Simulation of a spherical loudspeaker array using a flexible membrane model

Lucas Fernando Cóser

UNIVERSIDADE ESTADUAL DE CAMPINAS

FACULDADE DE ENGENHARIA MECÂNICA

COMISSÃO DE PÓS-GRADUAÇÃO EM ENGENHARIA MECÂNICA

Lucas Fernando Cóser

Simulação de um arranjo esférico de alto-falantes usando um modelo de membrana flexível

Campinas, 2010.

73/2010

Lucas Fernando Cóser

Simulação de um arranjo esférico de alto-falantes usando um modelo de membrana flexível

Dissertação apresentada ao Curso de Mestrado da Faculdade de Engenharia Mecânica da Universidade Estadual de Campinas, como requisito para a obtenção do título de Mestre em Engenharia Mecânica.

Área de concentração: Mecânica dos Sólidos e Projeto Mecânico

Orientador: Prof. Dr. José Roberto de França Arruda

Campinas

2010

i

UNIVERSIDADE ESTADUAL DE CAMPINAS

FACULDADE DE ENGENHARIA MECÂNICA

COMISSÃO DE PÓS-GRADUAÇÃO EM ENGENHARIA MECÂNICA

DEPARTAMENTO DE MECÂNICA COMPUTACIONAL
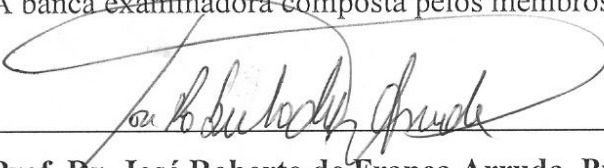
DISSERTAÇÃO DE MESTRADO ACADÊMICO

Simulação de um arranjo esférico de alto-falantes usando um modelo de membrana flexível

Autor: Lucas Fernando Cóser
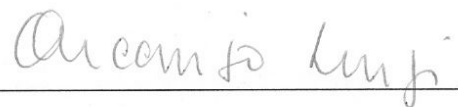
Orientador: Prof. Dr. José Roberto de França Arruda

A banca examinadora composta pelos membros abaixo aprovou esta dissertação:

_____

Prof. Dr. José Roberto de França Arruda, Presidente

Unicamp - Faculdade de Engenharia Mecânica

_____

Prof. Dr. Arcanjo Lenzi

UFSC - Departamento de Engenharia Mecânica

_____

Prof. Dr. José Maria Campos dos Santos

Unicamp - Faculdade de Engenharia Mecânica

Campinas, 09 de Agosto de 2010.

iii

Agradecimentos

Seria muito injusto não agradecer todas as pessoas que de alguma maneira tiveram participação nessa incrível jornada chamada vida. Embora todos os nomes não possam ser lembrados, é certo que cada pessoa contribuiu na minha história pessoal de uma forma peculiar que não pode ser descrita porque mesmo as frases mais complexas ou palavras não teriam um significado completo. De qualquer forma eu gostaria de agradecê-las, especialmente aquelas que me demonstraram que andar é a única forma de se construir um caminho.

Numa posição muito especial eu agradeço minha família por todo suporte, incentivo e amor que eu sempre tive mesmo nos tempos mais difíceis. Meus pais Sérgio e Elenice pela sua presença contínua e preocupação com a nossa educação e bem-estar; meu tio Edison e minhas tias Eunice, Eliana e Ecleide, por me levarem ao planetário quando eu era um garoto e me mostrarem que o mundo é tão grande quanto nossa imaginação pode ser; meus avós Justino e Diva, por me presentearem com um microscópio num Natal distante e me ensinarem que molhar seu jardim todo dia é importante; meu irmão Thiago por sempre instigar meu lado direito do cérebro e me mostrar o lado iluminado de todas as coisas e por último, mas não menos importante, minha esposa Renata, que se tornou minha inestimável companheira nessa jornada e me dá todos os dias muitas razões para continuar indo sempre além.

Gostaria de expressar ainda minha gratidão aos colegas do Departamento de Mecânica Computacional da Unicamp, especialmente a Alexander Mattioli Pasqual, cujas contribuições cruciais não apenas guiaram este trabalho, mas também me ensinaram tópicos importantes que eu nunca esquecerei. Tenho ainda muito orgulho de ter trabalhado com meu orientador José Roberto de França Arruda que, desde os meus tempos de graduação, tem sido uma referência pessoal e profissional sempre presente em minha memória.

Acknowledgments

It would be really unfair not to thank all the people who have somehow participated in this amazing journey called life. Although not all names can be remembered, it is certain that each person has contributed in my personal history in a peculiar way which cannot be described because even the most complex phrases or words would not have a complete meaning. Anyway I would like to thank all of them, especially those who have demonstrated me that walking is the only way of constructing a path.

In a special place I thank my family for all the support, incentive and love I have always had, no matter how hard the times were. My parents Sérgio and Elenice for their continuous presence and concern about our education and well being; my uncle Edison and my aunts Eunice, Eliana and Ecleide, for taking me to the planetarium when I was a kid and showing me that the world is as big as our imagination can be; my grandparents Justino and Diva, for giving me a microscope in a distant Christmas and teaching me that watering your garden everyday is important; my brother Thiago for always stimulating the right side of my brain and showing me the bright side of all things and last, but not the least, my wife Renata, who became my inestimable partner along this journey and gives me everyday many reasons to keep going further and further.

I would like also to express my gratitude to my colleagues of the Department of Computational Mechanics at Unicamp, especially to Alexander Mattioli Pasqual, whose crucial contributions not only guided this work but also taught me important topics that I will never forget. I am also very proud to have worked with my advisor José Roberto de França Arruda who, since my undergraduate times, has been both a personal and professional reference for me who I will always remember.

At last I express here my special thanks to the Brazilian company SmartTech for all the

Resumo

CÓSER, Lucas Fernando, *Simulação de um arranjo esférico de alto-falantes usando um modelo de membrana flexível*. 2010. 144 p. Tese (Mestrado em Engenharia Mecânica): Faculdade de Engenharia Mecânica, Universidade Estadual de Campinas, Campinas, Brasil.

Duas abordagens para a simulação do campo sonoro produzido por um arranjo esférico de alto-falantes são apresentadas e comparadas a resultados experimentais. Na primeira, modos estruturais obtidos da análise modal experimental da membrana são usados em simulações vibroacústicas por elementos de contorno no software LMS Virtual.Lab®. Na segunda, adota-se uma solução analítica baseada na expansão dos harmônicos esféricos de um padrão de velocidades sobre uma calota esférica. Os resultados são apresentados em termos de potência sonora e de padrões de diretividade para o arranjo. No primeiro caso, são observadas as mesmas tendências na faixa de baixa freqüência em todas as curvas analisadas, havendo distorções consideráveis na faixa de alta freqüência para a solução analítica devido ao fato desta não incluir os efeitos dos modos estruturais da membrana. Por outro lado, os padrões de diretividade demonstram um alto grau de similaridade em todos os casos analisados e não são fortemente afetados pelos modos estruturais da membrana.

As diferenças observadas nos resultados e as amplificações não realistas nas curvas de potência sonora das simulações são causadas por três fatores principais: modos de cavidade acústica do arranjo esférico, desconsideração do acoplamento acústico entre os alto-falantes durante seus funcionamentos e utilização de um mesmo conjunto de FRFs para todos os alto-falantes. De uma forma geral, pode-se dizer que a simulação usando o modelo de membrana flexível melhora consideravelmente a previsão da potência sonora na alta freqüência, o que não pode ser obtido com o modelo analítico comumente usado na análise de arranjos esféricos de alto-falantes.

Palavras-chave: radiação acústica, arranjos de alto-falantes, diretividade sonora, fontes esféricas, síntese de diretividade.

Abstract

CÓSER, Lucas Fernando, *Simulation of a spherical loudspeaker array using a flexible membrane model*. 2010. 144 p. Thesis (M.Sc. in Mechanical Engineering): Faculty of Mechanical Engineering, State University of Campinas, Campinas, Brazil.

Two approaches for sound field prediction of a spherical loudspeaker array operation are presented and compared to experimental measurements. In the first, real membrane modes from experimental modal analysis are used as input for BEM vibroacoustic simulations using LMS Virtual.Lab® software. In the second, an analytical solution based on the spherical harmonic expansion of an idealized velocity pattern over the spherical array is used. Results are presented in terms of sound power and directivity patterns, showing that the former has the same trend in all comparisons for the low frequency range, and that the analytical solution cannot be used for the high frequency range since it does not include the effect of the flexible membrane modes. Directivity patterns, however, show a good degree of similarity in all cases, and are not strongly affected by the flexible membrane modes.

The differences found in the results and the unrealistic amplifications in the sound power curves from the simulations are caused mainly by three factors: acoustic cavity modes of the array, neglecting the acoustic coupling among loudspeakers for the operating condition and utilization of the same set of FRFs for all loudspeakers in the array. In a general way, it can be said that the flexible membrane modeling improves considerably the prediction of radiated sound power in the high frequency range, which cannot be obtained by the analytical model commonly used in the analysis of spherical loudspeaker arrays.

Keywords: acoustic radiation, loudspeaker array, sound directivity, spherical sources, directivity synthesis.

List of figures

List of tables

List of symbols and abbreviations

Mathematical operators

$\{\,\cdot\,\}$, $\mathbf{x}$	-	Vectors
$[\,\cdot\,]$, $\mathbf{X}$	-	Matrices
$\lvert\,\cdot\,\rvert$	-	Absolute value
$\vec{\cdot}$	-	Vector quantity
$\times$	-	Curl
$\nabla(\cdot)$	-	Nabla
f(t)	-	Function of t (time domain)
f(s)	-	Function of s (Laplace domain)
$\Re\{\cdot\}$	-	Real part of
$*$	-	Complex conjugate
$\langle\,\cdot\,\rangle$	-	Spatial mean operator

Latin letters

$F_{in}(t)$	-	Force applied to the loudspeaker diaphragm (N)
a(t)	-	Diaphragm acceleration (m/s²)
v(t)	-	Diaphragm velocity (m/s)
x(t)	-	Diaphragm displacement (m)
e(t)	-	Input voltage (V)
i(t)	-	Current (A)
L_e	-	Voice coil inductance (H)
R_e	-	Voice coil resistance (Ω)
S	-	Diaphragm area (m²); effective area of a vibrating surface (m²)
m_m	-	Diaphragm moving mass
r_m	-	Diaphragm mechanical losses
c_m	-	Diaphragm suspension compliance
K	-	Loudspeaker amplification constant
p	-	Acoustic pressure (Pa)
A_{mn}	-	Constant for the series solution of the Helmholtz equation
Y_n^m	-	Spherical harmonic function of order n and degree m

$h_n^{(1)}$	-	Spherical Henkel function of first kind
$h_n^{(2)}$	-	Spherical Henkel function of second kind
P_n^m	-	Associated Legendre function of the first kind
k	-	Wave number (1/m)
c	-	Speed of sound (m/s)
f	-	Frequency (Hz)
F	-	Force (N)
I	-	Electrical current (A)
l	-	Element or loudspeaker coil lengths
L	-	Loudspeaker degree of freedom
B	-	Magnetic field vector (T)
Bl	-	Force factor (T.m)
W	-	Radiated acoustic power
$\mathbf{n}_{out}$	-	Normal vector point outwards of the domain
$\mathbf{x}_s$	-	Point on the radiator surface
$\mathbf{u}$	-	Column vector of velocity amplitude coefficients
$\mathbf{C}$	-	L by L real symmetric matrix

Greek letters

α, β, γ	-	User-defined constants for the general BEM problem
δ	-	Dirac delta function
ρ	-	Fluid density (kg/m³)
ω	-	Frequency (rads/s)
ω_n	-	Loudspeaker resonance frequency
ε	-	Infinitesimal radius
θ	-	Angle between the coil length vector and the magnetic field; zenith angle in a spherical coordinate system
ζ	-	Electromechanical damping factor
ϕ	-	Azimuth angle in a spherical coordinate system
Y	-	Acoustic particle velocity
Γ	-	Physical domain
σ	-	Radiation efficiency
υ_n	-	Acoustic particle normal velocity
Ψ	-	Eigenvector; structural mode; acoustic radiation mode
λ	-	Eigenvalue; wavelength
$\xi(\cdot)$	-	Set of orthogonal functions

Λ - L by L diagonal matrix containing the eigenvalues λ

Superscripts

H	-	Hermitian (complex conjugate)
T	-	Transpose
-1	-	Inverse of a matrix or number
m	-	Degree of a spherical function

Subscripts

r	-	Mode number
d	-	Diagonal matrix
ε	-	Infinitesimal volume
m	-	Degree of a spherical harmonic
n	-	Order of a spherical harmonic
max	-	Maximal value sought

Abbreviations and acronyms

AC	-	Alternating Current
ARM	-	Acoustic Radiation Mode
BC	-	Boundary Condition
BEM	-	Boundary Element Method
CAD	-	Computer Aided Design
CLF	-	Common Loudspeaker Format
CPU	-	Central Processing Unit
DC	-	Direct Current
DSP	-	Digital Signal Processing
EMF	-	Electric Motor Force
FEM	-	Finite Element Method
FMBEM	-	Fast Multipole BEM
FRF	-	Frequency Response Function
IRCAM	-	Institut de Recherche et Coordination Acoustique/Musique (Paris, France)
LDV		Laser Doppler Vibrometer
LMA	-	Laboratoire de Mécanique et d'Acoustique (Marseille, France)
MIF	-	Modal Indication Factor
MIMO	-	Multiple Input Multiple Output

RAM	-	Random Access Memory
SISO	-	Single Input Single Output
SLA	-	Spherical Loudspeaker Array
T-S	-	Thiele-Small
WFS	-	Wave Field Synthesis

Summary

"Take stock of those around you and you will see them wandering about lost through life, like sleep-walkers in the midst of their good or evil fortune, without the slightest suspicion of what is happening to them. You will hear them talk in precise terms about themselves and their surroundings, which would seem to point to them having ideas on the matter. But start to analyze those ideas and you will find that they hardly reflect in any way the reality to which they appear to refer, and if you go deeper you will discover that there is not even an attempt to adjust the ideas to this reality. Quite the contrary: through these notions the individual is trying to cut off any personal vision of reality, of his own very life. Life is at the start a chaos in which one is lost. The individual suspects this, but he is frightened at finding himself face to face with this terrible reality, and tries to cover it over with a curtain of fantasy, where everything is clear. It does not worry him that his "ideas" are not true, he uses them as trenches for the defense of his existence, as scarecrows to frighten away reality. The man with the clear head is the man who frees himself from those fantastic "ideas" and looks life in the face, realizes that everything in it is problematic, and feels himself lost. As this is the simple truth - that to live is to feel oneself lost - he who accepts it has already begun to find himself, to be on firm ground."

José Ortega y Gasset, The Revolt of the Masses

Capítulo 1

1. Introdução

1.1. Campos sonoros e sua síntese

O sentido da audição desempenha um papel extremamente importante na vida cotidiana dos seres humanos não apenas como um mecanismo de detecção, mas também por proporcionar sensações psicológicas complementadas pela visão e os outros sentidos (Olson, 1967). As propriedades de localização características do sistema auditivo são de extrema importância em muitos aspectos práticos (Vorländer, 2008), e se a reprodução de um campo sonoro específico é desejada, suas propriedades espaciais devem certamente ser levadas em conta, tornando o problema bastante complexo e mantendo-o numa área ativa de pesquisa e desenvolvimento.

Campos sonoros são caracterizados pela propagação de ondas sonoras e são caracterizados por quantidades acústicas de partícula (pressão acústica, potencial de velocidade, velocidade e deslocamento de partícula) numa posição e instante específicos (Fahy, 2001). Essas quantidades podem ser facilmente previstas no caso de fontes simples como um monopolo, porém serão geralmente muito mais complexas em fontes reais devido aos seus sofisticados mecanismos de geração. Devido à dependência espacial, posições diferentes terão quantidades acústicas distintas variando no tempo, resultando assim numa distribuição espacial complexa que caracteriza a diretividade da fonte. Como conseqüência desse fato, um instrumento como um violino radia seu som de maneira diferenciada dependendo de qual nota está sendo tocada e afetando, portanto, a maneira como os ouvintes o percebem dentro de uma sala de concerto (Figura 1.1).

Independentemente da técnica utilizada para gravar e reproduzir o som, a cadeia de reprodução sempre possuirá um elemento em sua extremidade final responsável pela geração das

1

ondas sonoras. Esse elemento é o alto-falante e, embora muitas técnicas de construção sejam empregadas, a maioria absoluta fabricada nos dias atuais usa um mecanismo de acionamento eletromecânico (Rossi, 1988). Para sistemas acústicos usando esse tipo de alto-falante, os parâmetros T-S (Thiele-Small) fornecem as orientações gerais para o seu desenvolvimento, sendo extremamente importantes e amplamente disseminados entre fabricantes e pesquisadores.
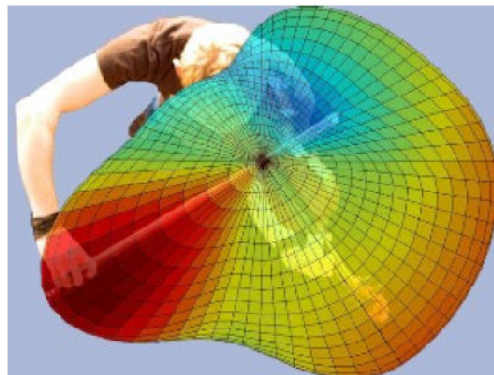
Figura 1.1 - Características de radiação sonora de um violino em médias freqüências (Behler, 2007).

Alto-falantes podem ser também combinados com outros para fornecer ao ouvinte uma melhor percepção dos campos sonoros que aquela encontrada com apenas um dispositivo. Uma solução comumente usada para atingir esse objetivo é a sua colocação ao redor do ouvinte, tal como encontrado nos sistemas *surround* convencionais. Tal metodologia pode ser melhorada com a utilização de processamento digital de sinais (DSP) para o controle eletrônico dos canais tal como usado na técnica *Ambisonics* (Gerzon, 1973) ou para a criação de frentes de onda artificiais sintetizadas por um grande número de alto-falantes individuais tal como encontrado no *Wave Field Synthesis* (WFS) e detalhado por (Berkhout et al., 1993). Entretanto, a predição das interações entre todos os alto-falantes e as interações com a sala são difíceis de serem computadas, colocando a complexidade do problema num nível ainda maior. Além disso, para os casos nos quais o DSP é utilizado, cálculos intensivos são necessários para se recriar padrões de campos sonoros complexos (Pasqual, 2010).

Outra alternativa para lidar com o problema da recriação de um campo sonoro complexo é utilizar um dispositivo eletroacústico multicanal. Esse método lida com a síntese direta da fonte sonora ao invés do campo sonoro resultante, ou seja, a complexidade da fonte é trabalhada na

origem do som e não no estágio de reprodução, evitando assim o problema da interação com a sala e simplificando o problema previamente estabelecido. De forma diferente do WFS, uma fonte multicanal pode ser um arranjo compacto de alto-falantes desenhado para simular radiadores complexos tais como instrumentos musicais (Pasqual, 2010).

Na prática, pode-se criar um arranjo esférico de alto-falantes (SLA) com a distribuição destes numa superfície esférica de acordo com uma geometria sólida de Platão, de maneira a se obter uma configuração altamente simétrica. Como os alto-falantes podem ser individualmente controlados por tensões elétricas diferentes, qualquer campo sonoro poderia em teoria ser gerado, atingindo então o objetivo previamente estabelecido pela reprodução da fonte ao invés do campo sonoro resultante e eliminando o problema da interação com a sala uma vez que a fonte seria virtualmente a mesma que a original. Pesquisas sobre esse tópico começaram com Caussé et al. (1992) e são ainda um tópico ativo de estudos, com variações no projeto e estratégias de controle diferenciadas (Warusfel et al., 2004). Devido às características previamente descritas, os SLAs podem também ser totalmente aplicados em controle ativo de ruído (Boaz, 2009) e na obtenção de respostas ao impulso de salas para uso em auralização (Behler, 2007). Outras aplicações possíveis dos SLAs são (Pasqual, 2010):

- Música eletroacústica;
- Medições acústicas em salas;
- Difusão da informação em direções privilegiadas e ajustadas;
- Controle por *feedback* de microfones.

France-2001 (IRCAM)   EUA–2003 (CNMAT – Berkeley)   EUA–2006   Germany-2007 (ITA – Aachen)   Austria-2007 (IEM – Graz)   Brazil/France-2008 (Unicamp/CNRS)

Figura 1.2 - Linha do tempo dos SLAs construídos e seus modelos (Pasqual, 2010).

Modelos analíticos para esses sistemas foram propostos por alguns autores como Kassakian et al. (2004) e Zotter et al. (2007), mas não levam em conta o efeito de uma membrana flexível, ou seja, o diafragma do alto-falante é normalmente tratado como um corpo rígido oscilando com um padrão constante de velocidade ao invés de um comportamento flexível com modos de vibração diferenciados em freqüências distintas. Embora bastante confiável na faixa de baixa freqüência, nota-se que esses modelos começam a divergir seriamente de resultados experimentais na faixa de alta freqüência, indicando assim que os efeitos das ressonâncias da membrana possuem efetivamente uma influência nessa região (Klippel, 2007).

1.1. Objetivos

O presente trabalho é uma contribuição à pesquisa realizada por Pasqual (2010) no sentido de estender o conhecimento sobre os SLAs pela utilização de uma nova abordagem computacional usando um *software* comercial de simulação. O termo *membrana flexível* significa que a análise modal experimental é aplicada ao diafragma e usada em todo o SLA, de maneira a proporcionar novas compreensões sobre o funcionamento do arranjo ao permitir o estudo da faixa de alta freqüência não contemplada pelos modelos analíticos até então existentes. Todos os experimentos foram realizados por Pasqual (2010) no Laboratoire de Mécanique et d'Acoustique em Marselha, França, num trabalho de cooperação entre a Unicamp e a instituição estrangeira. Mais ainda, pode-se dizer que este trabalho fornece uma nova visão sobre os dados até então disponíveis, permitindo que novas pesquisas possam ser investigadas rapidamente com o uso das simulações computacionais tal como resumido pela Figura 1.3. Uma descrição detalhada dos passos da simulação também é fornecida, o que não apenas documenta a complexidade do modelo, mas também proporciona uma referência para pesquisas futuras.
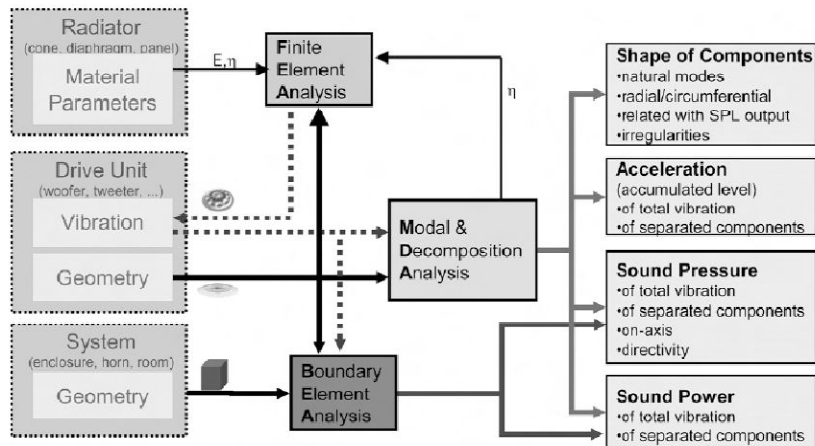
Figura 1.3 - Visão geral das análises de vibração e radiação para o desenvolvimento de alto-falantes conforme Klippel et al. (2009).

1.2. Resumo dos capítulos

Este trabalho está organizado da seguinte forma:

- Capítulo 2: inicia com a discussão sobre alto-falantes através de uma revisão histórica e um resumo dos tipos de dispositivo disponíveis. Os parâmetros T-S são então apresentados, seguidos por uma revisão da literatura sobre modelagem de membranas flexíveis. As características acústicas de campos próximo e distante são discutidas juntamente com o conceito de padrões de diretividade, e a seção sobre alto-falantes finaliza com uma revisão sobre o formato CLF usado para intercâmbio de dados de alto-falantes. Em continuidade, as duas abordagens relativas à modelagem dos SLAs (harmônicos esféricos e modos de radiação acústicos) juntamente com a solução analítica usada por Pasqual (2010) são apresentadas. O capítulo finaliza com uma descrição do arranjo experimental usado por Pasqual (2010) para a determinação dos padrões de diretividade dos ARMs do protótipo em forma de dodecaedro construído por ele;

- Capítulo 3: no início uma explicação sobre a análise modal da membrana é feita, a partir da qual os parâmetros modais foram extraídos para uso nas simulações. Uma

5

descrição detalhada de todos os passos envolvidos é então feita de maneira a proporcionar o leitor uma compreensão aprofundada das hipóteses e os parâmetros necessários para simular o SLA construído por Pasqual (2010);

- Capítulo 4: estabelece os parâmetros de comparação utilizados entre os resultados analítico, simulado e experimental e fornece uma análise dos resultados obtidos em termos da potência sonora radiada e os padrões de diretividade do SLA construído por Pasqual (2010);

- Capítulo 5: interpreta os resultados do capítulo anterior e discute-os, proporcionando assim uma compreensão geral sobre os dados obtidos. Sugestões para pesquisas futuras também são fornecidas no final do capítulo.

Chapter 1

1. Introduction

1.1. Sound fields and their synthesis

The sense of hearing plays an important role for humans in the everyday life not only as a detection mechanism but by allowing them to have psychological experiences complemented by vision and the other senses (Olson, 1967). The localization mechanisms proportioned by the auditory system are extremely important in many practical aspects (Vorländer, 2008), meaning that if the reproduction of a particular sound field is wanted, its spatial properties must certainly be taken into account, which makes the problem extremely challenging and thus remaining an active field of research and development.

Sound fields are generated whenever sound waves propagate and are characterized by acoustic particle quantities (acoustic pressure, velocity potential, particle velocity and displacement) at a specific position and instant (Fahy, 2001). Those quantities can be easily predicted in the case of simple sources like a monopole, but will generally be far more complex in real sources due their sophisticated sound generating mechanisms. Because of the space dependence, different locations will have distinct acoustic quantities, thus resulting in fact a complex spatial distribution which characterizes the source directivity. As a consequence of that, a musical instrument like a violin radiates sound in different ways depending on which musical note is being played, therefore greatly affecting how listeners in a concert hall will perceive it (Figure 1.1).

No matter which technique is used to record and play sound, the reproduction chain will always have an element at its very end responsible for sound generation. Although many

construction approaches for loudspeakers are available, the vast majority manufactured today uses an electromechanical driving mechanism (Rossi, 1988). For acoustic systems using such type of loudspeakers, the T-S (Thiele-Small) parameters provide the key guidelines in their design, therefore being extremely important and disseminated throughout manufacturers and researchers.
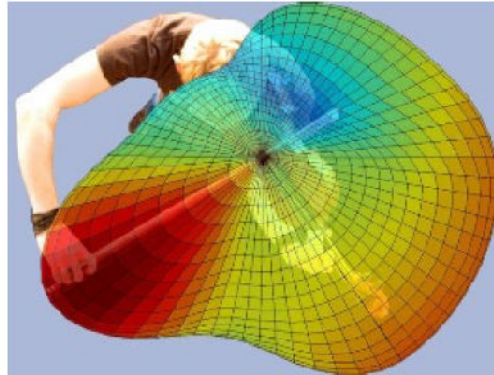
Figure 1.1 - Sound radiation characteristics of a violin player at mid frequencies (Behler, 2007).

Loudspeakers can also be combined in order to give to the listener a better perception of sound fields than by using a sole device. A solution commonly implemented to achieve such goal is to place them around the listener as found in conventional surround. That method can also be improved with DSP (Digital Signal Processing) for electronic channel mixing like used in Ambisonics (Gerzon, 1973) or to create artificial wave fronts synthesized by a large number of individual speakers used in WFS (Wave Field Synthesis) and detailed by Berkhout et al. (1993). However, the prediction of the interactions among all loudspeakers and the interactions with the room are difficult to account for, putting the complexity of the problem in an even higher level. Besides, for the cases where DSP is used, massive computations are needed in order to recreate sophisticated sound field patterns (Pasqual, 2010).

Another approach to tackle the problem of recreating a complex sound field consists of using a multichannel electroacoustic source. That method deals with the direct sound source synthesis instead of the resultant sound field itself, i.e., the complexity of the source is dealt with the sound at the origin and not at the reproduction stage, thus avoiding the problem of the room interaction and simplifying the problem stated above. Unlike the WFS, a multi-channel source can be a

compact array of loudspeakers designed to simulate complicated sound radiators such as musical instruments (Pasqual, 2010).

In practice, one can create a Spherical Loudspeaker Array (SLA) by distributing the loudspeakers over the spherical surface according to a Platonic solid geometry, so that a highly symmetrical configuration is obtained. As speakers can be individually controlled by independent voltages, any sound field could be in theory generated, thus achieving the previous goal by reproducing the source instead of the resultant sound field and getting rid of room interaction problem since the source would be virtually the same as the original. Research concerning such devices have started by Caussé et al. (1992) and are still an active topic, with many variations in design and control strategies (Warusfel et al., 2004). Due to the characteristics previously described, SLAs can also be applied in active noise control (Boaz, 2009) and room impulse responses for auralization purposes (Behler, 2007). Other applications of SLAs mentioned by Pasqual (2010) are:

- Electroacoustic music performance;
- Room acoustics measurements;
- Information diffusion in privileged adjustable directions;
- Microphone feedback control.

Figure 1.2 - Timeline of SLAs constructed and their models (Pasqual, 2010).

Analytical models for such systems have been proposed by some authors like Kassakian (2004) and Zotter (2007), but they do not take in account the effect of a flexible membrane, with

the loudspeaker's diaphragm normally treated as a rigid body oscillating with a constant velocity pattern instead of a flexible behavior with different mode shapes at distinct frequencies. Although very reliable in the low frequency range, those models start do severely diverge from experimental results in the high frequency range, thus indicating that the effects of membrane resonances do have an influence in such region (Klippel, 2007).

1.1. Objectives

The present work is a contribution to the previous research made by Pasqual (2010) in order to extend the knowledge on SLAs by using a new simulation approach made with commercial software. The term *flexible membrane* means that a structural modal identification approach from experimental data is applied to the diaphragm and used in the simulations of the SLA, thus providing new insights in the array operation by allowing the study of the behavior in the high frequency range, which is not contemplated by the analytical models available so far. All the experiments were performed by Pasqual (2010) in the Laboratoire de Mécanique et d'Acoustique in Marseille, France, in a cooperative work between Unicamp and that institution. Moreover, it can be said this work gives a new look to already available data in order to enable quicker future research by the use of computational simulations as summarized in Figure 1.3. Also, a detailed description of the simulation steps taken is provided, which not only documents the complexity of such simulation but also provides a starting point for future reference.
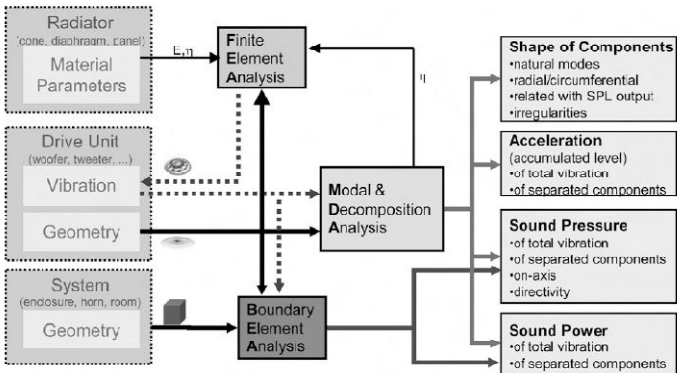
Figure 1.3 - Overview of vibration and radiation analysis in loudspeaker design after Klippel et al. (2009).

The work structure starts with loudspeaker technology research by including a brief review of the device history and its types. Since the predominant transducer mechanism in industry is the electrodynamic, a detailed analysis concerning its internal parts and modeling is made, the latter relying on the T-S (Thiele-Small) parameters that are then presented and discussed. Afterwards, the SLA construction and modeling is treated with the description of its construction techniques, geometrical and acoustical properties that allow the synthesis of a sound field, neglecting the control strategies fully discussed by Pasqual (2010) in his work. Finally, a complete description of the flexible membrane model is presented and the simulation steps described, the results being compared at the end with the previously mentioned analytical and experimental results.

1.2. Summary of chapters

This work is organized as follows:

- Chapter 2: starts with a discussion about loudspeakers through a historical review and a summary of its construction types. The Thiele-Small parameters are then presented, followed by a review of the literature available on flexible membrane modeling. Near- and far-field propagations are discussed together with directivity pattern concept and the loudspeaker section ends with a revision about the CLF format for loudspeaker data exchange. Afterwards the two approaches concerning SLA modeling (spherical harmonics and ARMs) and the analytical solution used by Pasqual (2010) are presented. The chapter ends with a description of the experimental setup used by him in order to determine the directivity patterns for the ARMs of the dodecahedral prototype constructed;

- Chapter 3: in the beginning an explanation of the membrane modal analysis is made, in which the structural modal parameters were extracted. The results of this analysis were then used in the simulations, and a detailed description of all steps is then made in order to provide the reader a deep insight of the assumptions taken and the necessary parameters used to simulate the SLA constructed by Pasqual (2010);

5

- Chapter 4: establishes the comparison criteria used to compare the results obtained from analytical, simulated and experimental data and analyses the results obtained in terms of the radiated sound power and the directivity patterns for the SLA;

- Chapter 5: interprets the results obtained in the previous chapter and discusses them in order to better understand all the data. Suggestions for further research are also provided at the ender of the chapter.

Chapter 2

2. Loudspeakers and spherical arrays

A discussion about loudspeakers and spherical arrays is presented in this chapter in order to provide the reader a deeper knowledge about the two subjects which indeed complement each other. In the beginning focus is given to loudspeakers, its construction types and design based on the T-S parameters. After that, a discussion about loudspeaker arrays is presented and some insights concerning its construction parameters and design are given, finishing with a presentation of the experimental setup used by Pasqual (2010) in order to evaluate the proposed analytical model.

2.1. Loudspeakers

According to Olson (1962) "*a loudspeaker is an electroacoustic transducer intended to radiate acoustic power into the air, the acoustical waveform being essentially equivalent to that of the electrical input*". The process of transforming an electrical signal into a mechanical oscillation can be performed in many ways, but the flatter the response inside the audible frequency range, the better will be the sound reproduction quality achieved by the device (Dickason, 2005).

The design goal mentioned above is always hard to achieve since the two ends of the audio-frequency spectrum are the most difficult to reproduce with efficiency when compared the mid range (Olson, 1962). Some construction approaches are used in practice to increase the low audio-frequency radiation and are essentially based on the diaphragm size, quantity and mounting (baffles, cabinets and horns). In the high audio-frequency range loss of efficiency is essentially caused by a relative large mass reactance compared to the sound radiation resistance of the air and can be reduced by using multiple loudspeakers and horn mountings (Dickason, 2005).

7

In the following sections a brief presentation of loudspeaker history and design types will be made. Further attention will be especially given to electrodynamic (or electromechanical) loudspeakers which comprehend the majority of devices used today and can be fully described in terms of the T-S parameters. A description of the CLF (Common Loudspeaker Format) will also be made at the end in order to present this file format and its applications for researchers and manufacturers.

2.1.1. Historical background and loudspeakers types

The development of electrodynamic loudspeakers is related with the invention of the telephone (Pedersen, 2008), which can be verified in two patents from Siemens (1874) and Bell (1876). A description given by Siemens (1874) to his invention was "(…) *for obtaining the mechanical movement of an electrical coil from electrical currents transmitted through it.*" which can be promptly correlated to the electromechanical loudspeaker working principle available in the present time. In another approach, Bell was developing a new way of information transmission through the available wires by using continuous signals that could be combined like musical notes to produce more complex sounds instead of just intermittent tones available in telegraphy. Both innovations not only culminated in the development of the telephone as known today, but also needed rapid developments in the process of transforming electrical signals into audible sound.

The moving-coil motor was patented by Lodge (1898) who introduced the air gap construction as found today, but the transducer was not used until the vacuum tube was developed and radio was established as an information broadcast standard (Pedersen, 2008). The electrodynamic loudspeaker as know today appeared first in a patent by Rice et al. (1925), which became a widely spread part in many consumable products and devices like home audio music, television and toys.
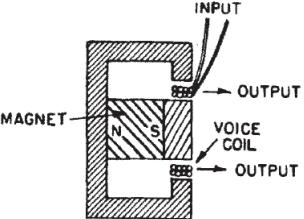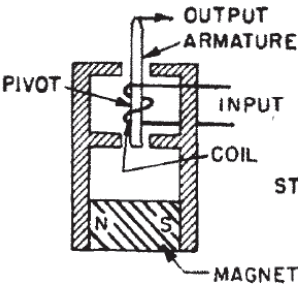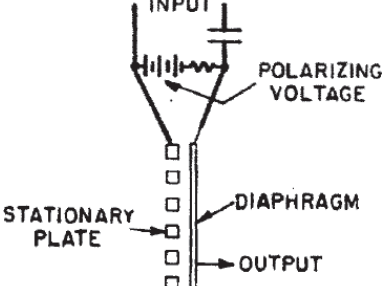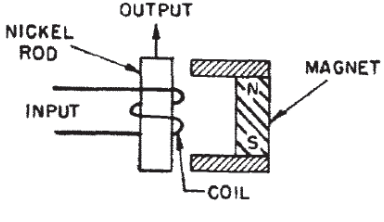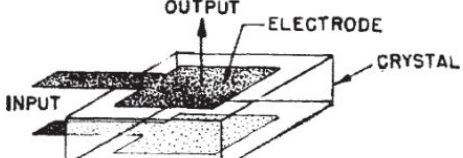
The key point behind almost all loudspeakers is the fact that that they employ either an

electromechanical or electroacoustic transducer for converting electrical current variations into corresponding acoustical changes. It is interesting to note that the driving systems available in the 1960s and summarized by Olson (1962) in Table 3.1 are surprisingly nearly the same of most predominant types found today. It is clear to see that, although new driving mechanisms have been developed in the past fifty years, the dominant construction types are still equal, which is mainly caused by poor economical feasibility of new designs and concentrated efforts in improving actual systems in terms of efficiency and flatter frequency responses (Dickason, 2005).

Electrodynamic loudspeakers are not commonly found in practice since a DC (Direct Current) supply is needed to keep the electromagnetic field active, thus resulting in higher power consumption for the system as a whole. Differing from the electrodynamic loudspeaker only by the fact that the magnetic field is generated by a current source instead of being just steady, it can be said that that the electromagnetic type has equivalent acoustical characteristics compared to the former, with good, reasonable and poor frequency responses in the low, mid and high frequency ranges respectively (Olson, 2002). Advantages do exist due the fact that the magnetic field can be totally controlled, allowing the usage of variable or powerful electromagnetic fields in compact designs due the absence of the permanent magnet, which has a limited magnetic flux directly related to its size. However its applications are limited due the higher power consumption caused by the necessary current source for the electromagnet.

The main advantage in electrostatic loudspeakers is their extremely flat frequency response (similar to an electrostatic microphone), which is achieved by the totally in-phase movement of the membrane as the thin statically charged diaphragm is driven by the electric field. On the other hand, the membrane displacement is very limited due construction constraints and, the further the diaphragm is located from the stationary plate, the higher will be the electric field necessary to keep acceptable the system's working principle, which normally causes the appearance of electric arcs and dust attraction that can damage the driver (Wikipedia, 2010).

Table 2.1 - Main loudspeaker types according to Olson (1962).

Type	Principle for development of mechanical forces	Figure
Electrodynamic	Interaction of the electric current passing through the coil and the transverse magnetic field.	
Electromagnetic	Magnetic reactions between the magnetized armature and the magnetic field of a permanent magnet. Another variation can be obtained by using the same construction as in the electrodynamic case, but replacing the permanent magnet by an electromagnet, i.e., a magnet controlled by the flow of a DC electric current.	
Electrostatic	Electrostatic reactions between a high voltage electric field and a statically charged membrane.	
Magnetostrictive	Deformation of a ferromagnetic material possessing direct magnetostrictive properties.	
Piezoelectric	Deformation of a crystal or ceramic having converse piezoelectric properties.	

Magnetostrictive transducers are based on an effect called magnetostriction by which ferromagnetic materials undergo a small mechanical change when magnetic fields are applied, either expanding or contracting slightly (Nave, 2006); a common example of this property is the humming noise found in AC (Alternate Current) transformers caused by the response of the iron

core due the magnetic field impressed on it. The essential advantages of the technology are: massive force generation, stationary magnetizing coil which can be easily cooled and absence of suspension mechanisms (less fragile assembly). A patent for a giant device was published by Ijima (2006) according to Foster[1] and some other structure-embedded construction techniques were presented by FeONIC Technology[2], which has a proprietary technology called *Whispering Windows*[3] in which a magnetostrictive driver is used to vibrate a wall or a window in order to produce audible sound that could be used in advertisement for instance (FeONIC Technology, 2010).

Piezoelectric speakers are normally found in everyday electronic products with beeping sounds (alarm clocks, timers, etc) and are sometimes used as tweeters in less-expensive speaker systems, such as computer speakers and portable radios. Their advantage is the fact that they support overloads much better than any conventional loudspeaker, but distortions can be observed in amplifiers due the high capacitive loads and the frequency response is not good compared to other technologies, enabling them to be used mainly in single frequency tone applications (Wikipedia, 2010).

As mentioned before, some new driving devices have been developed in past years and, although not included in Table 2.1, are worth to be mentioned. It is important to note though that they are very specific devices intended for dedicated applications:

- Ribbon: developed by the European Acoustic Laboratory after the First World War (Sequerra, 1998), a thin metal-film ribbon suspended in a magnetic field moves as an electrical signal is applied. As the driver has very little mass, it can accelerate very quickly, thus having very good high-frequency response. The disadvantage though is that the device is often very fragile and needs generally powerful magnets which make them costly to manufacture;

---

[1] http:// www.foster.com
[2] http://www.feonic.com
[3] http://www.whisperingwindow.com

11

- Bending wave: in this design the stiffness of the diaphragm material increases from the center to the outside, making shorter and longer wavelengths radiate from the inner and outer areas of the speaker. A surrounding damper is also used to absorb longer waves to be reflected and such transducers can cover a wide frequency range from 80 Hz up to 35 kHz and many construction techniques were employed by manufacturers, most notably Ohm Walsh[4];

- Plasma arc: electrical plasma is used as a radiating element. Since it has a minimal mass and is charged, an electric field can manipulate the plasma in order to produce very flat frequency responses far higher than the audible range. The device still remains mostly as a curiosity since problems of maintenance and reliability make it unsuitable for mass market use and the most remarkable commercial version was presented by Plasmatronics company in 1979 (Olson, 2002);

- Air motion: invented by Oskar Heil in the 1960s. In this approach, a pleated diaphragm is mounted in a magnetic field and forced to close and open under control of a music signal. Air is forced from between the pleats in accordance with the imposed signal, generating sound. The drivers are less fragile than ribbons and considerably more efficient, being able to produce higher absolute output levels than ribbon, electrostatic, or planar magnetic designs (Wikipedia, 2010). The first commercial models were sold by ESS[5] in the 1970s and 1980s and nowadays only two notably companies still produce this kind of speaker: Precide[6] and ADAM Audio[7].

2.1.2. Electromechanical loudspeakers

As presented before, the most common type of loudspeaker is the electromechanical (or

---

[4] http://www.ohmspeakers.com/
[5] http://essspeakersusa.com/
[6] http://www.precide.ch/
[7] http://www.adam-audio.com/

electrodynamic) device, which will be examined in detail in this section. Before starting the discussion of this topic, it is convenient to analyze the individual parts of such device as depicted in Figure 2.1.
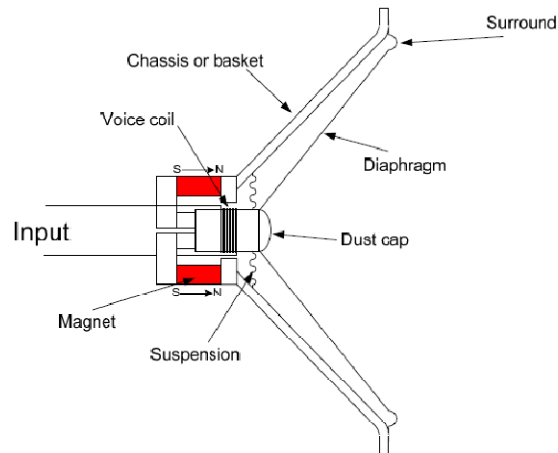
Figure 2.1 - Common electromechanical loudspeaker parts (Pedersen, 2008).

Parts presented in Figure 2.1 are better detailed by Pedersen (2008) and Dickason (2005):

- Diaphragm (or membrane): converts the mechanical movement established by the interactions between the magnetic field and the coil into sound waves;

- Suspension (or spider): behaves like a spring and fixes the diaphragm to a defined rest position, thus introducing stiffness into the membrane;

- Surround (or edge suspension): fixates the edge of the membrane to the chassis, limiting the movement of the diaphragm to one direction, preventing excessive displacements and avoiding air leakage from the back of the membrane to the front;

- Dust cap: prevents the intrusion of any unwanted particles inside the air gap;

- Chassis (or basket): provides the structural support for the surround, the membrane and the magnet;

13

- Magnet: permanent magnet normally manufactured with ferrite and inserted in a soft iron structure which directs the magnetic flux to the magnet gap in order to concentrate it;

- Voice coil: mounted onto the diaphragm and placed in the air gap, is responsible for converting the electric current into force using the Lorentz principle (further explained below).

The electromechanical operation occurs because of the Lorentz principle, in which a wire inserted in a magnetic field will have a force exerted perpendicularly to the plane formed by the current flow and the magnetic field vector when a current flows through it (Tipler, 2002). That principle is better described by equation (2.1):

$$\vec{F} = I\,(\vec{l} \times \vec{B}) = I\,|\vec{l}|\,|\vec{B}|\,\sin(\theta) = I\,l\,B\,\sin(\theta) = I\,l\,B \tag{2.1}$$

where l is the length of the wire in meters, I the current flow in Ampères and B is the magnetic flux density in Teslas. The product Bl is usually called as *force factor* (Dickason, 2005), having units of *T.m* and it is an important parameter in loudspeaker analysis because it is directly related to the power of the mechanical system, i.e., an increase in that product means an automatically increase of the system total output power.

The coil displacement will follow the voltage applied to the loudspeaker. If it starts to increase, the effective number of windings inside the magnetic field will be smaller and consequently reduce the Bl term. According to Dickason (2005), when the number of windings inside the magnetic field is constant, the speaker is said to operate in the linear range, entering the non-linear region when this quantity starts to decrease. Dickason (2005) also mentions that two construction approaches for the coil are normally used in practice: short and long windings as illustrated in Figure 2.2. The X_{max} distance seen in Figure 2.2 represents the maximal course in which the coil can move keeping the speaker in the linear range and characteristics of both construction approaches are summarized in Table 2.2.
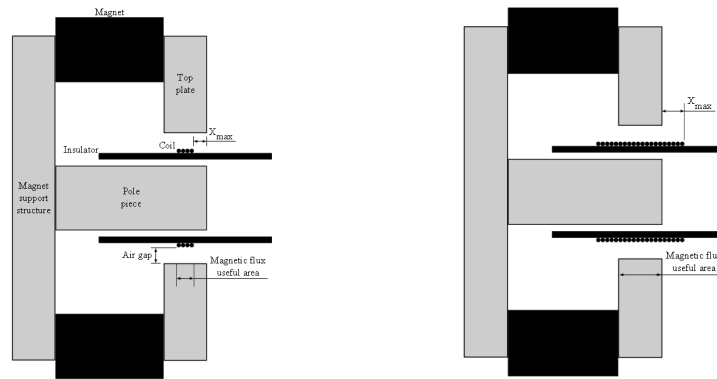
Figure 2.2 - Details in the two coil construction approaches as demonstrated by Dickason (2005) with short coil on the left and long coil on the right. The magnetic flux useful area indicates the path used by the magnetic circuit to close its loop from north to south magnetic poles.

It is worth noting that different combinations of coil lengths and geometries can be used in order to produce different values for X_{max}. However, even two different loudspeakers having the same X_{max} value will have different behaviors in terms of linearity due the different interactions inside the electromechanical driving system (Dickason, 2005). The short coil has a very linear behavior for small displacements with a smaller *Bl* factor caused by a larger air gap, while the contrary can be observed for the long coil construction, which makes it a preferable construction in practice because of the higher allowable displacements inside the linear range.

Table 2.2 - Qualitative comparison of the two coil construction approaches (Dickason, 2005).

Parameter	Short coil	Long coil
Linearity	Good for small displacements	Reasonably good
Magnet flux useful area	Small compared to the surrounding structure	Total
Magnetic flux	Stronger to compensate the smaller previous parameter	Weaker due to the higher previous parameter
Bl factor	Smaller	Higher
Mass	Usually smaller	Usually bigger
Price	Normally expensive (heavily depends on magnet construction)	Normally cheaper

2.1.2.1. The Thiele-Small (T-S) parameters

Designing loudspeakers requires a great amount of research and development of many factors.

The fundamentals for which speaker enclosures are designed today are specifications called Thiele-Small (T-S) parameters, developed by Neville Thiele and Richard Small. These parameters can be used to predict the performance of a speaker in different types of speaker enclosures.

The two articles from Thiele (1971) are a reprint of his published works made in 1961 concerning loudspeakers studies in different types of vented speaker enclosures. Small (1972), also published another series of two articles based on the works of Thiele (1971) for other configurations of loudspeakers and enclosures. Those works are widely referred to even today because the acoustic output and characteristics of a speaker was made much simpler by simply using electrical circuit analysis from which the T-S parameters can be extracted and used in loudspeaker and enclosure design. The next sections investigate a linear loudspeaker in order to establish its T-S parameters.

2.1.2.1.1. Mechanical part

Taking a generic linear loudspeaker given by Figure 2.3,
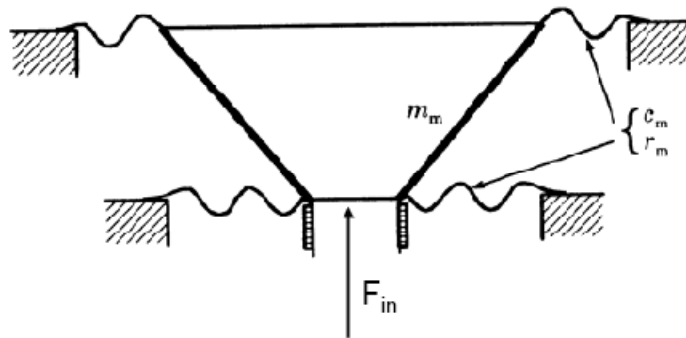
Figure 2.3 - Free body diagram of a linear loudspeaker as demonstrated by (Pedersen, 2008).

by applying Newton's second law, the mechanical part can be described as:

$$F_{in}(t) = m_m\, a(t) + r_m\, v(t) + \frac{1}{c_m}\, x(t)$$

(2.2)

16

where $F_{in}(t)$ is the force applied to the diaphragm, $a(t)$, $v(t)$ and $x(t)$ are respectively the diaphragm acceleration, velocity and displacement, m_m is the moving mass, r_m are the mechanical losses and c_m is the suspension compliance. Equation (2.2) can be thought in terms of a block diagram as:
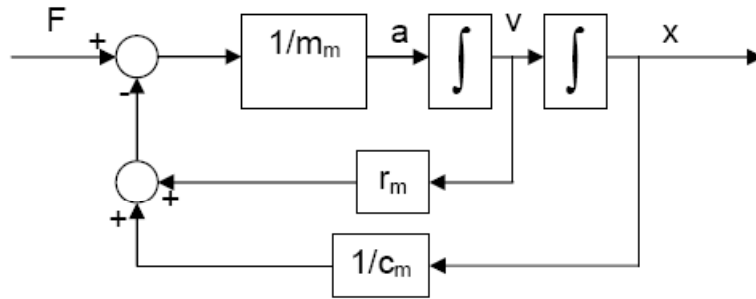
Figure 2.4 - Block diagram of the mechanical system (Pedersen, 2008).

2.1.2.1.2. Electrical part

Considering the electrical circuit given by:
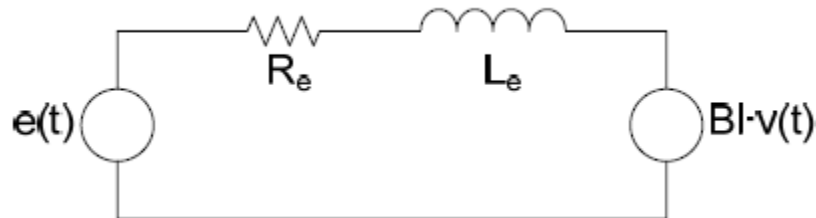
Figure 2.5 - Electrical circuit of a linear loudspeaker (Pedersen, 2008).

Using Kirchoff's voltage law one has:

$$e(t) = L_e \frac{di}{dt} + R_e \, i(t) + B \, l \, v(t)$$
(2.3)

where $e(t)$ and $i(t)$ are the loudspeaker input voltage and current respectively, L_e and R_e the voice coil inductance and resistance respectively and Bl the force factor. Equation (2.3) includes the back electrical motor force (EMF) from the movement of the voice coil in the magnetic field and

can be also represented by:
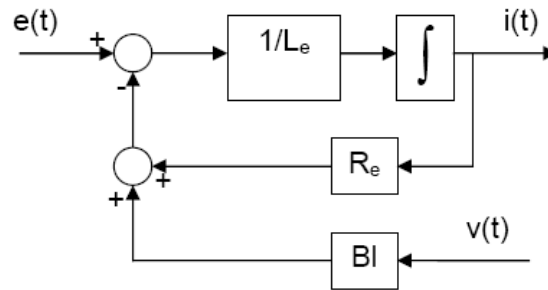
Figure 2.6 - Block diagram of the electrical system (Pedersen, 2008).

2.1.2.1.3. Electromechanical conversion

The electro-mechanical conversion is characterized by the conversion from current to force and is dependent on the force factor *Bl* which, as previously described, also occurs in the back EMF when the voice coil is moving. Therefore:

$$F_{in}(t) = B \, l \, i(t) \tag{2.4}$$

Equation (2.4) sets the link between the two block diagrams presented by Figure 2.4 and Figure 2.6. Therefore, a complete block diagram for the loudspeaker is given by:
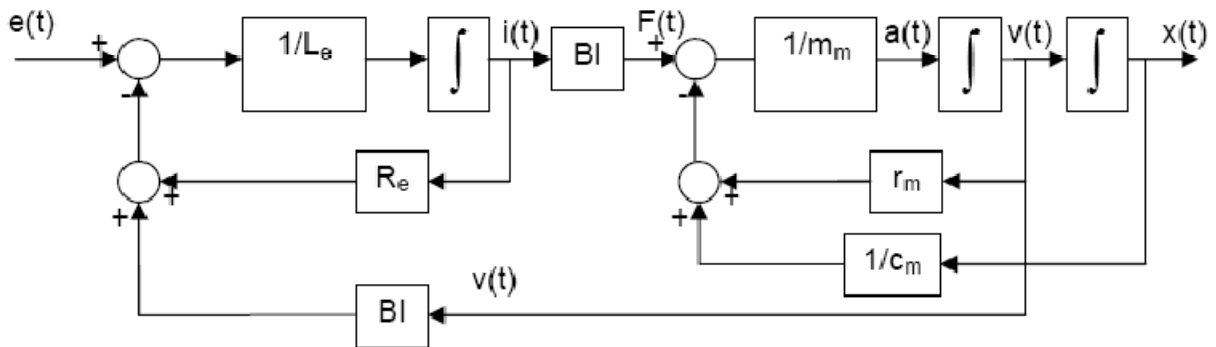
Figure 2.7 - Block diagram of the entire linear loudspeaker (Pedersen, 2008).

This can be depicted in an equivalent electrical circuit as:

18
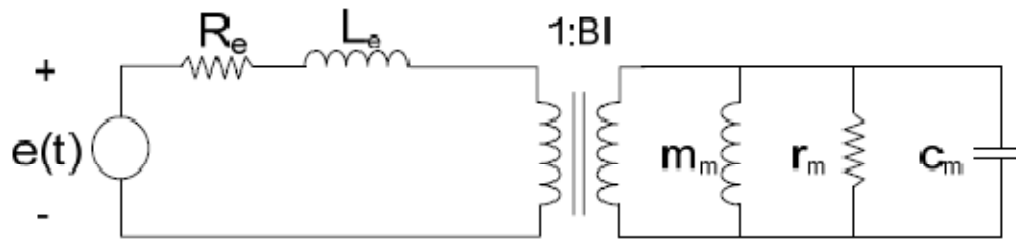
Figure 2.8 - Electrical equivalent circuit for the linear loudspeaker (Pedersen, 2008).

2.1.2.1.4. Acoustic load

The air on the back and front of the diaphragm is called as acoustic load and must be taken into account in order to represent a complete model. Under normal conditions, a loudspeaker unit is mounted in a box, known as the rear cabinet. Hence, the acoustic load can be simplified into two elements: in the front of the loudspeaker the moving air mass can be added to the moving mass, m_m; at the back side of the rear cabinet the air inside acts like a compliance, so it can be included in the term c_m (Pedersen, 2008).
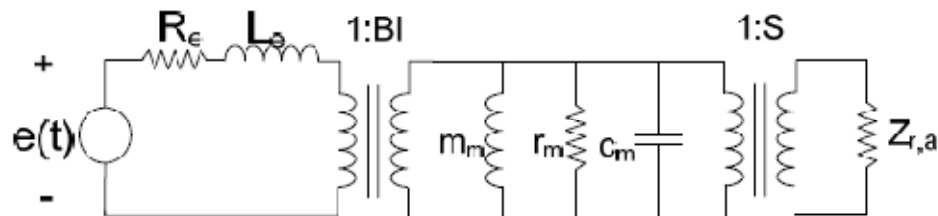
Figure 2.9 - Electrical equivalent circuit for the linear loudspeaker including a complex resistor on the right side (Pedersen, 2008).

Although the moving air mass is recalculated to mechanical parameters, it can also be included as an acoustic parameter by applying the mechanical acoustic transformation of the effective diaphragm area S and the acoustic load is shown as a complex resistor on the acoustic side (Figure 2.9).

2.1.2.1.5. Frequency response

The reason for using a linear model is that it gives a simple overview of loudspeaker

19

characteristics. By applying a Laplace transformation in equations (2.2), (2.3) and (2.4) one has:

$$F_{in}(s) = m_m \, s^2 \, x(s) + \, r_m \, s \, x(s) + \frac{1}{c_m} \, x(s) \tag{2.5}$$

and

$$e(s) = L_e \, s \, i(s) + R_e \, i(s) + \, B \, l \, s \, x(s) \tag{2.6}$$

and

$$F_{in}(s) = B \, l \, i(s) \tag{2.7}$$

Typically, the output of interest is the diaphragm acceleration due to its proportionality to the sound pressure in the far field (Thiele, 1971). However, in relation to loudspeaker design, the displacement of the diaphragm is of interest and the transfer function between displacement and input voltage is given by Pedersen (2008):

$$H(s) = \frac{x(s)}{e(s)} = \frac{\dfrac{Bl}{m_m \, (L_e \, s + R_e)}}{s^2 + \left[\dfrac{Bl^2}{m_m(L_e \, s + R_e)} + \dfrac{r_m}{m_m} \right] s + \dfrac{1}{c_m \, m_m}} \tag{2.8}$$

The transfer function between acceleration and voltage is also given by Pedersen (2008) as:

$$H(s) = \frac{a(s)}{e(s)} = \frac{\dfrac{Bl}{m_m \, (L_e \, s + R_e)} \, s^2}{s^2 + \left[\dfrac{Bl^2}{m_m(L_e \, s + R_e)} + \dfrac{r_m}{m_m} \right] s + \dfrac{1}{c_m \, m_m}} \tag{2.9}$$

By eliminating the voice coil inductance to consider only the low frequency range (low inductor impedance) the transfer function in equation (2.8) can be simplified to:

$$H(s) = \frac{x(s)}{e(s)} = \frac{\dfrac{Bl}{R_e \, m_m}}{s^2 + \left(\dfrac{Bl^2}{R_e \, m_m} + \dfrac{r_m}{m_m}\right) s + \dfrac{1}{c_m \, m_m}}$$

(2.10)

which can be rewritten as:

$$H(s) = \frac{x(s)}{e(s)} = K \frac{\omega_n^2}{s^2 + 2 \zeta \omega_n s + \omega_n^2}$$

(2.11)

where ζ is the electromechanical damping factor, ω_n the resonance frequency and K the amplification constant. From equation (2.8) those values are given by:

$$\zeta = \frac{Bl^2 \sqrt{c_m}}{2 \, R_e \, \sqrt{m_m}} + \frac{r_m \sqrt{c_m}}{2 \sqrt{m_m}}$$

(2.12)

$$\omega_n = \frac{1}{\sqrt{m_m c_m}}$$

(2.13)

$$K = \frac{B \, l}{R_e \, m_m}$$

(2.14)

It can be seen from the equations above that the formulation for the linear loudspeaker is very similar to a single DOF mechanical system. Indeed this is what makes the T-S parameters so useful because they can provide a very good insight into the loudspeaker operation by using some pre-defined parameters. Experimentally there are many ways of determining them as can be seen in the classical articles by Thiele (1971) and Small (1972), and variations concerning variable components in frequency can also be introduced in order to improve the model like performed by Pasqual et al. (2009), in which a lossy inductor is used instead of a linear component.

2.1.2.2. Flexible membrane modeling

As seen in the previous section, the T-S parameters provide a very consistent way of determining

lumped parameters for electrodynamic loudspeakers. However, the membrane flexibility is normally not taken into account since the structural interactions between the component and the suspension are very complex, thus posing additional complexities to the simulation (Knudsen et al., 1993). Another major challenge found is the correct determination of the properties of all materials involved and non-linearities, which are suppressed either by simplifying the model or by using extracted modal parameters (distributed model) as demonstrated by Skrodzka et al. (2000) and the first paper in series of two published by Klippel et al. (2009). This series has indeed valuable guidelines for identifying problems in loudspeakers, with extremely concise information from measurement setup to data interpretation.

In Joly et al. (1996), the authors state the difficulties involved in modeling the membrane using the FEM in order to have simulated results comparable to the experimental ones. Although some results were obtained, a series of constraints existed in the model which almost invalidated it for a real world situation. However, an important contribution given by the authors concerns the membrane mesh, which has to be asymmetrical (nodes and elements not necessarily evenly spaced) in order to intentionally cause an uneven distribution of material properties as found in real membranes.

Non-linearities happen mostly during high vibrational amplitudes, affecting the electroacoustical behavior of electrodynamic transducers with distortions in the system response. Quaegebeur et al. (2008) investigate this effect and identify two main types of non-linearities: electrical (as already seen in Figure 2.2) and mechanical. Also, they propose a simulation structure composed by annular and circular plates in which a calculation methodology is performed. After studying the influence of both material properties and geometrical parameters involved, the authors conclude their research showing that non-linear effects can be substantially reduced by choosing appropriate material and geometrical parameters. Ravaud et al. (2009) propose a non-linear modeling based on the time variation of the T-S parameters in order to analyze non-linearities and time-varying effects. By investigating two identical loudspeakers subjected to different excitation conditions, the authors conclude that their resonance frequency is different and does not vary in time in the same way. Also, the solution of the time-varying non-linear differential equation of the electrodynamic loudspeaker shows that the theoretical

22

displacement spectrum is consistent with the experimental displacement spectrum found.

The suspension is treated in detail in the second paper in a series of two published by Klippel et al. (2009) and Knudsen et al. (1993). In the latter the authors work with creep (continued slow displacement under sustained force) modeling for the low frequency range by replacing the simple linear compliance with a dynamic transfer function in three different analytical models followed by experimental evaluation; results indicated a very good correlation between all data obtained in the two approaches used.

For future reference purposes, it is worth to mention the work of Ba et al. (2009), in which the authors investigate an electret loudspeaker in order to compare the experimental results to a distributed parameter model. However, the reader must bear in mind that this is a not a very common construction for loudspeakers which might not be fully applicable to electromechanical devices.

2.1.3. Near- and far-field propagations and directivity patterns

The efficiency with which vibrating surfaces convert vibrational energy into sound depends not only upon the level of vibration, but also upon the frequency of vibration, the shape of the vibrating body, the spatial distribution of the surface motion and the acoustic properties of the fluid. It is also influenced by the presence of other nearby objects or surfaces. Consider two small adjacent regions of a surface that undergo equal and opposite normal displacements and then halt. It is "easier" for the molecules in the compressed region of contiguous fluid to move into the rarefied region that into the unaffected fluid a little way from the surface. This mass movement tends to equalize the pressures and densities local to the surface, producing a much weaker disturbance in the surrounding fluid than if the two regions had moved in unison. This phenomenon is commonly kwon as radiation "cancellation". The more rapid the completion of the displacement, the less effective will be the cancellation (Fahy, 2001).

If the displacements are now reversed, the molecules will move to re-establish equibilibrium.

23

The more rapidly the reversal takes place, the less chance there is for the molecules to effect the cancellation process, and the more effectively sound will be radiated. On the basis of the argument that the average speed of molecular motion determines the speed of sound, the critical time is given by the distance between the centers of the oppositely displaced regions divided by the speed of sound. Hence, such a process taking place at high frequency will radiate more effectively than that taking place at lower frequency. In terms of harmonic vibration and spatially sinusoidal wave motion of a surface, the critical time is given by half of the surface wavelength divided by the speed of sound in the fluid. If the vibrational wave speed is less than that of sound in the fluid, radiation cancellation operates (Fahy, 2001).

When dealing with sound radiation problems under free-field conditions, it is important to distinguish the difference between near-field and far-field propagation. For an arbitrary radiator, if the sound field is evaluated at a distance sufficiently large from the source, the sound pressure magnitude will decrease linearly with distance along a radial line connecting with the source, which characterizes the far-field propagation. Otherwise, one has near-field propagation (Pasqual, 2010).

How far one must be from the source in order to ensure far-field propagation depends on the frequency and the complexity of the directivity pattern. The latter is represented by the largest n that must be retained in (A.7 in order to accurately describe the sound field. As frequency increases and/or the directivity pattern becomes simpler, the near-field effects take place closer to the source. However, it is worth noting that the directivity complexity of an actual source generally increases with frequency (Pasqual, 2010).

The directivity pattern of a transducer is a description, usually presented graphically, of the response of the transducer as a function of the direction of the transmitted or incident sound waves in a specified plane and at a specified frequency (Beranek, 1993). The difference between near-field and far-field behaviors of sources must always be in mind. When the directivity pattern of a loudspeaker or some other sound source is presented in a technical publication, it is always understood that the data were taken at a distance r sufficiently large so that the sound pressure was decreasing linearly with distance along a radial line connecting with the source (Beranek,

1993).

2.1.4. The CLF format for loudspeaker data

In order to simulate acoustic systems with loudspeakers it is imperative to have the characteristics of the latter, especially those concerning the radiation patterns and frequency responses of the driver. In the past this was a problem since many proprietary data formats were available from different measurement systems, hence making comparisons very difficult since the user needed time consuming processes to translate data from one format to another. Although not used in this work, the CLF (Common Loudspeaker Format) is better explained in this section for further reference in electromechanical loudspeaker research. A comprehensive database with many manufacturers and free for download[8] can be found in the CLF website and demonstrates the enormous variety of drivers available together the complexity of their radiation patterns along the frequency range.

The CLF was first released in 2005 by group of companies[9] whose purpose was to provide an open file format that could allow loudspeaker manufacturers to supply data to their customers using a standardized platform (CLF Group, 2005). Although a free viewer is also available in the group website[10], manufacturers who wish to use the format must use a paid authoring kit[10] which generates a secure binary file containing loudspeaker information. This binary is generated from a TAB delimited text file, with special identification fields filled with measurement results, i.e., the CLF reader software parses the text file, displays the result for verification, and saves the data to a secure and traceable binary distribution file (Syn-Aud-Con, 2004). The extensions CF1 or CF2 can be used depending on the frequency resolution used in measurements (10º/octave or 5º/third octave, respectively). An example of the viewer screen is presented in Figure 2.10.

---

[8] As found in: http://www.clfgroup.org/files/index.php
[9] Namely CATT, Electro-acoustic Testing Company Inc., IfbSoft, Integral Acoustics, Odeon A/S and Syn-Aud-Con
[10] CLF download section: http://www.clfgroup.org/clfdocuments.htm.
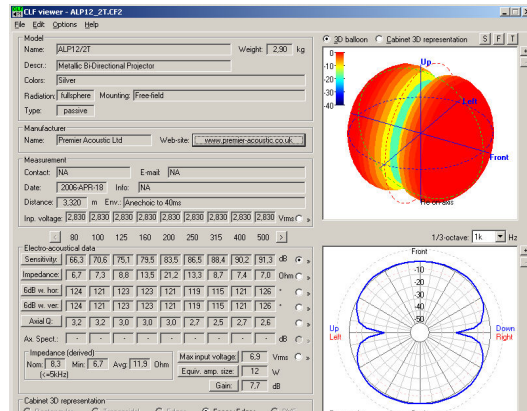
Figure 2.10 - CLF main screen showing frequency characteristics of a metallic bi-directional projector manufactured by Premier Acoustic Ltd. at 1 kHz.

(a) 100 Hz   (c) 2,5 kHz   (d) 5 kHz   (d) 10 kHz
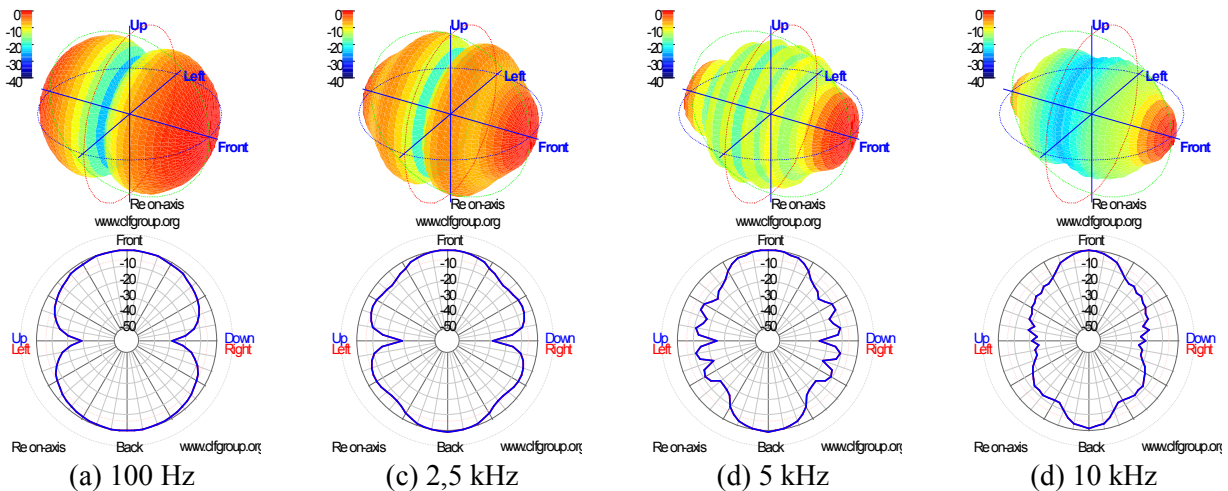
Figure 2.11 - Plots for the same loudspeaker of Figure 2.10 showing the increase in the complexity of directivity patterns for the same loudspeaker as the frequency increases.

Besides providing an electronic datasheet for drivers with traceable results (the authoring kit includes a unique identifier so that binary data is always tagged with its source), the format also standardizes the way loudspeakers are characterized in order to obtain a meaningful way for acoustic predictions (Syn-Aud-Con, 2004). In that sense, the experimental setup derives from the anechoic impulse response measurement made at each angular position around the loudspeaker, which assures that future refinements, including higher frequency resolution and support of phase information could be implemented without the need to re-measure devices that had previously been measured. Some examples of directivity patterns for the same driver of Figure 2.10 in different frequencies are presented in Figure 2.11 and show the increasing complexity as the

frequency increases. This case can be considered as a dipole radiation example found in ARMs #02 to #04, which is very close to the formats found in Chapter 4.

2.2. Spherical loudspeaker arrays

This section concerns presentation of some details about the array modeling and construction and starts with a discussion about near-field and far-field radiation. Afterwards the directivity pattern concept is presented, followed by the acoustics in spherical coordinates which culminates in two distinct approaches for radiation studies: the spherical harmonics found in the solution of the Helmholtz equation and the acoustic radiation modes (ARMs). A brief introduction to the analytical solution is presented in sequence, and the section ends with the description of the experiment performed at the LMA in France by Pasqual (2010) in order to evaluate the directivity patterns of the prototype constructed. The wave equation in spherical coordinates and simple multipole sources are fundamental topics for this section, and the reader is asked to check Appendix A and Appendix B in order to get further information about them.

2.2.1. Spherical acoustics

Two distinct subspaces for directivity representation are discussed in this section: the subspace spanned by spherical harmonic functions and the subspace spanned by the acoustic radiation modes. Although it is not a comprehensive discussion, it provides de guidelines for a better understanding of the results obtained in the simulations and also the acoustic phenomena involved. A concise review and discussion about the topic was made by Zotter (2009), Pasqual (2010), Williams (1999) and Pollow (2007).

2.2.1.1. Spherical harmonics

A series solution for the Helmholtz equation in spherical coordinates concerning an outgoing wave is presented in Appendix A and given by:

$$p(r, \theta, \phi) = \sum_{n=0}^{\infty} \sum_{m=-n}^{n} A_{mn} \underbrace{h_n^{(1)}(k.r)}_{\text{radial term}} \cdot \underbrace{Y_n^m(\theta, \phi)}_{\text{angular term}} \tag{2.15}$$

The angular dependence of the solution in equation (2.15) is given by a linear combination of spherical harmonic functions, which constitute a natural basis for representation of sound source directivities (Pasqual, 2010). For $n \in \mathbb{N}$ and $m \in \mathbb{Z} : |m| \leq n$:

$$Y_n^m(\theta, \phi) = (-1)^m \sqrt{\frac{(2n+1)}{4\pi} \frac{(n-m)!}{(n+m)!}} \; P_n^m(\cos\theta) \; e^{im\phi} \tag{2.16}$$

where $Y_n^m(\theta, \phi)$ is the spherical harmonic sought, $P_n^m(\cdot)$ is the associated Legendre function of the first kind (Pasqual, 2010), n is the order and m the degree. Spherical harmonics span an infinite dimension subspace, as can be verified by noting that the index n in equation (2.15) is unbounded. Hence, truncation error generally arises from the spherical harmonic decomposition, which can be dealt with by retaining a larger number of terms (Pasqual, 2010).

Representation of the spherical harmonics for different values of n and m are show in Figure 2.12, where the colors indicate where the deformed mesh indicates the magnitude and the colors the phase angle. As said before, it can be promptly seen that in order to represent complex acoustic phenomena a high number of harmonics is necessary, which poses a problem in terms the control of the radiation patterns due to the necessary processing (Pasqual, 2010).
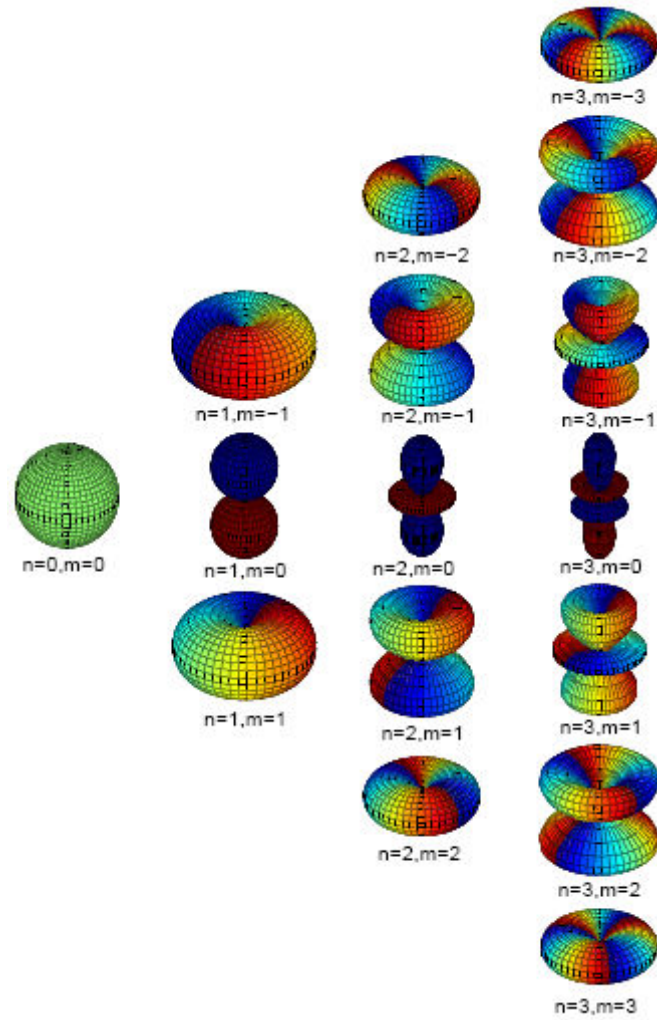
Figure 2.12 - Complex-valued spherical harmonics up to order n = 3 (Pasqual, 2010).

2.2.1.2. Acoustic radiation modes (ARMs)

Acoustic radiation modes are an important class of functions in sound radiation problems. They constitute a set of independent surface velocity distributions and are a useful representation of vibration patterns when one is mainly interested in the sound field radiated by a vibrating structure (Pasqual, 2010).

The expression "radiation mode" first appeared in Photiadis (1990) and the approach has been used since the 1990s as can be seen in the works of Borgiotti (1990), Borgiotti et al. (1994), Cunefare et al. (1994) and Elliott et al. (1993). Similarly to what occurs in the structural analysis

of a multi degree of freedom system where its behavior can be described by natural frequencies and mode shapes obtained from an eigenproblem, the radiation of acoustic sources can also be represented by an analogous description comparable to the modal approach for representing the exterior radiation characteristics of vibrating structures (Pasqual, 2010).

The acoustic radiation modes are real orthogonal functions describing surface velocity patterns. In addition, for a vibrating system with L degrees of freedom, these modal approaches both lead to a set of L linearly independent modes. On the other hand, unlike structural modes, radiation modes are defined so that they radiate sound energy independently, i.e., the total radiated sound power is given by a linear combination of the sound power produced by each mode. Then, in applications where one is mainly interested in the sound field, a reduced representation of the surface velocity can be achieved by neglecting the radiation modes which do not radiate efficiently (Pasqual, 2010).

Another advantage of radiation modes over structural modes is that, unlike the latter, the former do not depend on the mass and stiffness of the vibrating solid body, i.e., the material properties and thickness play no role in determining the radiation modes, which are only a function of the frequency, the body shape and the constraints it is subjected to. In addition, radiation modes of some radiators (like the continuous sphere) are frequency independent (Borgiotti et al., 1994).

In order to state the ARM eigenproblem previously mentioned, one must start with the acoustic power radiated by a source (Pasqual, 2010):

$$W = \int_{\Gamma} \Re\left\{\frac{1}{2} p^* \upsilon\right\} \cdot \mathbf{n}_{\text{out}} \, d\Gamma \tag{2.17}$$

where W is the radiated acoustic power, p the sound pressure, υ the acoustic velocity $\mathbf{n}_{out}$ the normal vector point outwards of the domain and Γ the domain. The asterisk indicates the complex conjugate. The radiation efficiency is a relation which indicates how much of W is effectively being radiated when compared with the energy existing due to the structural velocity at a specific

30

point. In other words:

$$\sigma = \frac{W}{\rho \, c \, S \, \langle |v_n(\mathbf{x}_s)|^2 \rangle} \qquad (2.18)$$

where σ is the radiation efficiency, S the effective area of the vibrating surface, v_n the acoustic velocity normal to S, $\mathbf{x}_s$ is a point on the radiator surface and $\langle \cdot \rangle$ is the spatial mean operator (Pasqual, 2010). The calculations of the acoustic power radiated from a discrete structure generally leads to expressions of the form (Pasqual, 2010):

$$W = \rho \, c \, S \, \mathbf{u}^H \, \mathbf{C} \, \mathbf{u} \qquad (2.19)$$

where $\mathbf{u}$ is a column vector of velocity amplitude coefficients and $\mathbf{C}$ is an L by L real symmetric matrix which couples the power radiated by the elements of $\mathbf{u}$. Evaluation of the term $\langle |v_n(\mathbf{x}_s)|^2 \rangle$ in the denominator in equation (2.18) yields (Pasqual, 2010):

$$\langle |v_n(\mathbf{x}_s)|^2 \rangle = \mathbf{u}^H \, \mathbf{V} \, \mathbf{u} \qquad (2.20)$$

with the superscript H denoting the complex conjugate transpose (Hermitian). The term $\mathbf{V}$ is a L by L matrix defined by:

$$V = \frac{1}{2 \, S} \int_S \xi^*(\mathbf{x}_s) \, \xi^T(\mathbf{x}_s) \, d\mathbf{x}_s \qquad (2.21)$$

where $\xi(\cdot)$ is a set of orthogonal functions. Using equations (2.19) and (2.20) in equation (2.18) yields:

$$\sigma = \frac{\mathbf{u}^H \, \mathbf{C} \, \mathbf{u}}{\mathbf{u}^H \, \mathbf{V} \, \mathbf{u}} \qquad (2.22)$$

The radiation efficiency is in the form of the generalized Rayleigh quotient (Pasqual, 2010). Also, the solution of the generalized eigenproblem problem $\mathbf{C} \, \psi = \lambda \, \mathbf{V} \, \psi$ leads to a set of L real orthogonal eigenvectors corresponding to real eigenvalues ordered as $\lambda_1 \geq \lambda_2 \geq \ldots \geq \lambda_L$. Those

31

eigenvectors are the acoustic radiation modes (ARMs) and the eigenvalues are their radiation efficiency coefficients, i.e., $\sigma_l \equiv \sigma(\psi_l) = \lambda_l$. The generalized eigenproblem can then be written as:

$$\mathbf{C}\,\Psi = \mathbf{V}\,\Psi\,\Lambda \qquad\qquad (2.23)$$

where Λ is a L by L diagonal matrix containing the eigenvalues λ.

It is important to emphasize that ARMs have to do with the radiation efficiency and the sound power, i.e., how the fluid behaves in terms of sound power as a function of the boundary condition of the vibrating surface. Another important observation is the fact that the eigenproblem varies with frequency because the matrices also vary, but Platonic solids have a special property (probably due to their high symmetry) so that the radiation modes are not affected by frequency change (Pasqual, 2010).

Table 2.3 - Modal matrix containing the ARMs for a dodecahedron based on a Platonic solid. The matrix has been normalized so that $\Psi^T \mathbf{V} \Psi = \mathbf{I}$. The gray values represent the reference loudspeakers used in the array measurements and the red value is the maximal component between all ARMs.

Driver	ARM											
	01	02	03	04	05	06	07	08	09	10	11	12
01	1,4143	2,4495	0	0	**3,1623**	0	0	0	0	0	0	2,4495
02	1,4143	1,0954	2,1908	0	-0,6325	2,1908	2,1908	0	0	2,1908	0	-1,0954
03	1,4143	1,0954	0,677	2,0835	-0,6325	-1,7725	0,677	2,0835	-1,2879	-1,7725	-1,2879	-1,0954
04	1,4143	1,0954	-1,7725	1,2879	-0,6325	0,677	-1,7725	1,2879	2,0835	0,677	2,0835	-1,0954
05	1,4143	1,0954	-1,7725	-1,2879	-0,6325	0,677	-1,7725	-1,2879	-2,0835	0,677	-2,0835	-1,0954
06	1,4143	1,0954	0,677	-2,0835	-0,6325	-1,7725	0,677	-2,0835	1,2879	-1,7725	1,2879	-1,0954
07	1,4143	-1,0954	-2,1908	0	-0,6325	2,1908	2,1908	0	0	-2,1908	0	1,0954
08	1,4143	-1,0954	-0,677	-2,0835	-0,6325	-1,7725	0,677	2,0835	-1,2879	1,7725	1,2879	1,0954
09	1,4143	-1,0954	1,7725	-1,2879	-0,6325	0,677	-1,7725	1,2879	2,0835	-0,677	-2,0835	1,0954
10	1,4143	-1,0954	1,7725	1,2879	-0,6325	0,677	-1,7725	-1,2879	-2,0835	-0,677	2,0835	1,0954
11	1,4143	-1,0954	-0,677	2,0835	-0,6325	-1,7725	0,677	-2,0835	1,2879	1,7725	-1,2879	1,0954
12	1,4143	-2,4495	0	0	3,1623	0	0	0	0	0	0	-2,4495

Finally, a modal matrix for the dodecahedron is presented in Table 2.3. This matrix is crucial for the simulation and the experiments since the combination of each driver will lead to a specific ARM which can then be further combined in order to synthesize a desired source as discussed in the SLA control strategy presented by (Pasqual, 2010).

2.2.1.3. Analytical solution

Some attempts have been made to predict the interaction of the radiated sound fields produced by the independent drivers of a compact spherical loudspeaker array and are demonstrated by Kassakian et al. (2004), Zotter et al. (2007), Pollow et al. (2009) and Pasqual (2010). The spherical caps approach proposed by Zotter et al. (2007) is the most used radiation prediction model for a spherical array, in which the drivers are modeled as convex spherical caps, each one oscillating with constant radial velocity amplitude over its surface. This model presents the advantage of having an analytical solution and is inspired in a previous work dealing with a single driver mounted on a rigid sphere (Meyer et al., 2000). However, it cannot predict the non-rigid body behavior of real drivers and neglects their actual geometry. A concise review of the spherical caps approach is given by Zotter et al. (2007) and Pasqual (2010).

The analytical solution used in this work for comparisons derives from discrete sphere model used by Pasqual (2010), in which the sound radiation from a loudspeaker mounted on a rigid sphere is approximated by modeling the loudspeaker diaphragm as a spherical cap that oscillates with a constant radial velocity. This model better approximates the actual loudspeaker sound field as the aperture angle of the cap is made smaller and allows the utilization of an electromechanical model developed by Pasqual et al. (2009) which also used in this work.

2.2.2. Prototype measurements

Measuring a spherical loudspeaker array is a complex task since in order to obtain its directivity patterns, an antenna of microphones and an anechoic chamber is necessary. A good reference for array measurements can be found in an article by Leishman et al. (2006), in which the authors compare the directivity patterns of a series of SLAs constructed using different Platonic solids.

The spherical array prototype made by Pasqual (2010) consists of twelve Aurasound® NSW2-326-8A drivers (nominal diameter 2 inches or 0.051 m) mounted on a rigid sphere with

radius 0.075 m shown Figure 2.13. Using a microphone circular antenna with a radius of 700 mm, the directivity patterns corresponding to the ARMs of the prototype were measured in an anechoic chamber at the LMA, with the array positioned right on the center of the circle as depicted in Figure 2.13. Measurements were taken in 49 successive angular positions of the antenna in order to form a field with 1372 points surrounding the loudspeaker array.
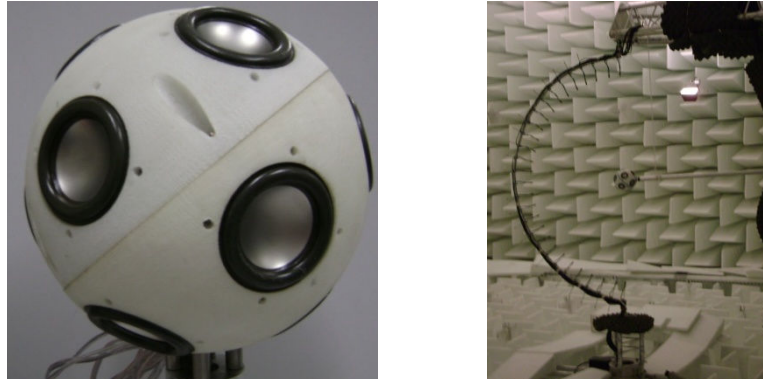
Figure 2.13 - Detail of the dodecahedral array prototype (right) and array measurement setup (left).

In order to measure each ARM, voltages must be applied to all loudspeakers following the components of Table 2.3. For instance, if one wants to measure ARM #01, it is necessary to apply 1.4143 V to all loudspeakers; for ARM #02, it is necessary to apply 2.4495 V to driver #01, 1.0954 V to drivers #02 to #06, -1.0954 V to drivers #07 to #11 and -2.4495 V to driver #12 and so on. Instead of just applying in the drivers the necessary voltages for each ARM and measuring the pressure field with the microphone antenna, the experiment performed by (Pasqual, 2010) determined the FRFs between the pressures at the microphones and the voltage at a specific driver grayed out in Table 2.3, therefore having units of Pa/V. The FRF information is much more valuable than just the pressure since it characterizes the system based on the input voltage, which is the driving parameter for the loudspeakers.

Since the maximal modal component among all ARMs in Table 2.3 is at driver #01 in ARM #05 (red value in Table 2.3), this was set as the driver with the superior limit for white noise voltage application. After preliminary tests to find a high signal-to-noise ratio in measurements, the maximal voltage amplitude determined to be 0.93 V_{RMS}. Hence, in order to determine the necessary voltages applied to the loudspeakers to reproduce a specific ARM, it was necessary to

calculate the proportion between the components and driver #01 in ARM #05. To better demonstrate the process described above, consider ARMs #03 and #12 in Table 2.3. The voltages applied to the driver #07 in both cases were:

$$U_{\text{Driver \#07, ARM \#03}} = 0.93 \ V_{\text{RMS}} \ \frac{-2.1908}{3.1623} = -0.6443 \ V_{\text{RMS}} \tag{2.24}$$

and

$$U_{\text{Driver \#07, ARM \#12}} = 0.93 \ V_{\text{RMS}} \ \frac{1.0954}{3.1623} = 0.3221 \ V_{\text{RMS}} \tag{2.25}$$

The FRFs were obtained instead the information for a specific operating condition, therefore it is then possible to determine the sound pressure field information for each ARM by changing the voltage applied to the reference driver and recalculating the proportions between the components as it will become clearer in section 3.6.

Chapter 3

3. Membrane modal analysis and simulations

This chapter deals with the simulations concerning the prototype spherical loudspeaker array constructed at Unicamp. The structural membrane modal analysis is analyzed in order to obtain the flexible membrane characteristics, which were then used as boundary conditions for the simulations. A complete description of the simulation steps is done to provide a comprehensive and consistent analysis of the results.

3.1. Computational tools

Two main computer programs from LMS International[11] were used in the analyses explained in this chapter. A brief description of both is given below, and all the details concerning modal parameters extraction and simulations are given the subsequent sections.

Test.Lab® is a complete software solution for structural and vibroacoustic problems with many functional and effective features for experiment setup, data acquisition and processing. The easiness of use and data handling, consistent and reliable calculations and the idea of modules which can be enabled or disabled according to the problem in study allow the software to be used in a considerable amount of situations. Concerning modal analysis only, it has extremely optimized routines for modal parameters extraction and visualization of modes that are really useful in practice by leaving the operator concentrated in solving the problem using tools which make decisions easier to make.

Virtual.Lab® is a simulation software broadly used in industry and academic fields for

---

[11] http://www.lmsintl.com/

simulating structural, vibroacoustic and many other problems such as mechanism analysis and durability. A core element behind the acoustics module in Virtual.Lab® is Sysnoise®, a software also developed by LMS which has become a well established simulation platform for both BEM (Boundary Element Method) and FEM (Finite Element Method) acoustical analyses. It can be said that Virtual.Lab® is a friendly interface based on Catia® for model manipulation with optimized features for pre and post processing while Sysnoise® is the responsible for all the solving steps, making them a powerful combination for many kinds of vibroacoutics problems. Sysnoise® is also capable of running in Linux servers, which allows it to deal with very complex models demanding intense calculations, large amounts of RAM (Random Access Memory) and considerable storage capacities.

Before starting this chapter it is important to note that the experimental modal analysis performed in the membrane derives directly from Pasqual et al. (2009) i.e., no experiments were performed in the present work. Finally, it is important to note that all loudspeakers in the array are named by the prefix "HP" (from the French word *Haute Parleur*) followed by their respective numbers.

3.2. Structural modal analysis of loudspeaker membranes

Surface velocity measurements of the dodecahedral array prototype shown in the left side of Figure 3.1 using a scanning laser Doppler vibrometer (LDV) were performed at the LMA (Laboratory of Mechanics and Acoustics, UPR7051, Marseille, France) with measurement points forming a circular pattern following the geometry of the membrane (Pasqual et al., 2009). Since a complex movement in the suspension area was expected, its point grid density was increased as depicted in Figure 3.1.

The goal of all measurements was to obtain the FRFs (Frequency Response Functions) between velocities at the nodes and a voltage input applied to the loudspeaker coil, so the FRFs have units of (m/s)/V. As it can be noticed, this is not the classical approach used in structural modal analysis in which responses are caused by force(s) applied to the structure. Nevertheless,

voltage is used instead of force in the loudspeaker because it is the driving parameter of the electromechanical device.

Nodal velocity responses were measured with all loudspeakers installed in the spherical array whilst only a selected one was operating. It is important to say that the prototype has a hollow spherical cavity, which leads to internal acoustic coupling between drivers. Therefore, the FRFs so obtained remain strictly valid only if just one driver of the array is made active as the coupling between the excitation of the driver and the responses at the other drives is neglected. In other words, all loudspeakers in the simulations use the same set of FRFs corresponding to a randomly selected driver among all others available, thus strengthening the assumption of neglecting coupling.
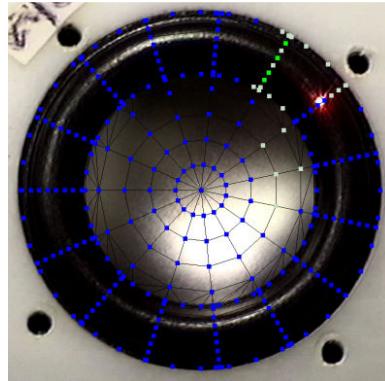
Figure 3.1 - Measurement grid with a better refinement around the suspension area.

With the definition of all measurement points as shown in Figure 3.1, a white noise with a RMS (Root Mean Square) value 1 V was applied to the loudspeaker terminals and velocity responses were automatically measured by the laser scanning system until data for all points were acquired. The FRFs were then automatically computed by the laser software using the $\hat{H}_1$ estimator (Newland, 1993) in the range of 0 Hz to 10 kHz with fifty subsequent averages and 50% overlap. Results were exported in the "svd" extension which was opened in LMS Test.Lab® software for processing using the Polymax® modal parameter extraction method and further exported in the Universal File Format (unv extension) with mass-normalized modal parameters fur utilization in LMS Virtual.Lab® for the simulations.

It is important to emphasize for future reference that opening the svd extension inside Test.Lab® is a straightforward process which depends on two items: installation of the Polytec® Scan Viewer software[12] and Test.Lab® license availability. The latter must be specified upon license buying in order to have the proper module available for use, and this is not normally requested by software dealers due to a lack of knowledge on the topic. Once the two prerequisites are met, the user must install first the viewer and afterwards enable the "Polytec Data Driver" add-in inside Test.Lab®, which will not only enable the access to all measurement information but also to the geometry as seen in Figure 3.2.
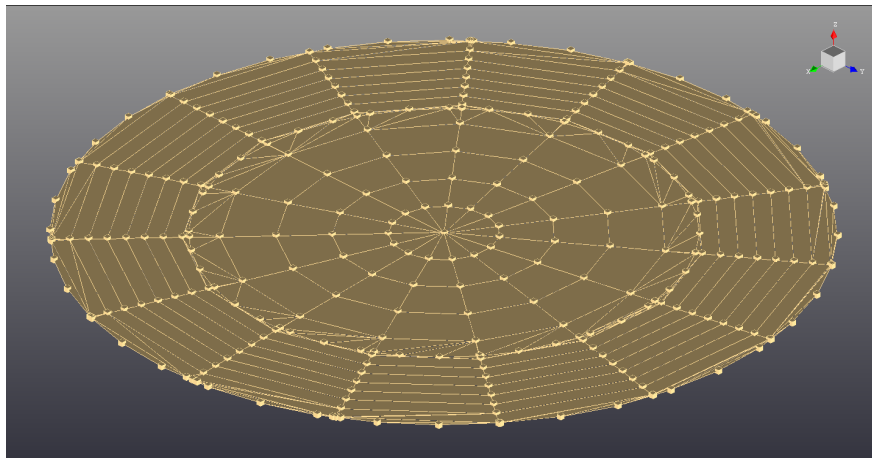
Figure 3.2 - Experimental mesh extracted from laser scan file with 312 scan points.

The PolyMAX® method is a further evolution of Least-Squares Complex Frequency-Domain (LSCF) estimation method and provides very consistent and reliable results either for SISO (Single Input Single Output) or MIMO (Multiple Input Multiple Output) systems. A comprehensive discussion about the method is made by Peeters et al. (2004) and using it in Test.Lab® consists basically in three main steps which are summarized below:

- Define the analysis band: the frequency range for the analysis (20 Hz to 10 kHz) was defined and all FRFs together with their reference point (number one in this case) were selected. The features "Sum" (summation of all FRFs) and "MIF / Imaginary Sum" (Modal Indicator Factor) were also checked as complementary detection tools in the case

---

[12] Available at http://www.polytec.com/usa/_print/158_7786.asp.

of modes with very close frequencies;

- Selection of stabilized frequencies from stabilization diagram: in this step the maximum order of the modal model was defined and a stabilization diagram was then plotted indicating the presence of modes (Figure 3.3) which were then manually selected for both modal parameters and shape extraction. Although the computational cost for order calculation is not high, an order of forty was used as a good compromise between reliable detection and quick computations. Also, factors of 2% in mode vector, 1% in frequency and 5% in damping were used as tolerance parameters for stabilization criteria[13];
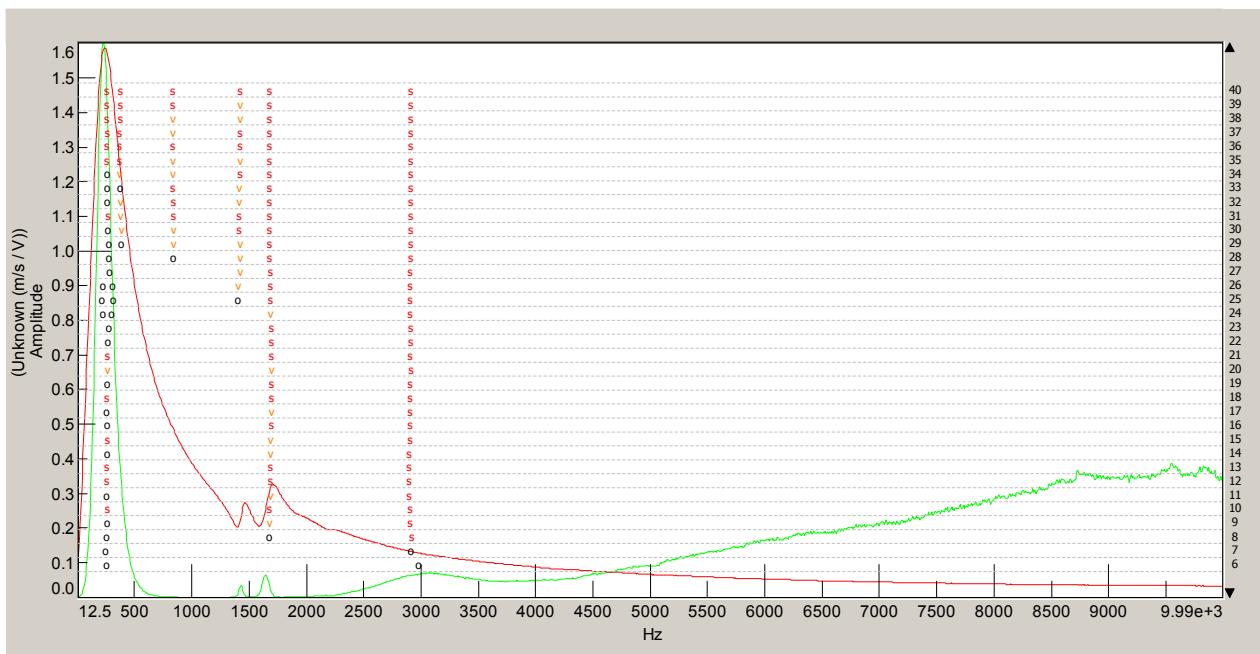
Figure 3.3 - Stabilization diagram for the modal analysis performed with all measured membrane FRFs with dashed lines connected to right vertical axis indicating increasing model order. The FRF summation and MIF curves can be also seen, indicating correct mode detection by the diagram ("s" stands for stabilization under tolerances for frequency, damping and mode vector, "v" for unchangeable pole inside tolerances and "o" for unstable pole).

- Shapes: the last step took all the information computed in the previous steps and determined the mode shapes for each selected frequency. It also produced the cyclic animations based in the relative displacements of nodes, giving thus a complete description of the structure behavior as it will be seen in Chapter 4.

---

[13] The stabilization criteria tell the software the tolerances inside which detected parameters can be considered stable when estimated in subsequent orders.

After extraction of modal parameters, they were exported together with the measurement geometry using the universal file format (unv extension) normalized by the modal mass matrix, which is an important parameter for the simulation as discussed in Appendix D.

3.3. Spherical array design and membrane meshing

To simulate the spherical loudspeaker array a 3D mesh model derived from its geometrical CAD (Computer Aided Design) drawing was created in Abaqus®. All internal walls, fixation holes and loudspeaker mounting cavities were removed, the latter being replaced by circular planes in order to close up the holes like shown on the right side of Figure 3.4. The reason for closing them with a plane is supported by the fact that the structural modal analysis was actually performed in the normal direction relative to the membrane and does not take its curvature into account.
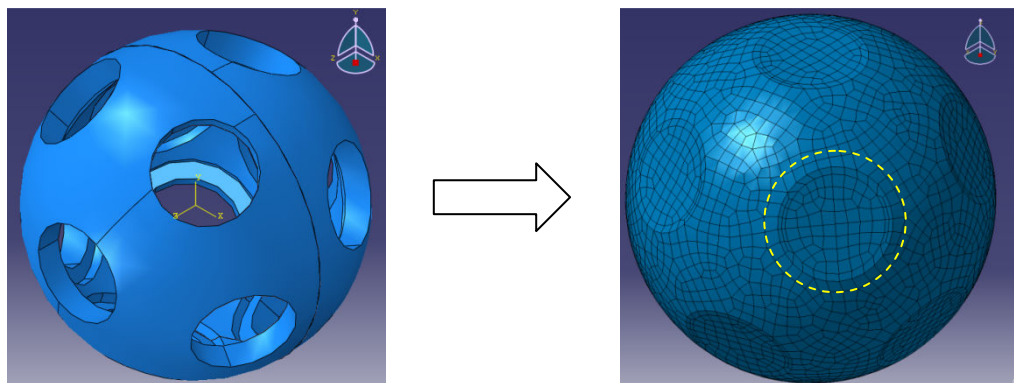
Figure 3.4 - CAD design (left) and its respective mesh (right) with the refinement detail.

The mesh was generated in Abaqus® using 3288 linear quadrilateral shell elements type S4R[14] with four nodes and a higher element density around the loudspeaker suspension area in order to better accommodate the projected velocities discussed in the next steps. Also, an important remark for the simulation concerns the average size of 5 mm used for the elements which is directly related to the maximal frequency that can be calculated with the acoustic mesh.

---

[14] According to the nomenclature used in Abaqus®, "S" stands for Shell, "4" is the number of nodes and "R" means that the element has a reduced integration (item not considered in Virtual.Lab® since no thickness is used for the acoustic simulation).

Analogously to the frequency aliasing observed in time signals in which there is a lack of representation caused by an insufficient signal sampling rate, a spatial aliasing caused by a deficient spatial representation (too large elements) must be prevented in the geometry, and a common practice in acoustics simulations is to consider that there must be at least six elements per wavelength as given by equation (3.1) so the wave can be spatially discretized properly (von Estorff, 2000). Hence, mathematically speaking:

$$l = \frac{c}{6.f_{max}}$$

(3.1)

where l is the element average length, c is the speed of sound in air and f_{max} the maximum simulation frequency sought. Equation (3.1) can be thought as a general guideline for acoustic mesh definition and does not take in account the complexity of the geometry. Nonetheless, Virtual.Lab® has an interesting feature called "Material maximum frequency" which checks the whole acoustical mesh considering the fluid properties and geometrical parameters to determine the maximal frequencies achievable with such geometry, thus promptly demonstrating the acoustic quality of the mesh for the desired simulation purposes. As can be seen in Figure 3.5, the low frequency limit for the mesh is around 6 kHz, which is proper considering the simulation range sought, from 20 Hz to 5 kHz.

Figure 3.5 - Material maximum frequency calculated by Virtual.Lab® for the acoustic mesh of Figure 3.4.

3.4. Spherical array simulations using membrane modes
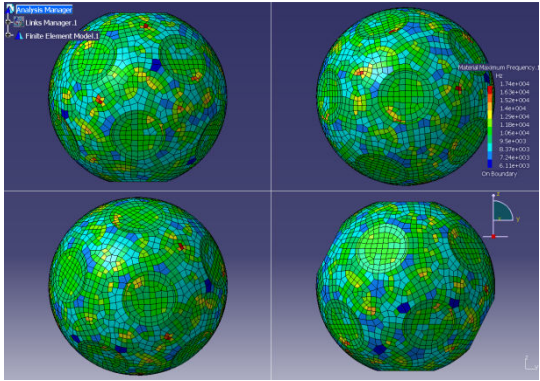
As simulations rely totally on the experimental modal analysis presented in section 3.2, it is important once more to emphasize that they were made using loudspeaker #07 and its measurement conditions, especially the one concerning the fact that the loudspeaker was operated with all others assembled but turned off. In order to give a better understanding of the simulations, steps for a single membrane operating in the spherical array will be explained at first, being the others combinations of this case as explained in section 3.5. All simulations range from 20 Hz to 5 kHz in steps of 10 Hz and the choice for that range was made merely based in RAM (Random Access Memory) shortage problems caused by increasing processing needs of Virtual.Lab® as the number of active membranes in the simulation increased.

3.5. Methodology for one membrane simulation

Briefly speaking, any linear vibroacoustic simulation in Virtual.Lab® can be performed once the acoustic mesh, fluid properties (density and speed of sound), position of field points and boundary conditions are known. However, the usage of the modal analysis in the simulations brings an extra challenge since the information contained in the FRFs must be transformed into velocity data by solving a forced response problem. Those velocities cannot be directly used in indirect BEM approach as Boundary Conditions (BCs) as explained in Appendix C, therefore needing an interpolation over the surface in order to determine usable surface velocities.

Since the primary objective of membrane measurements was to only obtain its modal properties, i.e., no simulations were foreseen at that time, another critical issue for the computational model was the fact that the measurement geometry of Figure 3.2 was not well suited for direct use in the simulations because of its very sharp elements with a considerable amount of distortion. Also, measurements were performed out of the membrane plane (Z direction), which means that they had to be somehow transported to the membrane local reference frame on the sphere. Those steps are summarized in Figure 3.6 and detailed explanations for them will be given in the following items of this section.

43
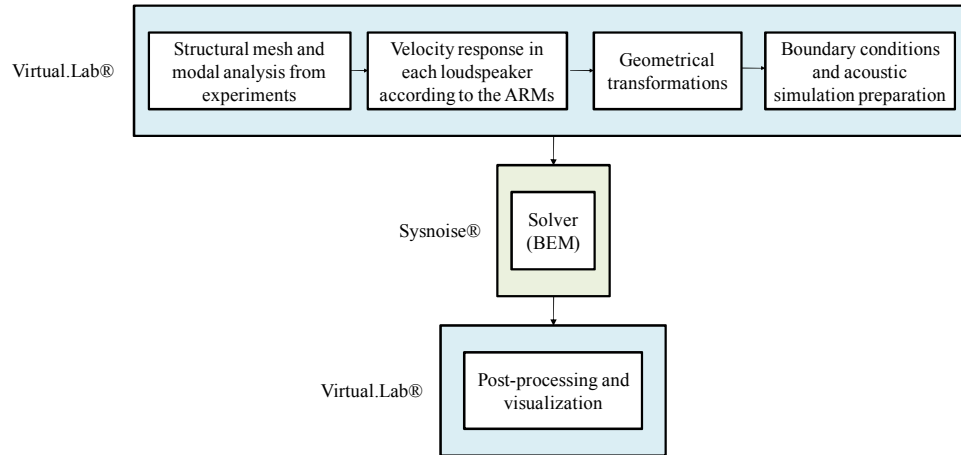
Figure 3.6 - Sequence of steps followed in the vibroacoustic simulation.

3.5.1. Structural experimental mesh and associated modal analysis

In this step both the structural mesh and its associated modal analysis are imported inside Virtual.Lab® either from a FEM simulation software or from an experimental modal analysis processed from measurement data like the one performed for the membrane in section 3.2. One important remark at this stage is that the imported modal data should always be mass-normalized in order to conform to the modal superposition principle discussed in Appendix D.

Another approach for this step can be done using directly the FRFs and their associated input and output points which would lead, in theory, to the same results as found by using the modal superposition. It was noticed though that the usage of the FRFs directly was not possible due to some software issues, most noticeably the necessity of matching exactly the same name for all nodes used in the experiment. Hence, the velocities at the nodes, although calculated using the forced response analysis, could not be interpolated as described in step 3.5.3 because of either null or incorrect results, which definitely invalidated the direct use of the FRFs.
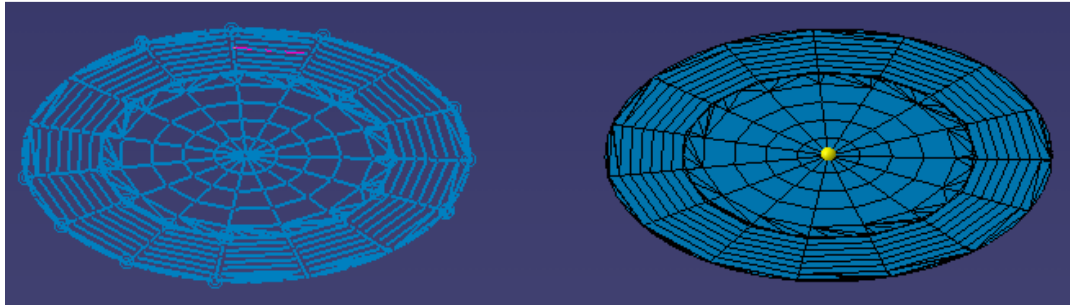
Figure 3.7 - Experimental (left) and shell element (right) meshes. A transformation feature was needed in order to convert the experimental geometry into a proper shell mesh. The point on the right shows the location of the reference point.

Once the universal file containing both the modal analysis results and the geometry was imported into Virtual.Lab®, a new problem concerning the mesh had to be solved. In fact, the mesh used in Test.Lab® is not a rigorous mesh representation of the real structure in the sense that it is just a collection of points linked by bar elements and filled with surfaces in-between. Although recognized by Virtual.Lab®, they cannot be used in vibroacoustic simulations, and a solution was found by converting all faces into shell elements using an automated feature available in the software which preserved all node identifications as found in the experimental setup demonstrated in Figure 3.7 and prevented any information mixing among all response points available. That new mesh was also separated from the modal analysis data in order to have a better file management and to allow the individual controlling of the exact association between the modal analysis and the experimental shell mesh.

Another important remark was that the version of Virtual.Lab® used for all simulations (release 8B) is designed to follow the classical modal analysis approach where the only driving parameter for the FRFs can be force. Also, no physical excitation point existed for the analysis due the experimental utilization of voltage as the driving parameter, thus creating a gap in the software workflow to compute the nodal responses. Both problems were solved with the following solutions:

- FRFs: as the software understands just forces and not voltages for excitations, it was assumed that the input is done in Volts but represented in Newtons, i.e., all references to forces found in the simulations are implicitly known to be in reality voltages. In fact that procedure has no effect concerning units consistency since

they will be cancelled out when the forced response problem is solved with the application of the excitation force;

- Reference point: in order to have a reference point where the excitation force is applied, an individual point over node one (central point in the dashed circle of Figure 3.7) was created with all FRFs related to it as a reference, thus enabling the introduction of the force and the computation of nodal velocities based in the modal analysis imported from Test.Lab®.

As discussed at the beginning of the current section, one last and important topic concerns the normalization of modes when importing them into Virtual.Lab® since all modes must be normalized by the modal mass matrix, which was done during the exporting process inside Test.Lab® described in section 3.2. An additional check to proceed in the next simulation steps was also performed inside Virtual.Lab® after importing the modes by double clicking the item "Modal Editing" in the features tree, where modes can also be enabled, disabled or have its viscous damping changed according to the user needs (Figure 3.8).

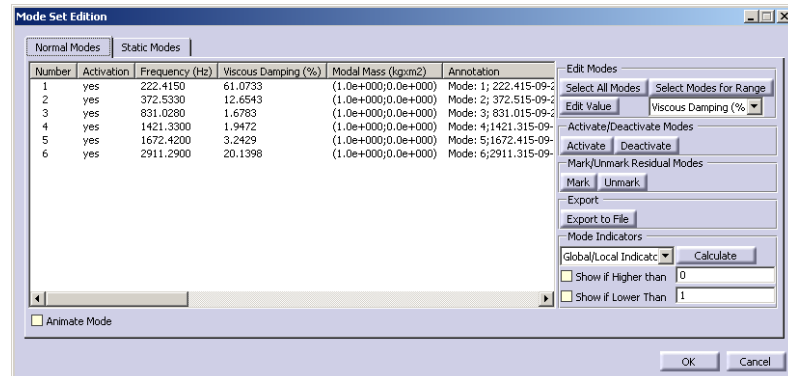**Figure 3.8 - Modal editing screen showing manual mode selection and edition.**

3.5.2. Structural mesh nodal velocities

After the previous step and the presented solutions, the forced response problem could be arranged in order to determine the nodal velocities in the structural mesh. It is worth remembering that from now on the term "force" refers to "voltage" anytime it appears, agreeing

with the convention used to make the simulation possible inside Virtual.Lab®.

For the input point previously described a continuous force with amplitude of 1 N was created ranging from 20 Hz up to 5 kHz in 10 Hz steps (white noise spectrum). That amplitude is a key parameter in the simulation since it will determine the magnitude of the nodal velocities and is a straightforward process in Virtual.Lab® done by the "Load Function Editor" feature, which consists in setting the force name, its orientation (in this case +Z just like the measurement direction) and the numerical force values over the frequency range, which can be either entered manually or imported from a text file or Microsoft Excel® spreadsheet.

Once the force is created, it was necessary to attach the force to its application point (reference) by using the "Load Function Set" feature. After the attachment, a "Modal-Based Forced Response Case" was then created with the desired frequency range for the calculations and the output response velocity at the output points selected. As the name suggests, the described procedure determines the responses by means of a forced response in which the system is assumed to be linear, therefore solving the problem $\{F\}=[H].\{\dot{x}\}$, where $\{\dot{x}\}$ is a vector with resultant nodal velocities, $[H]$ is the modal matrix and $\{F\}$ is the force vector. As all data is frequency dependent, results can also be displayed in terms of displacement or acceleration by dividing them by $(j\omega)$ or multiplying by the same term, respectively.

3.5.3. Surface velocity response

Before starting the discussion of the current topic, it is important to inform the two types of data used in Virtual.Lab® for information handling:

- Functions: two dimensional data arrays representing the variation in time, frequency or rotational speed of a specific quantity (same as SORT2 format used in Nastran®). Examples: forces applied to the structure as a function of frequency, sound pressure level in a specific field point as a function of frequency, FRFs, etc;

- Vectors: three dimensional data arrays (XYZ components) at specific time, frequency or rotational speed (same as SORT1 format used in Nastran®). Examples: displacement, velocity or acceleration fields in a structure resultant from a forced response analysis, acoustic intensity in a field point mesh, mode shapes, etc.

The second type presented above is directly related to the boundary conditions applied in the BEM simulation since it satisfies the requirements explained in Appendix C. The problem though comes from the fact that the forced response performed in the step 3.5.2 produces as results only nodal velocities, which are understood by the software as "function" data and cannot be further used in the BEM simulations as boundary conditions.

A solution for this problem was found by using the "Running Modes on Load/Response Functions" feature from Virtual.Lab®. Its primary use is for allowing the display of all forcing or response functions at many different points simultaneously and it is very similar to the animation of structural modes or vibrations (which are intrinsically in "vector" format). In other words, that feature can be thought as an interpolation done between all nodes from each element in order to create "vector" data understood by BEM as boundary conditions. The drawback of this procedure is that there is no control from the user side, which means that the software assumptions are unknown and can be a source of error.

The experimental mesh presented in the previous sections is centered in the global coordinate system, i.e., its central point has coordinates (0, 0, 0) in a (X, Y, Z) orthonormal basis. However, it needs to be transported into the correct loudspeaker locations of Figure 3.4, which means that it had to be both translated and rotated depending on the loudspeaker position on the sphere's surface. For the top surface (loudspeaker #01) this is relatively an easy task since it is just a translated version of the experimental mesh, but the others needed more complex geometrical transformations further explained.
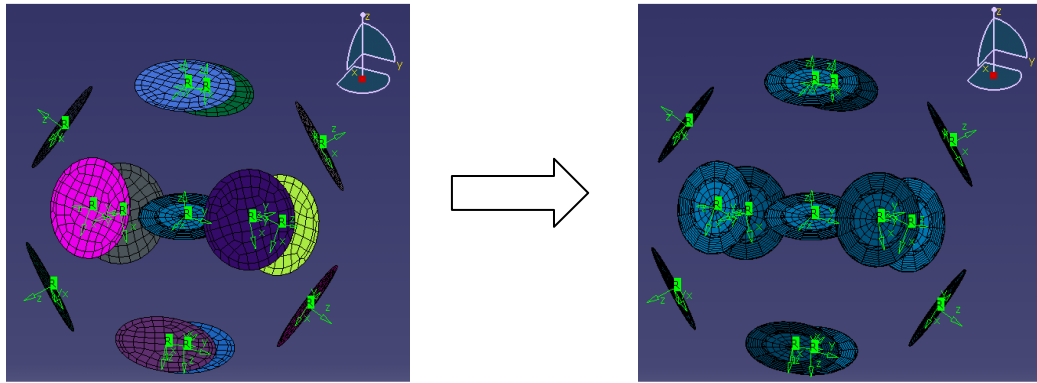
Figure 3.9 - Acoustical mesh with only membrane surfaces and experimental mesh ready for geometrical transformation (left) and transformed experimental meshes (right).

The solution found was first to remove the spherical geometry from the acoustic mesh in Figure 3.4 and to leave just the plane surfaces corresponding to the membranes as shown on the left side of Figure 3.9. The green arrows on the surfaces are local Cartesian coordinate systems with the Z direction pointing outward the membrane in the same way of the experimental mesh (seen in the middle of left picture). Those reference systems are used to transport the experimental mesh by aligning its local coordinate system to the others, thus positioning it right on the location of each membrane. The results for all loudspeakers can be seen on the right side of Figure 3.9, which shows the transported experimental meshes in their final position. Each membrane mesh was individually exported in order to be further used, and an important remark is the fact that the node IDs (identification numbers) had to be changed for all the transformed meshes in order to avoid possible number conflicts.

The previous procedure was able to solve the geometrical transformation problem by aligning the two local coordinate systems. However, it was not possible to perform local forced response analysis like seen in step 3.5.2 because Virtual.Lab® does not accept forces in directions different from the XYZ coordinate system. Hence, instead of solving local forced response problems for each membrane, the methodology adopted was to solve the problem in the original coordinate system and transform the velocity results to the local meshes seen in the right side of Figure 3.9.

Such task was achieved by using the "Correlation" workbench available in Virtual.Lab®, which was originally designed for correlating modes from experimental (reference) and

computational (verification) structures in modal analysis. Since the latter has usually a more discrete representation of the structure, it is necessary to adopt some points for geometrical equivalence that will guide the software to project experimental and computational modes into a common reference frame in which both results can be compared. In this work there were no differences between the reference and the verification structures since they were exactly the same, and the workbench is capable of calculating all the transformation parameters (rotations and translations) that allow the surface velocities to be positioned exactly on the meshes of the right side of Figure 3.9 as will be seen below.
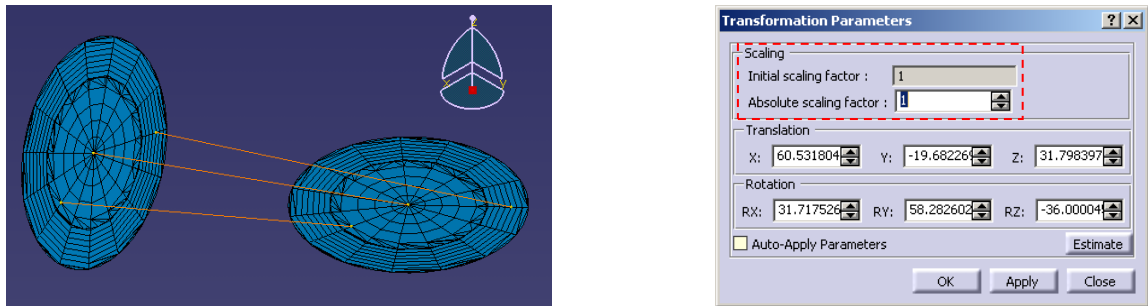
Figure 3.10 - Points used for mesh transformation (left) and transformation parameters with scaling control (right).

The transformation process starts by setting at least three mapping points in the original and destination meshes and finishes with the calculation of all necessary geometrical transformations for them (left side of Figure 3.10). Since the meshes were exactly the same, an important control parameter in the process was the fact that no scaling should occur and only translations and rotations should be detected by the transformation algorithm (right side of Figure 3.10). The three points selected must be exactly the same in both membranes in order to achieve a scaling factor of 1, which means that they need to be properly found in the transformed meshes in the right side of Figure 3.9. Another important remark is that Virtual.Lab® needs to have separate documents for the correlation to work properly, i.e., the user must create a first document with the experimental data and the forced response analysis and a second document where the desired transformed membrane and the previous document will be imported and the correlation parameters calculated.

Figure 3.11 - Mesh mapping indicating the transfer between origin and destination nodal information (left) and options used in the process (right).

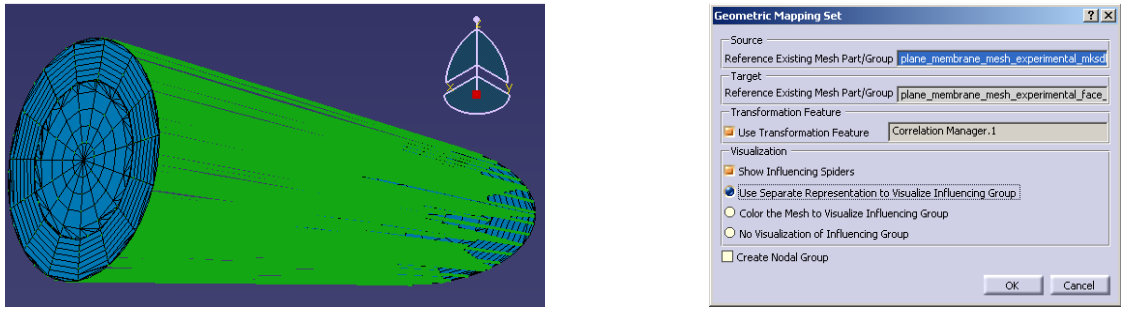The correlated model will, as expected, place the forced response results on the membrane location on the sphere with a crucial difference: differently from just aligning the local coordinate systems in the meshes, the transformation parameters were now stored, which means that they can be used in further procedures which need transformations between the two involved meshes. At this point velocities could then be finally transferred to the destination mesh by using data transfer process in which three parameters are necessary:

- Mesh mapping: tells the software the criteria to map one mesh onto the other. In the membrane case no interpolation is necessary since the nodes are exactly the same, and an interesting feature that can be used to understand the process is given by the "Show the influence spiders" option, which indicates the origin and the destination of the nodal information (Figure 3.11);

- Set to be transferred: the velocities obtained in the running modes interpolation;

- Transformation feature: calculated parameters demonstrated in Figure 3.10.

Finally, after obtaining the correlation parameters and transporting the velocities to the transformed experimental meshes, it is necessary to project those velocities onto the final acoustical simulation surface, which is done by another geometrical mesh mapping. That process is done by setting the original (transformed version of the experimental mesh) and destination (corresponding planar surfaces of Figure 3.9) meshes and selecting a projection algorithm. The "max distance" interpolation method was used with five nodes and a radius of 15 mm, which

means that the software will take all values found inside a sphere of radius 15 mm and interpolate the results for the first five nodes available. This process was done several times in order to define the best possible combinations for those parameters, and the selection criterion was based upon comparisons with the translated surface velocities discussed before. It should be noticed that this step is another source of error since the correct selection of the proper projection parameters relies solely on the user's experience. Also, the circular refinement close to the membrane edge presented on Figure 3.4 is importing in this case because it will provide more interpolation points compatible to the higher number of points in the suspension area used in the FRF measurements.

3.5.4. Setup of boundary conditions and acoustic simulation

By successfully concluding the previous steps, surface velocities BCs related to the twelve surfaces in Figure 3.9 could be then associated with the acoustic mesh. It is worth to note that only the planar surfaces have associated velocities and the spherical geometry has zero velocity since it should not have any movement. Afterwards, a radial field point mesh with a radius of 700 mm similar to the experimental microphone antenna used by Pasqual (2010) and air properties at 15 ºC (c = 343 m/s and ρ = 1,225 kg/m³) were defined. The simulation was solved for a frequency range from 20 Hz to 5 kHz in 10 Hz steps using Sysnoise® Linux parallel solver and one important remark about this step was the utilization of the same frequency discretization used in step 3.5.2 in order to avoid any possible further interpolations[15] performed by LMS Virtual.Lab®, hence providing a frequency match during the solution process.

3.6. Important remarks on setting force amplitudes

The reader must realize that the previous steps are for each membrane in the array i.e., the geometrical transformations must be used for each loudspeaker position in order to position the

---

[15] The interpolations performed at the frequency response solution are performed on all available data in order to match the necessary frequency points. In that case, a linear interpolation is performed and it was noticed in the simulations that usage of very different frequency points can lead to incorrect results.

velocities from the forced response analysis in their respective places. However, in order to reproduce the ARMs, it is necessary to correctly set the amplitude of the forces in step 3.5.2 so they can have comparable results in all the approaches studied (analytical, simulated and experimental).

A normalized ARM vector was used in the simulations by dividing all components of each vector in Table 2.3 by its reference driver (gray component) as summarized in Table 3.1 which demonstrates the constant value force spectra that must be used in each membrane to reproduce the ARM sought. Those parameters were also used as input for the analytical model and the calculation of the new sound pressure fields from the FRFs as previously discussed in section 2.2.2.
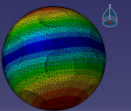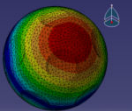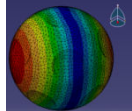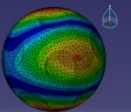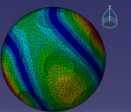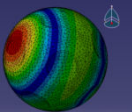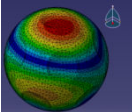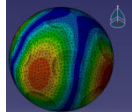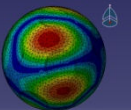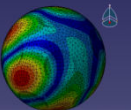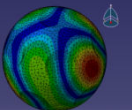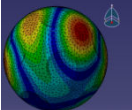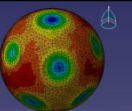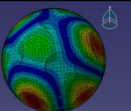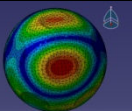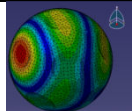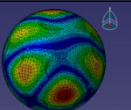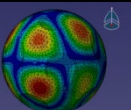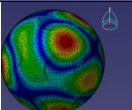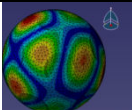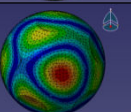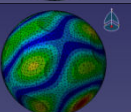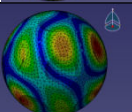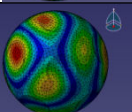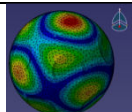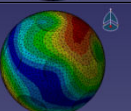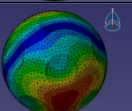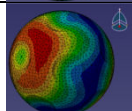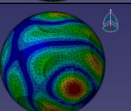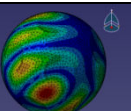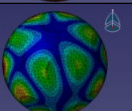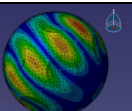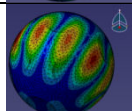
Table 3.1 - Constant force spectra applied to the membranes in the simulation according to the ARM sought.

Driver	ARM											
	01	02	03	04	05	06	07	08	09	10	11	12
01	1,0000	-1,0000	0,0000	0,0000	1,0000	0,0000	0,0000	0,0000	0,0000	0,0000	0,0000	-1,0000
02	1,0000	-0,4472	1,2360	0,0000	-0,2000	-1,2360	-1,2360	0,0000	0,0000	1,2360	0,0000	0,4472
03	1,0000	-0,4472	0,3819	1,0000	-0,2000	1,0000	-0,3819	-1,0000	-0,6181	-1,0000	0,6181	0,4472
04	1,0000	-0,4472	-1,0000	0,6181	-0,2000	-0,3819	1,0000	-0,6181	1,0000	0,3819	-1,0000	0,4472
05	1,0000	-0,4472	-1,0000	-0,6181	-0,2000	-0,3819	1,0000	0,6181	-1,0000	0,3819	1,0000	0,4472
06	1,0000	-0,4472	0,3819	-1,0000	-0,2000	1,0000	-0,3819	1,0000	0,6181	-1,0000	-0,6181	0,4472
07	1,0000	0,4472	-1,2360	0,0000	-0,2000	-1,2360	-1,2360	0,0000	0,0000	-1,2360	0,0000	-0,4472
08	1,0000	0,4472	-0,3819	-1,0000	-0,2000	1,0000	-0,3819	-1,0000	-0,6181	1,0000	-0,6181	-0,4472
09	1,0000	0,4472	1,0000	-0,6181	-0,2000	-0,3819	1,0000	-0,6181	1,0000	-0,3819	1,0000	-0,4472
10	1,0000	0,4472	1,0000	0,6181	-0,2000	-0,3819	1,0000	0,6181	-1,0000	-0,3819	-1,0000	-0,4472
11	1,0000	0,4472	-0,3819	1,0000	-0,2000	1,0000	-0,3819	1,0000	0,6181	1,0000	0,6181	-0,4472
12	1,0000	1,0000	0,0000	0,0000	1,0000	0,0000	0,0000	0,0000	0,0000	0,0000	0,0000	1,0000

3.7. Cavity modes for the loudspeaker array

In order to detect any possible cavity modes, another simulation was performed with the same mesh presented in section 3.3 but with a filled interior in order to proper represent the air inside the dodecahedral array. Although this is not exactly a representation of the geometry because of the thickness of the internal walls, it provides a reasonable understanding of the cavity behavior of the structure.

Table 3.2 - Cavity modes detected for the dodecahedral array geometry. The number of pictures represents the number of times the same mode appeared in the analysis.

Mode number	Frequency [Hz]	Symmetries				
1	1515		-		-	
2	2444					
3	3261					
4	3319					
5	3400		-		-	
6	4116					-
7	4220					
8	4450		-		-	
9	4965					

The simulation was also performed in Virtual.Lab® but using the FEM (Finite Element Model) module in which the acoustic mesh was a solid mesh composed by tetrahedrons. The same air properties for 15 ºC (c = 343 m/s and ρ = 1,225 kg/m³) were used, thus yielding the same conditions as those found in the previous BEM simulations described. After associating those properties to the solid acoustic mesh, an "Acoustic Mode Analysis Case" was created and solved for all modes detected between 0 and 5000 Hz. It is interesting to note that due to the high degree of symmetry in the structure, many similar but rotated acoustic modes appear, as it can be noticed in Table 3.2.

Chapter 4

4. Results and discussion

This section starts presenting the results for membrane modal analysis discussed in section 3.2. Results of the membrane modal analysis are presented at first, followed by results for the simulations in terms of sound power plots and directivity patterns.

4.1. Membrane modal analysis

Analyzing both Table 4.1 and the summation curve in Figure 3.3 it can be seen that the membrane behaves like a piston (all nodes moving in phase) in almost all structural modes in the frequency range of interest. The first structural mode was found at 253 Hz and has a high damping ratio of 54% due to the combined mechanical and electrical dissipative actions, where the latter is normally much higher than the former (Pasqual et al., 2009).
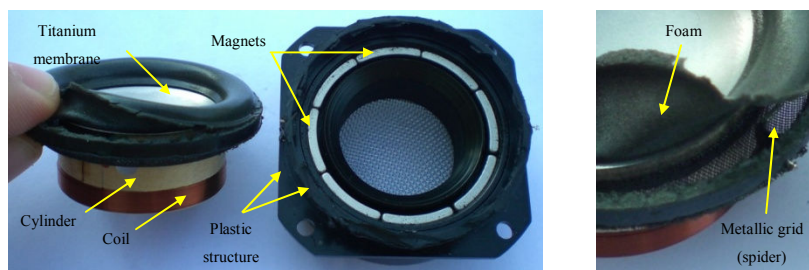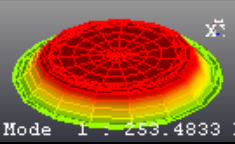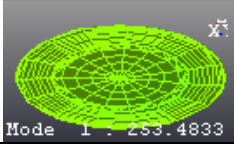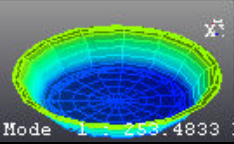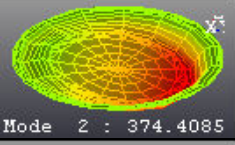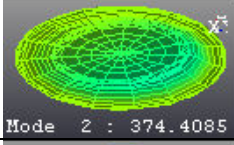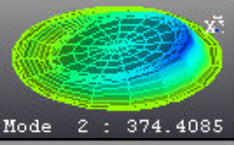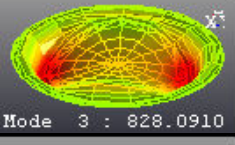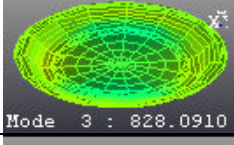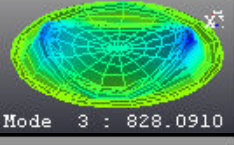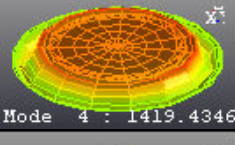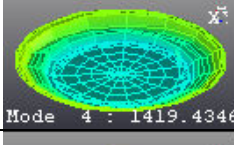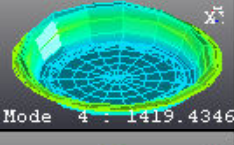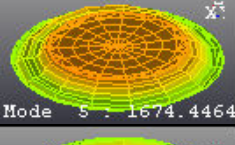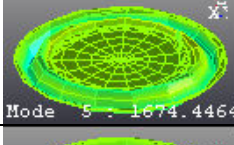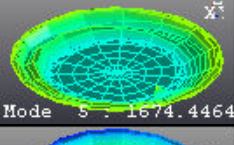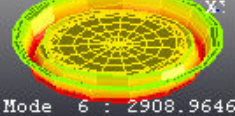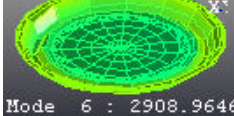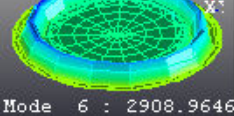
Figure 4.1 - Disassembled loudspeaker sample showing parts in detail. The right side demonstrates the suspension composed by foam and a metallic grid.

The stabilization diagram presented by Figure 3.3 indicates that poles corresponding to structural modes #02 and #03 (374 Hz and 828 Hz respectively) start to be stable only with high model orders, therefore indicating that their existence, although real, is being probably caused by an individual structural mode of the cylindrical element where the coil is installed (Figure 4.1)

55

and not by the membrane itself. Mode #04 at 1419 Hz is a cavity mode and above this frequency the structural modes can be characterized mainly by out-of-phase motion between the membrane and the suspension, leading to a discrepancy between analytical and experimental results in the high-frequency range as will be seen in the sound power plots.

Table 4.1 - Modal parameters and mode shapes extracted from experimental measurements for loudspeaker HP07.

Mode	Frequency [Hz]	Damping [%]	Mode shape		
01	253	54,06			
02	374	11,31			
03	828	1,58			
04	1419	1,83			
05	1674	3,17			
06	2908	20,12			

4.2. Comparison criteria for the simulations and the analytical model

Although the spherical field point meshes used in the analytical model and the simulations had similar radii, the exact positions of the field points could not be determined since the mesh generating mechanism developed in Matlab® by Pasqual (2010) was different from that available

in Virtual.Lab. Therefore, since sound power is a source characteristic, its behavior along the frequency range was chosen for specific ARMs as demonstrated in the next topics.

Directivity patterns are harder to compare since the amount of data generated for each ARM is very large. Therefore, only a few of them were chosen for comparison based on those demonstrated in Pasqual (2010). It is worth to note that the way figures are presented are not strictly equal since (Pasqual, 2010) uses the colors for identifying phase information while the amplitude of the deformed mesh represents the sound pressure vector amplitude. In Virtual.Lab® there is no possibility to show the two data together, therefore the colors represent only the magnitude of the sound pressure which does not have anything to do with phase information.

Finally, based on Table 4.2 and noting that some ARMs have similar and rotated versions according to the configuration chosen, their results can be grouped and were also used as a check for the simulation in order to verify if results were similar. It is worth noting that, since structural mode #02 does not involve the membrane and its influence was not found in experimental sound radiation measurements, it was decided do disable it from all simulations.

Table 4.2 - ARMs and associated similarities.

ARM number	Similarities?
01	No
02	
03	Yes
04	
05	
06	
07	Yes
08	
09	
10	Yes
11	
12	No

4.2.1. Sound power level comparisons

The next plots show the results in terms of sound power and directivity patterns for some ARMs.

It is worth mentioning that frequencies below 100 Hz are not shown in all plots because the microphone and the anechoic chamber used in the experiment did not provide a low signal-to-noise ratio in this frequency range.
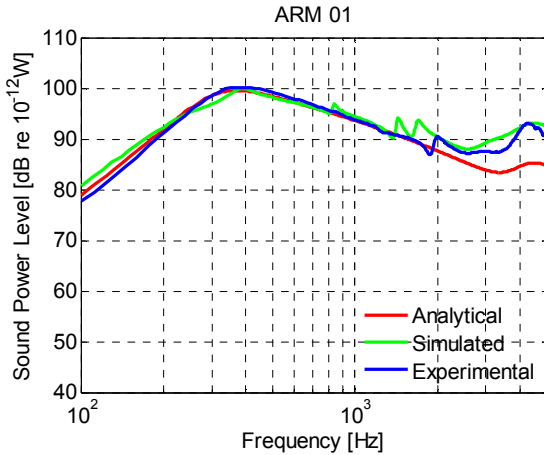
Figure 4.2 - Sound Power Level comparison for ARM #01.
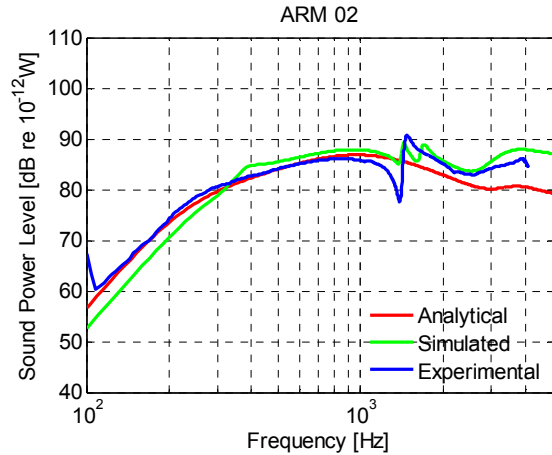
Figure 4.3 - Sound Power Level comparison for ARM #02.
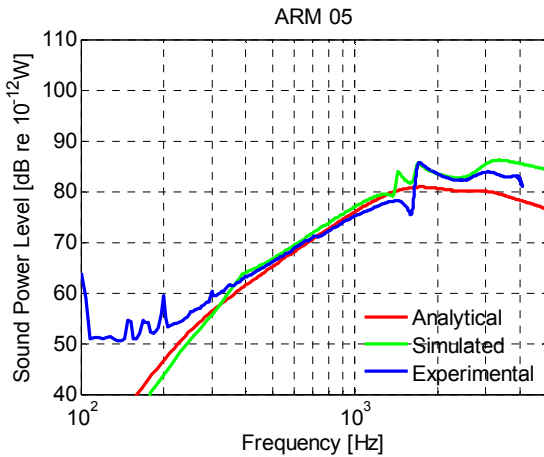
Figure 4.4 - Sound Power Level comparison for ARM #05.
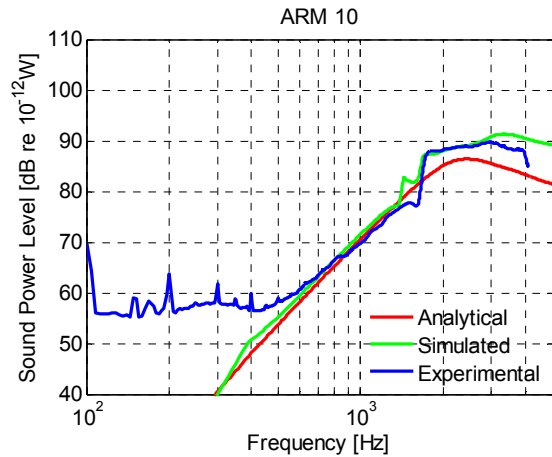
Figure 4.5 - Sound Power Level comparison for ARM #10.
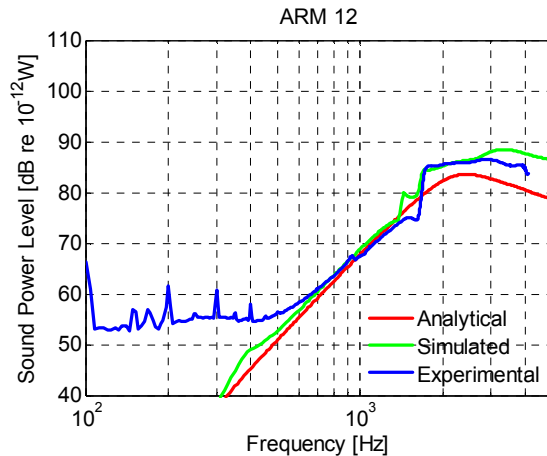
Figure 4.6 - Sound Power Level comparison for ARM #12.

For ARM #01 (Figure 4.2) it can be noticed that the three curves relate very well up to 1 kHz, with a difference of 3 dB for the lowest frequency which is gradually as frequency increases. The three subsequent peaks at 840 Hz, 1440 Hz and 1700 Hz found in simulated results can be directly associated to the structural modes #03, #04 and #05, but are not seen in the experimental results that shows only a peak at 1980 Hz, thus indicating an unrealistic amplification of radiated sound power probably caused by numerical issues with the interpolations used in the computational model. As expected, analytical results do not show any influence of structural modes, starting to deviate from experimental and simulated results above 1.5 kHz.

For ARM #02 (Figure 4.3) the sound power level in the low frequency range has a similar slope as observed for ARM #01, with a difference around 5 dB between simulated and experimental results that is practically constant until 300 Hz. The simulation correctly predicts the influence of structural mode #04 at 1476 Hz, but now the magnification factor is lower than found in the experimental results. Conversely, a peak in the sound power radiation appears at 1710 Hz and that can be correlated to structural mode #05 with a shift in frequency of around 50 Hz.

The values presented up to 400 Hz in Figure 4.4 show that ARM #05 has very low radiation efficiency, so the sound radiation level is not sufficient to distinguish noise from real measurements. Analytical and simulated results still present a 3 dB difference with similar slopes inside that range, and start to have the same level from that point up to 1500 Hz where the analytical results do not follow the same trend anymore. The simulation has detected two sound power level peaks at 1450 Hz and 1724 Hz, with the second coinciding with the measured results and that can be the same shifted version of structural mode #05 as seen for #ARM 02. Experimental and simulated results start to have divergent levels above 3 kHz.

ARM #10 shown in Figure 4.5 presents the same radiation efficiency problem stated before for ARM #05 which goes up to 600 Hz. Afterwards the curves behave practically the same quantity until 1500 Hz, with the same peaks occurring as for ARM #05. Above that frequency the analytical model starts to diverge, and the simulated and experimental results have the same

trends up to 3 kHz. The same behavior can be noticed for ARM #12 as demonstrated in Figure 4.6.

4.2.2. Directivity patterns comparisons

As mentioned before, not all directivity patterns can be shown due to the amount of information generated. However, the plots in Figure 4.7 to Figure 4.10 show that the sound pressure amplitudes and directivity patterns agree well with both experimental and analytical results, therefore demonstrating the good prediction capability of the proposed methodology.
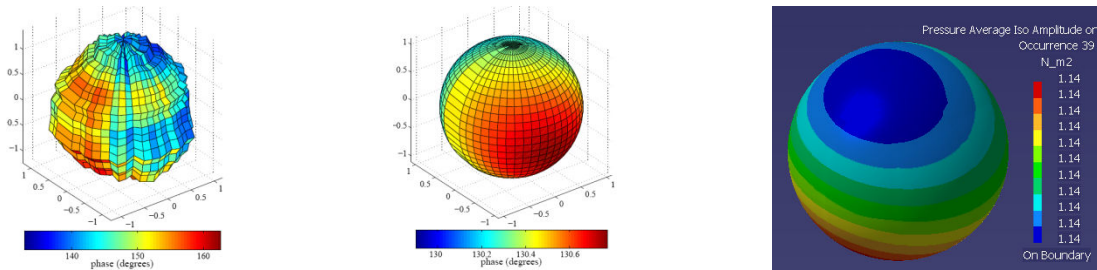
Figure 4.7 - Directivity patterns for ARM #01 at 400 Hz (experimental, analytical and simulated).
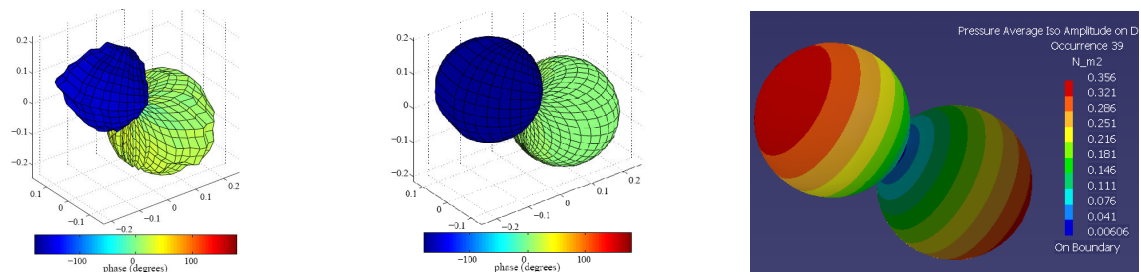
Figure 4.8 - Directivity patterns for ARM #02 at 400 Hz (experimental, analytical and simulated).
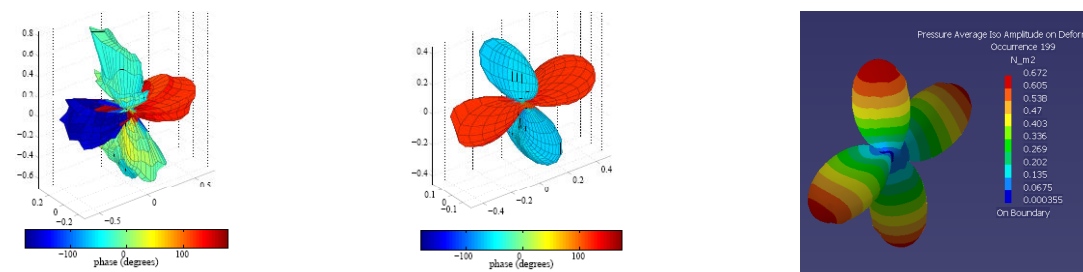
Figure 4.9 - Directivity patterns for ARM #07 at 2000 Hz (experimental, analytical and simulated).
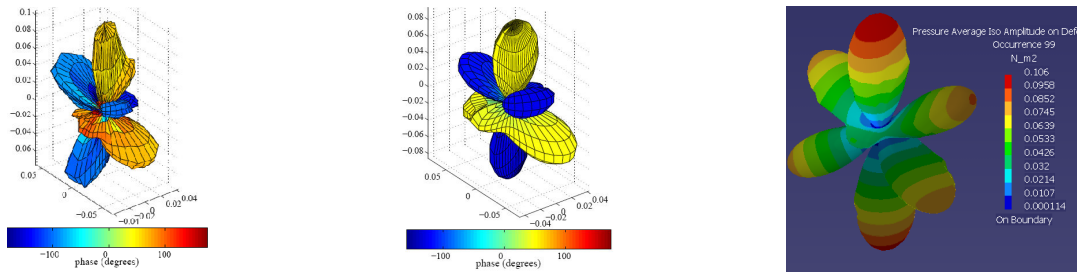
Figure 4.10 - Directivity patterns for ARM #10 at 1000 Hz (experimental, analytical and simulated).

Finally, it is important to note that slight differences in the directivity patterns can be observed when comparing experimental and simulated results. This was caused by the fact that only one set of FRFs in the simulations was used for all loudspeakers, since their electromechanical characteristics are very similar (Pasqual, 2010).

Capítulo 5

5. Conclusões

O modelo analítico desenvolvido por Zotter et al. (2007) e utilizado por Pasqual (2010) fornecem resultados muito bons até 1 kHz, sendo uma excelente referência para uma melhor compreensão do funcionamento do arranjo esférico de alto-falantes. O modelo analítico é capaz de prever tendências nessa importante faixa de operação em freqüência, mas nas freqüências superiores o modelo começa a falhar devido à contribuição de modos estruturais da membrana de ordem superior, que afetam o espectro de potência sonora com picos visualizados nos gráficos experimentais e simulados apresentados. Mais ainda, uma divergência nas curvas de nível de potência sonora pode ser sempre observada nessas faixas, o que é provavelmente causado pela influência da suspensão da membrana. Esse fato pode alterar significativamente a reprodução de campos sonoros complexos e precisa ser melhor investigado para atualizar o modelo analítico utilizado.

Embora os níveis de potência sonora sejam comparáveis, as simulações BEM parecem amplificar o efeito de alguns modos estruturais da membrana de uma forma não realista, causando picos em todas as curvas das simulações que não são encontrados nas curvas experimentais. Uma possível causa para esse problema é provavelmente as duas interpolações usadas no passo 3.5.3 e especialmente a segunda, que introduz um erro implícito devido ao processo de tentativa e erro usado na determinação dos melhores parâmetros para as projeções das velocidades. Além disso, como as FRFs usadas na simulação foram obtidas numa situação onde o primeiro modo de cavidade do arranjo foi excitado, os resultados obtidos com o BEM diferem dos experimentais em torno de 1,5 kHz, indicando assim outra possível causa para os desvios encontrados. Esse fato pode ainda explicar as diferenças encontradas na região de baixa freqüência para as curvas de nível de potência sonora apresentadas.

O mesmo pensamento anterior pode ser usado para justificar amplificações em freqüências superiores devido aos modos de cavidade apresentados na Tabela 3.2, mas outro fator existe e precisa ser levado em conta: o conjunto de FRFs usado nas simulações possui apenas um alto-falante operando, o que significa dizer que todas as simulações não podem corretamente predizer o comportamento acústico do arranjo quando todos os dispositivos estiverem em funcionamento. Logo, é esperado que o acoplamento entre todos os alto-falantes possua realmente uma influência nos resultados e, uma vez que todos os alto-falantes possuem características eletromecânicas muito similares conforme enunciado por Pasqual et al. (2009) e as irregularidades geométricas na esfera são desprezíveis, a estratégia de simulação poderia ser mudada para incluir tais efeitos. Na realidade, uma solução para isso seria usar conjuntos de FRFs "diretos" (medidos com apenas um alto-falante operando excitado por uma tensão conhecida tal como usado nas simulações) e "cruzados" (medidos entre a velocidade num alto-falante qualquer causada pela tensão aplicada num alto-falante conhecido no arranjo). Assumindo que as características dos dispositivos são muito similares, a simulação poderia então ser realizada somando-se os resultados dos dois tipos de FRFs, automaticamente levando em conta os efeitos de acoplamento mencionados.

De forma resumida, o modelo de simulação apresentado melhora os resultados para a região de alta freqüência, porém mais pesquisa é necessária para se levar em conta os efeitos de acoplamento mencionados acima e os possíveis erros numéricos. Vale ressaltar que a resolução dos *field points* acústicos foi mudada várias vezes, porém com alterações desprezíveis apenas na faixa superior do espectro de nível de pressão sonora. Além disso, alguns pontos adicionais de fontes de variabilidade existentes nas simulações são resumidos abaixo:

- Efeito da curvatura da membrana do alto-falante: a medição de uma superfície com um feixe laser capta apenas a componente na direção do feixe, o que significa que a componente da velocidade de partícula do ar normal ao feixe laser – e, portanto, normal à superfície do pistão plano equivalente – não é considerada (ela contribui principalmente para o campo próximo);

- Deslocamentos finitos da calota esférica: a junção entre a calota esférica e o SLA causa uma descontinuidade geométrica que não é considerada na solução analítica;

- Tamanho dos elementos na malha acústica: a regra dos seis elementos por comprimento de onda usada na geração da malha acústica pode não ser suficiente para a representação do problema, pois se sabe que a predição da potência irradiada necessita de grande precisão na representação do campo acústico;

- Modos de cavidade acústicos: a maneira como os alto-falantes excitam esses modos e internamente interagem não foi considerada no modelo.

Os padrões de diretividade estão de acordo nos modelos comparados, representando inclusive distribuições complexas de pressão na faixa de alta freqüência. A representação com a malha deformada mostra muito bem a complexidade do problema mesmo para fontes simples e pode fornecer uma compreensão valiosa nesses casos. Algumas pequenas diferenças podem ser vistas predominantemente no modelo computacional e são causadas pelo fato de que apenas um conjunto de FRFs foi usado para representar todos os alto-falantes no arranjo.

A razão para desmontar um dos alto-falantes como demonstrado na Figura 4.1 foi a tentativa de extração de algumas propriedades estruturais da membrana (módulo de Young, massa, espessura, etc.) de maneira a criar um modelo computacional por elementos finitos no software Abaqus®, a partir do qual uma análise da resposta estrutural pudesse ser calculada. No entanto, trabalhar com pequenas estruturas não é uma tarefa fácil e, embora alguns parâmetros como a espessura (aproximadamente 0,7 mm) fossem extraídos e um desenho geométrico da membrana tenha sido feito, as propriedades do material e da suspensão não foram encontrados ou determinados, o que infelizmente tornou a simulação impraticável. Pela experiência do pesquisador Philippe Herzog do LMA, a modelagem por FEM da membrana é realmente difícil principalmente devido aos problemas apresentados e, de acordo com ele, pesquisas passadas (Joly et al., 1996) indicaram que mesmo após uma grande quantidade de trabalho, os parâmetros obtidos foram muito próximos àqueles encontrados para o modelo T-S. Finalmente, como uma

recomendação, o pesquisador ainda mencionou a importância de se realizar uma malha para tais simulações de maneira mais assimétrica possível através de uma distribuição não uniforme de elementos com diferentes tamanhos e nós em posições diferenciadas para causar perturbações intencionais em modos que podem não ser detectados quando malhas simétricas são utilizadas.

Como sugestões para trabalhos futuros, alguns tópicos são resumidos abaixo:

- Desenvolver e empregar técnicas para determinação das propriedades das partes dos alto-falantes, especialmente a membrana e a suspensão que variam muito conforme o tipo de construção utilizado. Um bom ponto de partida para o tópico pode ser visto em Rocha (2010);

- Simulação da membrana do alto-falante usando o FEM e incluindo a interação da suspensão com os materiais previamente determinados;

- Simulação da interação entre o arranjo esférico e uma sala e auralização dos resultados obtidos para predição das características de percepção sonora da fonte;

- Inclusão de parâmetros não lineares no modelo eletromecânico utilizado na solução analítica;

- Estudo dos efeitos em alguns parâmetros T-S variáveis em freqüência para a introdução de não-linearidades na operação dos alto-falantes.

Finalmente, a importância de simular um dispositivo complexo como o arranjo esférico de alto-falantes reside no fato de que tanto ferramentas experimentais como de simulação poderem ser combinadas para a obtenção de resultados mais próximos daqueles encontrados num sistema real.

O SLA é uma nova ferramenta em desenvolvimento, mas com um enorme potencial devido às

suas características direcionais totalmente controláveis, permitindo aos usuários não apenas a compreensão de fenômenos acústicos numa nova perspectiva, mas também o trabalho com campos sonoros de forma mais concisa com um aumento significativo na eficiência de controle proporcionada pelos ARMs.

Chapter 5

5. Conclusions

The analytical model developed by Zotter et al. (2007) and used by Pasqual (2010) yields very good results up to 1 kHz, being an excellent reference for understanding the loudspeaker array operation. The analytical model is capable of predicting trends in this very important operating frequency range, but in upper frequencies the model starts to fail due to the contribution of higher order structural membrane modes, which affect the sound power spectrum with peaks that cannot be seen in the experimental and BEM simulation plots presented. Moreover, a divergence in the sound power curves can always be observed in such ranges, which is probably caused by the influence of the membrane suspension. That fact would alter significantly the reproduction of a complex sound field and needs to be further investigated in order to upgrade the analytical model used.

Although the sound power levels are comparable, the BEM simulations seem to amplify the effect of some structural modes in an unrealistic way, causing peaks in all simulation curves not found in the experiments. One possible cause for that problem is probably the two interpolations used in step 3.5.3 and especially the second one, which introduces an inherited error due to the trial and error process of finding the best parameters for the velocity projections. Also, as the FRFs used in the simulation were obtained in a situation where the first cavity mode was excited, the BEM results differ from the experimental ones around 1,5 kHz, indicating thus another possible cause for the deviations found. That fact can also explain the differences found in the low frequency region found in the sound power level curves presented.

The same thought above presented can be used to justify upper amplifications seen due to the cavity modes presented in Table 3.2, but another possible issue exists and must be taken into

account: the FRF set used in the simulations was for just one loudspeaker operating, which means that the simulations cannot correctly predict the acoustic behavior of the array when all the devices are working together, i.e., it is expected that coupling among all loudspeakers does have an influence in the results and, since all loudspeakers have very similar electromechanical characteristics as seen in Pasqual et al. (2009) and the geometrical irregularities in the sphere are neglegible, the simulation strategy could be changed to include such effects. Indeed, a solution for that problem would be to use the "direct" and "crossed" FRF sets, i.e., those measured with only one loudspeaker operating excited by a known voltage (as used in the simulations) and those measured between the velocity at any random loudspeaker membrane and a voltage applied to any other loudspeaker in the array. Assuming that the characteristics of the devices are very similar, the simulation could be performed for each loudspeaker by summing the results from the FRFs, therefore automatically taking into account the coupling effects.

Strictly speaking, the simulation model presented improves the prediction in the high frequency range, but more research would be necessary in order to take into account the coupling effects mentioned above and the possible numerical errors. It is worth to mention that the resolution of the acoustic field points were changed a few times, which only altered the upper end of the sound power level spectrum. Moreover, some additional variability sources for the simulations are listed below:

- Curvature of the loudspeaker: measuring a curved surface with a laser beam captures only the component along the beam direction, which means that the particle velocity component normal to the laser beam, and thus normal to the equivalent flat piston surface, is not considered (it contributes mainly to the acoustic near field);

- Finite displacements of the spherical cap: the junction between the spherical cap and the SLA can cause a geometrical discontinuity which is not considered in the analytical solution;

- Element size on the acoustic mesh: the six elements per wavelength rule used for

generating the acoustic mesh may not be sufficient for the problem discretization given that it is known that radiated power prediction demands a very accurate sound field representation;

- Acoustic cavity modes: the way loudspeakers excite those modes and internally interact through them was not considered in the model.

The directivity patterns agree very well in both compared models, even representing complex pressure distributions in the high frequency range. The deformed mesh representation shows very well the complexity of the problem even for simple sources and can provide a helpful insight in such studies. Some slight differences can be seen mostly in the computational model that are caused by the fact that only one set of FRFs was used to represent all loudspeakers in the array.

The reason for disassembling one loudspeaker as demonstrated in Figure 4.1 was that the author has tried to extract some structural parameters of the membrane (Young's module, mass, thickness, etc.) in order to create a computational model in Abaqus® from which a structural response analysis could be performed. Nevertheless, working with such small structures is not an easy task and, although some parameters like the thickness (approximately 0,7 mm) could be extracted and a geometrical drawing of the membrane was made, the material and suspension properties were neither found nor determined, which unfortunately made the simulation impossible. From the personal experience of Philippe Herzog from the LMA, modeling the membrane using the FEM is really hard mostly because of the issues presented here and, according to him, some research done in the past (Joly et al., 1996) indicated that even spending an enormous amount of work, the obtained parameters were very close to those found using the T-S parameters. Finally, as an advice, the researcher also mentioned that an important feature of the mesh for such simulation is to make it as asymmetrical as possible, i.e., an uneven distribution of elements with different sizes and badly positioned nodes is preferred to cause perturbations in the response, otherwise not seen when symmetrical meshes are used.

As suggestions for future research, some topics are summarized below:

- Development of techniques for determining properties in loudspeaker's parts, specially the membrane and the suspension, which dramatically varies according to the construction used. A good starting point could be the article from Rocha (2010);

- Simulation of the loudspeaker membrane using the FEM by including the suspension interaction and the materials previously determined;

- Simulation of the interaction of the array with a room and sound auralization for the prediction of the sound perception characteristics of the source;

- Investigation of the numerical issues behind the interpolations used for the simulation;

- Inclusion of non-linear parameters in the electromechanical model used for the analytical solution;

- Study of the effects of some frequency dependent T-S parameters to simulate non-linearities in the loudspeaker operation.

Finally, the importance of simulating such complex device as the spherical loudspeaker array relies in the fact that both experimental and simulation tools can be combined in order to deliver results closer to the actual behavior of the system.

The SLA is a new tool under development but with an immense potential due to its fully controllable directional characteristics, allowing users to not only comprehend acoustic phenomena in a new perspective but also to work with sound fields in a more concise with the dramatic increase in control efficiency introduced by the ARMs.

References

Albuquerque, E. L. 2009. *Boundary Elements Lecture Notes - Part I.* Campinas, Brazil : s.n., 2009.

Allemang, R. J. and Brown, D. L. 1987. *Experimental Modal Analysis and Dynamic Component Synthesis Volume V - Universal File Formats.* Cincinnati : United States Air Force, 1987.

Ba, Mingsian R., Chen, Rong-Liang and Wang, Chun-Jen. 2009. Electroacoustic analysis of an electret loudspeaker using combined finite-element and lumped-parameter models. *Journal of the Acoustical Society of America.* 125, March 12, 2009, 6, pp. 3632-3640.

Behler, G. K. 2007. Sound Source for the Measurement of Room Impulse Responses for Auralisation. Madrid : 19th International Congress on Acoustics - ICA, 2007.

Bell, Alexander Graham. 1876. *Improvement in telegraphy. Patent: 174.465* USA, March 7, 1876.

Beranek, Leo L. 1993. *Acoustics.* Cambridge, MA : Acoustical Society of America, 1993. ISBN: 088318914X.

Berkhout, A. J., de Vries, D. and Vogel, P. 1993. Acoustic control by wave field synthesis. *Journal of the Acoustical Society of America.* 93, May 1993, 5, pp. 2764-2778.

Boaz, R. 2009. Spherical loudspeaker array for local active control of sound. *Journal of the Acoustical Society of America.* 125, May 2009, Vol. 5.

Borgiotti, G. V. and Jones, K. E. 1994. Frequency independence property of radiation spatial filters. *Journal of the Acoustical Society of America.* 96, December 1994, pp. 3516-3524.

Borgiotti, G. V. 1990. The power radiated by a vibrating body in an acoustic fluid and its determination from boundary measurements. *Journal of the Acoustical Society of America.* 88,

October 1990, pp. 1884-1893.

Caussé, R., et al. 1992. Radiation of musical instruments and control of reproduction with loudspeakers. Tokyo, Japan : In: Proceedings of the International Symposium on Musical Acoustics, 1992. Electronic document available at <http://articles.ircam.fr/textes/Causse92a/>. Last access: 11-Mar-2010.

CLF Group. 2005. CLF Group Main Page. *CLF Group website.* [Online] 2005. [Cited: April 01, 2010.] http://www.clfgroup.org.

Colloms, M. and P., Darlington. 2005. *High Performance Loudspeakers.* 6th. West Sussex : John Wiley & Sons, Ltd, 2005. ISBN: 0-470-09430-3.

Cunefare, K. A. and Currey, M. N. 1994. On the exterior acoustic radiation modes of structures. *Journal of the Acoustical Society of America.* 96, October 1994, pp. 2302-2312.

Dickason, Vance. 2005. *The loudspeaker design cookbook.* 7th edition. Peterborough : Audio Amateur Publications Inc., 2005. ISBN 1882580478.

Dirac Delta Consultants Ltd. 2001-2010. Acoustic Sources. *Science & Engineering Encyclopaedia Version 2.4.* [Online] Dirac Delta Consultants Ltd., 2001-2010. [Cited: April 08, 2010.] http://www.diracdelta.co.uk/science/source/a/c/acoustic%20sources/source.html.

Elliott, S. J. and Johnson, M. E. 1993. Radiation modes and the active control of sound power. *Journal of the Acoustical Society of America.* 94, October 1993, pp. 2194-2204.

Ewins, D. J. 1984. *Modal testing: theory and practice.* New York : John Wiley & Sons, 1984. ISBN: 0863800173.

Fahy, Frank. 2001. *Foundations of Engineering Acoustics.* 2nd edition. London : Academic Press, 2001. 0122476654.

FeONIC Technology. 2010. The GENUINE FeONIC Whispering Window : Attract New Customers : Whispering Windows : Shop Window Speakers. [Online] FeONIC Technolgy, 2010. [Cited: March 02, 2010.] http://www.whisperingwindow.com/works.

Gerzon, M. A. 1973. Periphony: with-height sound reproduction. *Journal of the Audio Engineering Society.* 21, 1973, 1, pp. 2-10.

Gupta, Mohit. 2006. *Simulation and Visualization of Various Acoustic Sources in MATLAB.* Department of Aeronautical and Vehicle Engineering, Royal Institute of Technology. Stockholm, Sweden : EU Asia-Link ASIE/2005/111000, 2006. p. 61, Summer Internship Project Report.

Hallez, R. 2009. Fast Multipole BEM - A New Era for Acoustic Simulation. [LMS International Webinar]. 26 September, 2009.

Handi, M. A. 1981. Une formulation variationelle par euqations integrales pour la resolution de l'equation de Helmholtz avec des conditions aux limites mixtes. *Comtes Rendus Acad. Sc. Paris.* 1981, Vol. 292, Ser. II, pp. 17-20.

He, J. and Fu, Z. 2001. *Modal analysis.* 1st Edition. Oxford : Butterworh-Heinemann, 2001. 0-7506-5079-6.

Ijima, Tohji. 2006. *Giant-Magnetostrictive Speaker. WO/2006/118205* Japan, November 09, 2006. Patent. Foster Electric Company Ltd..

Joly, N. and Herzog, P. 1996. Analyse du profil de la membrane d'un haute-parleur. . [In: Proceedings of StruCoMe]. Paris : s.n., October 2-3, 1996.

Kassakian, P. and Wessel, D. 2004. Characterization of Spherical Loudspeaker Arrays. *117th Convention of the Audio Engineering Society.* San Francisco : s.n., October 28-31, 2004.

Klippel, Wolfgang and Schlechtel, Joachim. 2009. Distributed Mechanical Parameters of Loudspeakers - Part 2: Diagnostics. *Journal of the Audio Engineering Society.* 2009, Vol. 57, No. 9.

Klippel, Wolfgang and Schlechter, Joachim. 2009. Distributed Mechanical Parameters of Loudspeakers - Part 1: Measurements. *Journal of Audio Engineering Society.* 2009, Vol. 57, No. 7/8.

Klippel, Wolfgang. 2007. Dynamic Measurement of Loudspeaker Suspension Parts. *Journal of the Audio Engineering Society.* 2007, Vol. 55, No. 6.

Knudsen, M. H. and Jensen, J. G. 1993. Low-frequency loudspeaker models that include suspension creep. *Journal of the Audio Engineering Society.* Januray/February 1993, Vol. 41, 1/2.

Leishman, T. W., Rollins, S. and Smith, H. M. 2006. An experimental evaluation of regular polyhedron loudspeakers as omnidirectional sources of sound. *Journal of the Acoustical Society of America.* 2006, Vol. 120, 3, pp. 1411-1422.

Liu, Y. J. and Nishimura, N. 2006. The fast multipole boundary element method for potential problems: A tutorial. *Engineering Analysis with Boundary Elements.* March 15, 2006, Vol. 30, pp. pp. 371-381.

LMS International. 2008. The LMS Test.Lab Modal Analysis manual - Modal Analysis Theory. [Online help]. 2008.

LMS International. 2008. Virtual.Lab Online Help. [Online help]. 2008.

Lodge, Oliver Joseph. 1898. *Improvements relating to Telephones, and to Circuit Arrangements and Relays therefor. GB189809712* UK, April 27, 1898. Patent.

Mariem, J. B. and Hamdi, M. A. 1987. A new boundary finite element method for fluid-structure interaction problems. *International Journal of Numerical Methods in Engineering.* 1987, Vol. 24, pp. 1251-1267.

Meyer, P. S. and Meyer, J. D. 2000. Multi acoustic prediction program (MAPP): recent results. Stratford upon Avon,, UK : Meyer Sound Laboratories Inc., 2000. Techical report presented at the Institute of Acoustics.

Nave, Rod. 2006. Loudspeakers. *HyperPhysics Concepts.* [Online] Georgia State University, 2006. [Cited: Jan 06, 2010.] http://hyperphysics.phy-astr.gsu.edu/HBASE/audio/spk.html#c2.

Nave, Rod. 2006. Magnetostriction. *HyperPhysics Concepts.* [Online] 2006. [Cited: March 02, 2010.] http://hyperphysics.phy-astr.gsu.edu/hbase/Solids/magstrict.html.

Newland, D. E. 1993. *An introduction to random vibrations, spectral & wavelet analysis.* 3rd edition. Mineola : Dover Publications, Inc, 1993. 0486442748.

Olson, Harry F. 1962. Loudspeakers. *Proceedings of the IRE (Institute of Radio Engineers).* 1962, Vol. 50, 5, pp. 730-737.

Olson, Harry F. 1967. *Music, Physics and Engineering.* 2nd edition. New York : Dover Publications, 1967. ISBN: 0-486-21769-8.

Olson, L. 2002. The Art of Speaker Design - Part I. [Online] 2002. [Cited: March 02, 2010.] http://www.nutshellhifi.com/library/speaker-design1.html.

Olson, L. 2002. The Art of Speaker Design - Part II. [Online] 2002. [Cited: March 02, 2010.] http://www.nutshellhifi.com/library/speaker-design2.html.

Pasqual, A. M., Herzog, P. and Arruda, J. R. F. 2009. Theoretical and experimental analysis of the electromechanical behavior of a spherical loudspeaker array for radiation control. September 25, 2009.

Pasqual, Alexander Mattioli. 2010. Sound Directivity Control in a 3-D Space by a Compact Spherical Loudspeaker Array. *Ph.D. Dissertation.* Campinas, SP, Brazil : s.n., Feb 22, 2010.

Pedersen, Bo Rohde. 2008. Error Correction of Loudspeakers: A study of Loudspeaker Design supported by Digital Signal Processing. *PhD Thesis.* s.l., Esbjerg, Denmark : Department of Software, Medialogy and Electronics. Esbjerg Tekniske Institut. Aalborg University., 2008. 9878776060244.

Peeters, B., et al. 2004. A new procedure for modal parameter estimation. *Journal of Sound and Vibration.* January 2004, pp. pp. 24-28.

Photiadis, D.M. 1990. The relationship of singular value decomposition to wave-vector filtering in sound radiation problems. *Journal of the Acoustical Society of America.* 88, August 1990, pp. 1152-1159.

Pierce, A. D. 1994. *Acoustics: An Introduction to its Physical Principles and Applications.* Melville, NY : Acoustical Society of America, 1994.

Pierce, A. D. 1994. *Acoustics: An Introduction to Its Physical Principles and Applications.* Melville : Acoustical Society of America, 1994.

Pollow, M. and Behler, G. K. 2009. Variable directivity for Platonic sound sources based on spherical harmonics optimization. *Acta Acustica united with Acustica.* 2009, Vol. 95, 6, pp. 1082-1092.

Pollow, M. 2007. Variable directivity of dodecahedron loudspeakers. *PhD Thesis.* 2007.

Quaegebeur, N. and Chaigne, A. 2008. Nonlinear vibrations of loudspeaker-like structures. *Journal of Sound and Vibration.* 2008, Vol. 309, pp. 178-196.

Quaegebeur, N. and Chaigne, A. 2006. On the influence of the geometry on radiation for electrodynamic loudspeakers. *In: Proceedings of the 120th Audio Engineering Society Convention.* Paris, France, May 20-23, 2006.

Ravaud, R., Lemarquand, G. and Roussel, T. 2009. Time-varying non linear modeling of electrodynamic loudspeakers. *Applied Acoustics.* 2009, Vol. 70, pp. 450-458.

Rice, W. Chester and Edward, W. Kellogg. 1925. Notes on the Development of a New Type of Hornless Loudspeaker. *Notes on the Development of a New Type of Hornless Loudspeaker.* 1925, Vol. 44, pp. 461-475.

Rocha, M. L. 2010. Simulação mecânica de alto-falantes pelo método dos elementos finitos. *In: Proceedings of the 14th AES Brazil National Convention.* São Paulo, SP, Brazil : s.n., May 4-6, 2010. p. 12.

Rossi, Mario. 1988. *Acoustics and electroacoustics.* [trans.] Patrick Rupert Windsor Roe. Norwood : Artech House, 1988. p. 758.

Russell, Dan. 2001. Kettering University Applied Physics. *Radiation from monopoles, dipoles, quadrupoles.* [Online] 2001. [Cited: April 12, 2010.] http://paws.kettering.edu/~drussell/Demos/rad2/mdq.html.

Schenck, H. A. 1968. Improved integral formulatino for acoustic radiation problems. *The Journal of Acoustical Society of America.* 1968, Vol. 44, pp. 41-58.

Schoenherr, Steven E. 2001. Loudspeaker History. [Online] 2001. [Cited: March 01, 2010.] http://history.sandiego.edu/GEN/recording/loudspeaker.html.

Sequerra, Richard. 1998. Classical Ribbon Loudspeakers. [Online] 1998. [Cited: March 2010, 02.] www.sequerra.com/common/data/ribbons.doc.

Siemens, Ernst W. 1874. *Moving-coil transducer with a circular coil of wire in magnetic field. 149797* USA, April 14, 1874. Patent.

Skrodzka, E. B. and Scęcek, A. P. 2000. Comparison of modal parameters of loudspeakers in different working conditions. *Applied Acoustics.* 60, 2000, pp. 267-277.

Small, R. H. 1972. Closed-Box Loudspeaker Systems - Part I: Analysis. *Journal of the Audio Engineering Society.* 1972, Vol. 20, 10, pp. 798-808.

Small, R. H. 1973. Closed-Box Loudspeaker Systems - Part II: Synthesis. *Journal of the Audio Engineering Society.* 1973, Vol. 21, 1, pp. 11-18.

Small, R. H. 1972. Direct-Radiator Loudspeaker System Analysis. *Journal of the Audio Engineering Society.* 1972, Vol. 20, 5, pp. 383-395.

Suzuki, H. and Tichy, J. 1981. Sound radiation from convex and concave domes in an infinite baffle. *Journal of the Acoustical Society of America.* 1981, Vol. 69, 1.

Syn-Aud-Con. 2004. *Syn-Aud-Con Newsletter.* 2004. Vol. 32. Avaible at: <http://www.clfgroup.org/clf_SAC_Newsetter_fall_2004.pdf>.

Thiele, A. N. 1971. Loudspeakers in Vented Boxes - Part I. *Journal of the Audio Engineering Society.* 1971, Vol. 19, pp. 181-191.

Thiele, A. N. 1971. Loudspeakers in Vented Boxes - Part II. *Journal of the Audio Engineering Society.* 1971, Vol. 19, pp. 192-204.

Tipler, Paul Allen. 2002. *Physics for Scientists and Engineers.* New York, NY : W. H. Freeman and Company, 2002. ISBN: 1-572596732.

von Estorff, O. 2000. *Boundary Element Acoustics – Advances & Applications.* 1st Edition. Southampton : WIT Press, 2000. ISBN: 1-853-312-556-3.

Vorländer, Michael. 2008. *Auralization - Fundamentals of Acoustics, Modelling, Simulation,*

Algorithms and Acoustic Virtual Reality. 1st Edition. s.l. : Springer-Verlag Berlin Heidelberg, 2008. ISBN 978-3-540-48829-3.

Warusfel, O. and Misdariis, N. 2004. Sound Source Radiation Synthesis: from Stage Performance to Domestic Rendering. Berlin : s.n., May 8-11, 2004. Convention Paper 6018.

Weise, W. 2004. Investigation of the anisotropy of hemi-dodecahedron noise source radiation. *Journal of Sound and Vibration.* 270, 2004, pp. pp. 137-147.

Wikipedia. 2010. Loudspeaker. *Wikipedia - The Free Encyclopedia.* [Online] 2010. [Cited: March 01, 2010.] http://en.wikipedia.org/wiki/Loudspeaker.

Williams, E. G. 1999. *Fourier Acoustics.* London : Academic Press, 1999. 0-12-753960-3.

Wu, T. W. 2000. *Boundary Element Acoustics - Fundamentals and Computer Codes.* 1st Edition. Southampton : WIT Press, 2000. 1-85312-570-9.

Wu, X. F., Pierce, A. D. and Ginsberg, J. H. 1987. Variational method for computing surface acoustic pressure on vibrating bodies, applied to transversely oscillating disks. *IEEE Journal of Oceanic Engineering.* 1987, Vols. OE-12, pp. 412-418.

Zotter, F. 2009. Analysis and Synthesis of Sound-Radiation with Spherical Arrays. *PhD Thesis.* s.l., Austria : IEM - Institute of Electronic Music and Acoustics, 2009.

Zotter, F., Sontacchi, A. and R., Höldrich. 2007. Modeling a Spherical Loudspeaker System as a Multipole Source. *DAGA.* March 2007, Vol. 33, pp. 19-22.

Appendix A - The wave equation and its solution in spherical coordinates

The linearized wave equation is given by Fahy (2001):

$$\nabla^2 p(\vec{x}, t) - \frac{1}{c^2}\frac{\partial^2 p(\vec{x}, t)}{\partial t^2} = 0 \tag{A.1}$$

where $p(\vec{x}, t)$ is the particle sound pressure, c is the sound speed in the fluid, $\vec{x}$ is the position vector, t is time and $\nabla^2(\cdot)$ is the Laplacian operator. Particle velocity can be related to particle acoustic pressure by the linearized Euler equation (Fahy, 2001):

$$\rho\frac{\partial \upsilon(\vec{x}, t)}{\partial t} = -\nabla p(\vec{x}, t) \tag{A.2}$$

where ρ is the fluid density without any acoustic perturbation. Assuming a harmonic time dependence of the form $e^{-i.\omega.t}$, equations (A.1) and (A.2) become:

$$\nabla^2\bar{p}(\vec{x},\omega) + k^2\,\bar{p}(\vec{x},\omega) = 0 \tag{A.3}$$

and

$$i.\omega.\rho.\bar{\upsilon}(\vec{x},\omega) = -\nabla\bar{p}(\vec{x},\omega) \tag{A.4}$$

where $k = \omega/c$ is the wave number, $\bar{p}(\vec{x}, \omega)$ and $\bar{\upsilon}(\vec{x}, \omega)$ are the complex magnitude spectra of particle acoustic pressure and velocity respectively. Since the frequency domain is predominant in this work, the overbars are always omitted.

Equation (A.3) is an ordinary differential equation (ODE) named Helmholtz equation.

79

Assuming a spherical coordinate system (Figure A.1) and knowing that it is separable (Williams, 1999), the method of separation of variables leads to the general solution of the type:

$$p(r, \theta, \phi) = R(r).\Theta(\theta).\Phi(\phi)$$ (A.5)
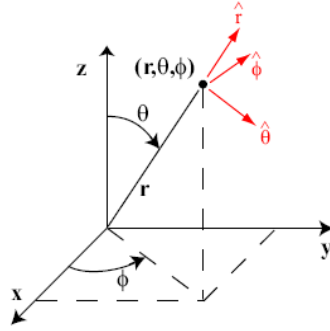
Figure A.1 - Spherical coordinate system.

Finding each separated function in equation (A.5) and combining them together as a series expansion (Pasqual, 2010) yields:

$$p(r, \theta, \phi) = \sum_{n=0}^{\infty} \sum_{m=-n}^{n} \left(A_{mn} h_n^{(1)}(k.r) + B_{mn} h_n^{(2)}(k.r) \right).Y_n^m(\theta, \phi)$$ (A.6)

where $h_n^{(1)}(k.r)$ and $h_n^{(2)}(k.r)$ are the spherical Henkel functions of the first and second kind (Williams, 1999), A_{mn} and B_{mn} are constants to be determined from the boundary conditions and related to outgoing and incoming waves and $Y_n^m(\cdot)$ is the spherical harmonic function discussed below. Since only free-field conditions are considered (neither scatters nor reflections), equation (A.6) can be rewritten as:

$$p(r, \theta, \phi) = \sum_{n=0}^{\infty} \sum_{m=-n}^{n} A_{mn} \underbrace{h_n^{(1)}(k.r)}_{\text{radial term}} . \underbrace{Y_n^m(\theta, \phi)}_{\text{angular term}}$$ (A.7)

An important observation concerning equation (A.7) and evidenced in Pasqual (2010) is the fact that it is divided in two main components for each series term: one radial – $h_n^{(1)}(k.r)$ – and other angular – $Y_n^m(\theta, \phi)$. Analyzing the radial term, it can be seen that for large arguments it decreases linearly with r (Williams, 1999) and for small arguments the near-field extends farther

out from the source. In other words, how far one must be from the source in order to ensure far-field propagation depends on the frequency and the complexity of the directivity pattern.

Appendix B - Simple multipole sources

The study of simple sources is very important in acoustics since their combination can describe the radiation characteristics in many situations like those found in the SLAs and other complex problems. The main types of acoustic sources and their formulations are presented below based on the works of Gupta (2006), Dirac Delta Consultants Ltd. (2001-2010) and Russell (2001). It is worth to note that the first author presents a very didactic review of acoustic sources with full Matlab® codes that can be used for teaching purposes.

1. Monopole

If a source of sound is much smaller than the wavelength of the sound it emits, it can be represented by a "point source" or a "monopole" characterized by an equal radiation in all directions (spherical symmetry). If a tiny spherical source generates sound by successively expanding and contracting, a pressure pulse will be followed by a rarefaction pulse, therefore resulting in the same sound field in all directions like represented in Figure B.1.
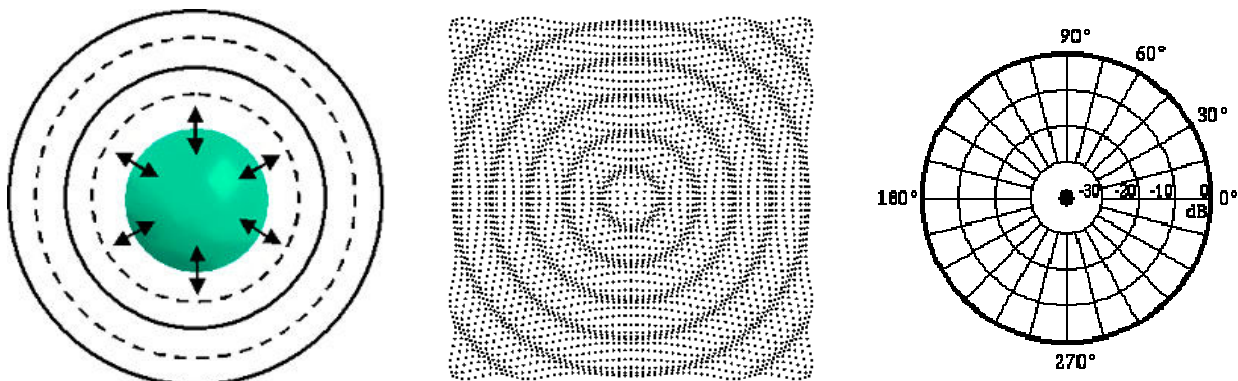
Figure B.1- Monopole operation (left), pressure distribution (center) and radiation pattern (right).

The equation for the monopole is given by:

$$p(r, t) = i \, \rho \, c \, \frac{Q_S \, k}{4 \, \pi \, r} \, e^{i \, (\omega \, t - k \, r)} \tag{B.1}$$

where $i = \sqrt{-1}$, ρ is the density of the fluid, c is the speed of sound, k is the wave number, r is the distance between the source and an arbitrary point, $Q_S = 4 \, \pi \, r^2 v$ is the volume velocity at r (also referred as source-strength function), ω is the frequency and t is the time. The intensity at distance r is given by:

$$I(r) = \frac{\rho \, c}{8} \left(\frac{Q_S}{\lambda \, r} \right)^2 \tag{B.2}$$

with λ equal to the wavelength and $I(r)$ the sound intensity at a distance r. Integrating the intensity over a sphere centered at the source gives the radiated power:

$$\Pi = \frac{\pi}{2} \, \rho \, c \left(\frac{Q_S}{\lambda} \right)^2 \tag{B.3}$$

where Π is the sound power. The simple monopole may be approximated by a loudspeaker with the rear closed off by a box, where the dimensions of the box in any direction are small compared to the wavelength.

A simple extension to this is to consider the source as being baffled in which case the pressure increases by a factor of two in the half space occupied by the source. This condition may be considered for a source above a rigid ground plane or for an element that is vibrating within an infinite baffle. This simple approximation allows a more complex source to be constructed from a number of discrete monopoles.

2. Dipole

A dipole source consists of two monopole sources of equal strength but opposite phase and separated by a small distance d compared with the wavelength of sound ($k.d << 1$). While one

83

source expands the other source contracts and the result is that the air near the two sources sloshes back and forth to produce the sound. A sphere which oscillates back and forth acts like a dipole source, as does an unboxed loudspeaker (while the front is pushing outwards the back is sucking in). A dipole source does not radiate sound in all directions equally, i.e., the directivity pattern shown in Figure B.2 shows that there are two regions where sound is radiated very well, and two regions where sound cancels.
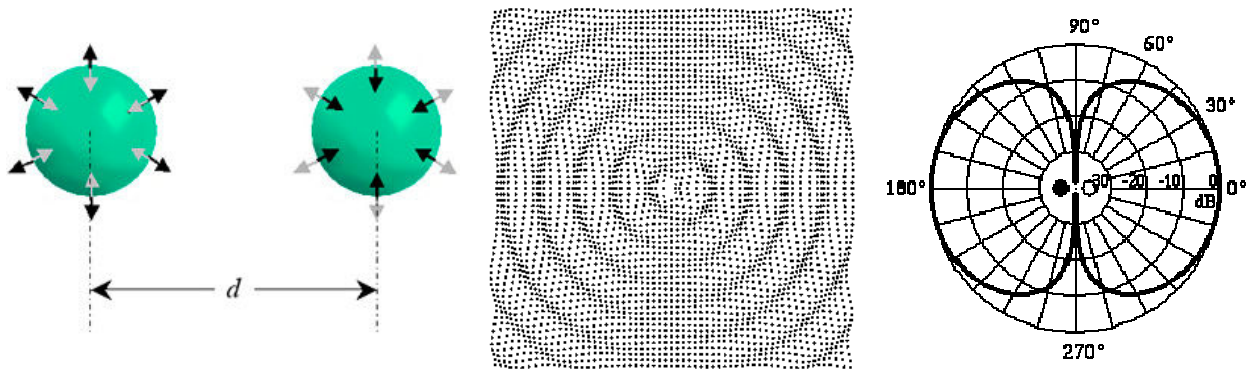
Figure B.2- Dipole operation (left), pressure distribution (center) and radiation pattern (right).

The near-field of this combination of sources is fairly complicated. However, the far-field expression for the pressure radiated by an acoustic dipole may be written as:

$$p(r, \theta, t) = - i \rho c \; \frac{Q_S \, k^2 \, d}{4 \, \pi \, r} \cos(\theta) \; e^{\, i.(\omega.t - k.r)} \qquad \text{(B.4)}$$

and the sound power is given by:

$$\Pi = \frac{Q_S^{\,2} \, \rho \, c \, k^4 \, d^2}{6 \, \pi} \qquad \text{(B.5)}$$

It is worth to note that the term *cos(θ)* in equation (B.4) controls the angular behavior of the directivity pattern.

84

3. Quadrupole

A quadrupole can be considered as four monopoles with two out of phase with the other two. They are either arranged in a line with alternating phase or at the vertices of a cube with opposite corners in phase. In both cases there is no net flux of fluid and no net force on the fluid: it is the fluctuating stress that generates the sound waves. However, since fluids do not support shear stresses well, quadrupoles are poor radiators of sound.

3.1. Lateral quadrupole

If two opposite phase monopoles make up a dipole, then two opposite dipoles make up a quadrupole source. In a lateral quadrupole arrangement the two dipoles do not lie along the same line (four monopoles with alternating phase at the corners of a square), and the directivity pattern (Figure B.3) indicates that sound is radiated well in front of each monopole source but canceled at points equidistant from adjacent opposite monopoles.
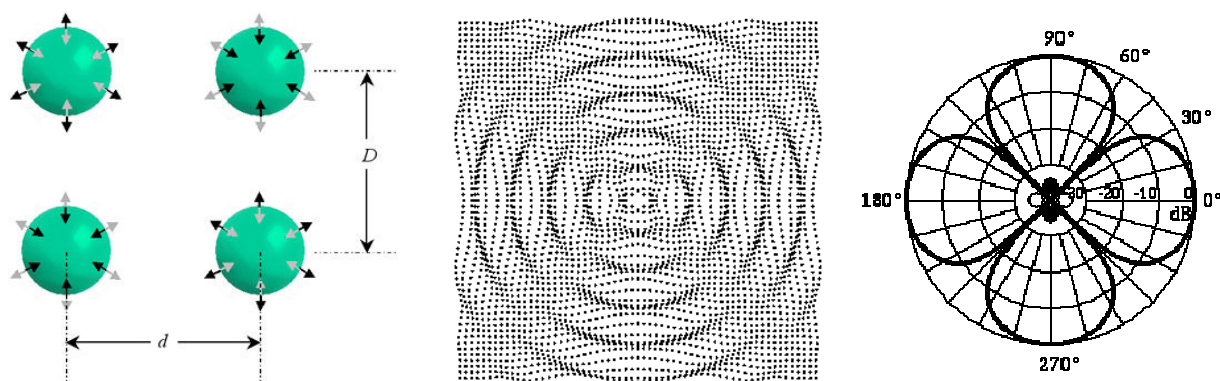
Figure B.3- Lateral quadrupole operation (left), pressure distribution (center) and radiation pattern (right).

The far-field sound pressure amplitude is given by:

$$|p(r, \theta, t)| = \frac{Q_S \, \rho \, c \, k}{4 \, \pi \, r} 4 \, k^2 \, d \, D \cos(\theta) \sin(\theta) \qquad \text{(B.6)}$$

where, again, the angular dependent terms is the major responsible for creating the directivity

85

pattern observed in Figure B.3.

3.2. Longitudinal quadrupole

If two opposite phase dipoles lie along the same line they make up a linear quadrupole source. A tuning fork is a good example of a linear quadrupole source, with each tine acting as a dipole as it vibrates back and forth in opposite directions. What makes the linear quadrupole interesting is that there is a transition from near-field to far-field. In the near-field there are four maxima and four minima, with the maxima along the quadrupole axis about 5 dB louder than the maxima perpendicular to the quadrupole axis. In the far-field there are only two maxima along the quadrupole axis and two minima perpendicular to the quadrupole axis as shown in Figure B.4. It is worth to note that that based on the previous fact the complexity of the directivity pattern is not constant and increases with frequency, which is normally observed in real world structures.

Near-field
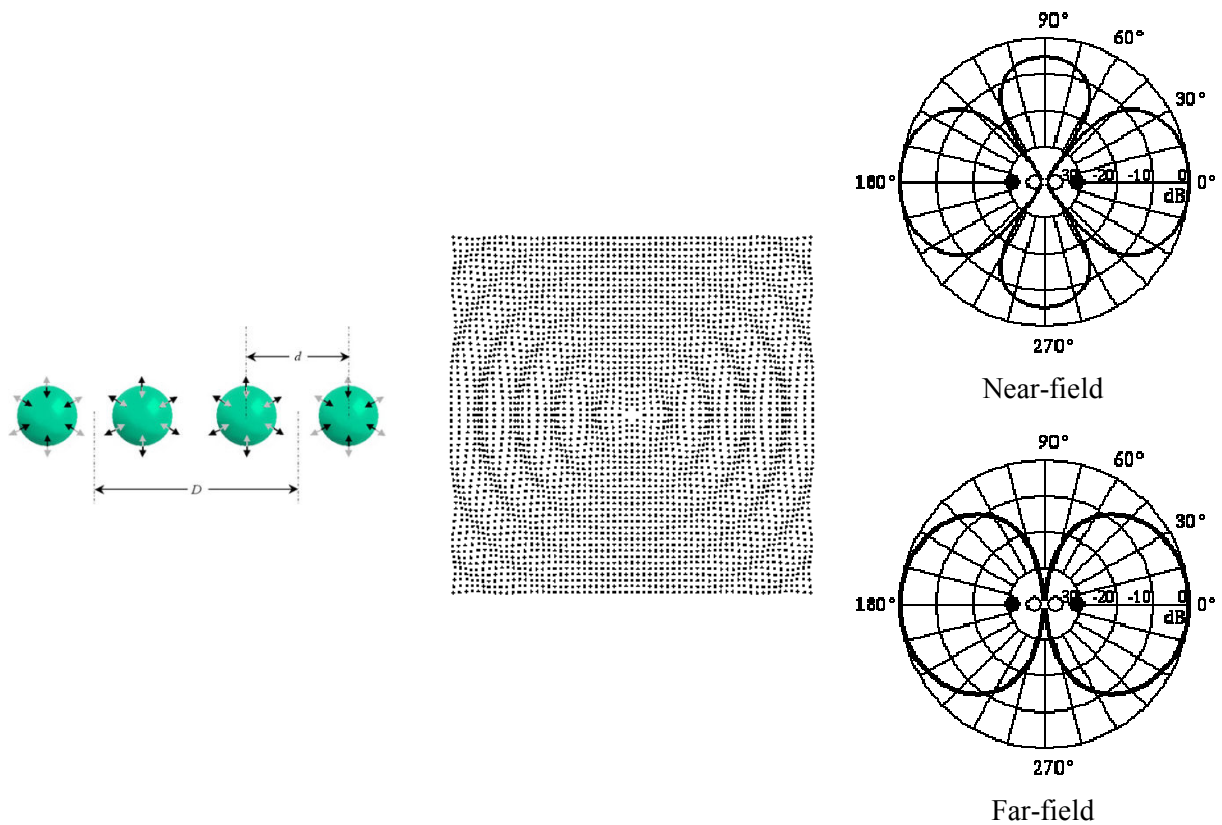
Far-field

Figure B.4- Longitudinal quadrupole operation (left), pressure distribution (center) and radiation patterns (right).

The far-field sound pressure amplitude is given by:

$$p(r, \theta, t) = \frac{Q_S\, \rho\, c\, k}{\pi\, r}\, k^2\, d\, D\, \cos^2(\theta) \qquad\qquad \textbf{(B.7)}$$

Appendix C - The boundary element method in acoustics

This section is mainly based in the works of Wu (2000), Albuquerque (2009) and von Estorff (2000). There are two kinds of principles available for acoustical analysis with the BEM: direct and indirect. The first is based on the classical Helmholtz integral equation with sound pressure as the primary variable, solving it in either a bounded interior domain or an unbounded exterior domain at a time. One important feature of the direct BEM is that it can use either discontinuous (constant) or continuous elements (linear and quadratic) as depicted in Figure C.1.
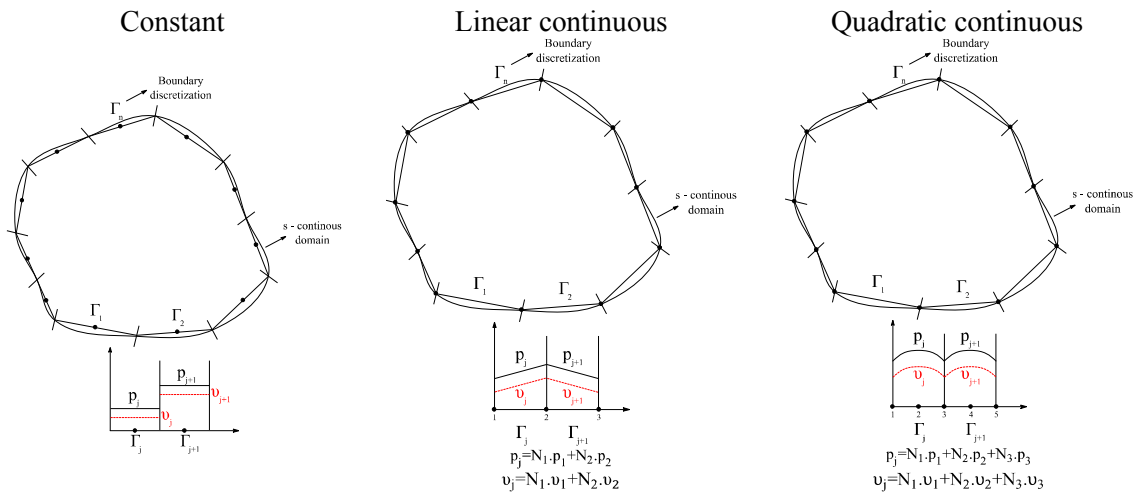
Figure C.1 - Illustration showing the different kinds of elements that can be used with the BEM.

Another approach used by Handi (1981), Wu et al. (1987) and Mariem et al. (1987) is the variational indirect BEM, which solves the Helmholtz equation in both the interior domain and the exterior domain simultaneously, even though one of the domains may not be needed for analysis or does not have even fluid. The primary variable used in the indirect BEM is the pressure jump across the boundary and, in general, it requires more CPU (Central Processing Unit) time to set up the system of equations. The resulting matrix though is symmetric and, unlike the direct BEM, the variation indirect BEM allows only continuous elements.

1. Fundamental solution

Before starting to understand the BEM, it is crucial to discuss about the fundamental solution which, in brief terms, is a solution that once applied to the original differential equation will result in the Dirac delta function (Albuquerque, 2009). In Cartesian coordinates, two important properties of the Dirac delta function are (Fahy, 2001):

$$\int_{-\infty}^{+\infty} \delta(\vec{x} - \vec{x}_0) \, d\vec{x} = 1 \qquad\qquad \text{(C.1)}$$

and

$$\int_{-\infty}^{+\infty} \phi(\vec{x}) \, \delta(\vec{x} - \vec{x}_0) \, d\vec{x} = \phi(\vec{x}_0) \qquad\qquad \text{(C.2)}$$

where $\phi(\vec{x})$ is an arbitrary function of $\vec{x}$, which can be a one-, two-, or three-dimensional variable and $\vec{x}_0$ is the application point. In other words, the property shown by equation (C.2) demonstrates that the Dirac delta function has a selection property which evaluates the function only at $\vec{x}_0$, with all the other values in the domain equal to zero. This is a key property for the BEM because it will allow the collocation of the fundamental solution at on specific element and the correspondent evaluation of the interactions with all other elements as it will be seen later.

As demonstrated before in Appendix A, the Helmholtz differential equation for the time-harmonic linear acoustics is defined by equation (A.3). Using the previous definitions and integrating the equation by knowing in advance that p is self-adjoint[16], a fundamental solution $p*$ can be found so when applied into equation (A.3) it yields the Dirac delta function:

---

[16] Mathematically speaking, a self-adjoint operator means that $p = p^H$, where H is the Hermitian operation. In physical terms, it is equivalent to say that the response at point Q caused by a source in P is equivalent to its reciprocal.

$$\nabla^2 p^* + k^2 p^* = -\delta(Q\text{-}P) \qquad (C.3)$$

where Q is any point in space, P is a singular point source and p^* is the fundamental solution at Q. Adopting a spherical coordinate system with coordinates (r, θ, φ) centered at P, a symmetrical solution (neglecting θ and φ angles) of equation (C.3) is (Wu, 2000):

$$\frac{d^2 p^*}{dr^2} + \frac{2}{r}\frac{dp^*}{dr} + k.p^{*2} = 0 \qquad (C.4)$$

and the general solution for equation (C.4) is:

$$p^* = \tilde{A}.\frac{e^{-i.k.r}}{r} + \tilde{B}.\frac{e^{i.k.r}}{r} \qquad (C.5)$$

where $\tilde{A}$ and $\tilde{B}$ are unknown complex coefficients and the first and second exponential terms in equation (C.5) represent an outgoing and incoming wave respectively. Since P is point source instead of a sink, $\tilde{B}$ can be eliminated from equation (C.5) yielding the fundamental solution sought:

$$p^* = \tilde{A}.\frac{e^{-i.k.r}}{r} \qquad (C.6)$$

The coefficient $\tilde{A}$ can be determined by using equation (C.6) in equation (C.3) and integrating it over a small spherical volume Ω_ε enclosing P, i.e., an infinitesimal volume which radius ε tends to zero:

$$\lim_{\varepsilon \to 0}\left(\iiint_{\Omega_\varepsilon} \nabla\cdot\nabla p^* + k^2 p^*\right)dV = \lim_{\varepsilon \to 0}\left(\iiint_{\Omega_\varepsilon} -\delta(Q\text{-}P)\right)dV = -1 \qquad (C.7)$$

with the volume under the Dirac delta function equals to one. Analyzing equation (C.7) and applying the fundamental solution from equation (C.6) on it, it can be seen that the term $e^{-i.k.r}$ tends to zero much slower than dV when the limit is taken, therefore eliminating the term $k^2 p^*$

from the integral. By using the divergence theorem:

$$\iiint_V \left(\nabla \cdot \vec{F} \right) dV = \oiint_S \left(\vec{F} \cdot \vec{n} \right) dS \tag{C.8}$$

and considering the limit evaluation, equation (C.7), can be rewritten as:

$$\lim_{\varepsilon \to 0} \left(\iint_{S_\varepsilon} \frac{\partial p^*}{\partial n} dS \right) = -1 \tag{C.9}$$

where S_ε is the boundary surface of the spherical volume Ω_ε and n is the unit normal pointing outward on S_ε. By differentiating p^* in the r direction and evaluating the integration in spherical coordinates of equation (C.9), one can find that $A = \frac{1}{4}\pi$. Substituting this value into equation (C.6) the final fundamental solution becomes:

$$p^* = \frac{e^{-i.k.r}}{4.\pi.r} \tag{C.10}$$

2. Interior problems

The objective of and interior problem is to solve the Helmholtz equation inside a cavity V of finite dimensions. The boundary conditions (pressure, normal velocity or impedance) on the cavity wall surface S may be represented by the general expression:

$$\alpha.p + \beta.v_n = \gamma \tag{C.11}$$

where v_n is the particle normal velocity and α, β and γ user-specified constants. Such problem can be solved by using the Green's second identity applied to the functions p and p^* and assuming a singular point P associated with the fundamental solution p^* located in the acoustic domain V. Since p^* is singular at P, a tiny spherical volume V_ε enclosing the singular point P is excluded

from the domain V must be used as shown in Figure C.2.
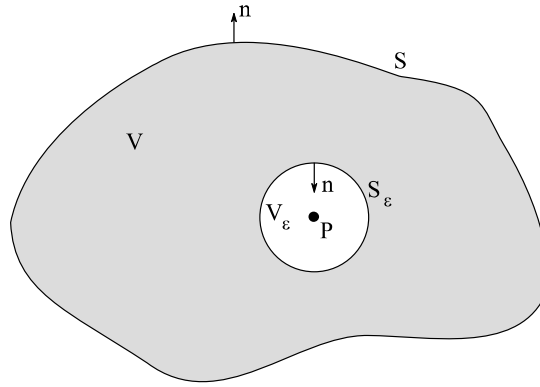
Figure C.2 - Point P excluded from the acoustic domain.

Application of Green's second identity in p and $p*$ and neglecting the internal volume yields:

$$\iiint_{V-V_\varepsilon} \left(p^* \nabla^2 p - p \nabla^2 p^* \right) dV = \oiint_{S+S_\varepsilon} \left(p^* \frac{\partial p}{\partial n} - p \frac{\partial p^*}{\partial n} \right) dS \qquad \text{(C.12)}$$

where the normal vector n is pointing away from the acoustic domain and S_ε is the boundary surface of V_ε. The normal on S is pointing away from the cavity, while the normal on S_ε is pointing towards the singular point P. Since the singular point is excluded from the domain, the Helmholtz equation can be rewritten in terms of p and $p*$ as:

$$\nabla^2 p + k^2 p = 0 \rightarrow \nabla^2 p = -k^2 p \qquad \text{(C.13)}$$

and

$$\nabla^2 p^* + k^2 p^* = 0 \rightarrow \nabla^2 p^* = -k^2 p^* \qquad \text{(C.14)}$$

because of the self-adjoint property of the p and $p*$ operators and the fact that the equations are equal to zero in the whole domain except at the singularity point. This result cancels out the left hand side of equation (C.12) and the right hand side becomes a boundary integral evaluated on two boundary surfaces: the cavity wall and the enclosing of singular point P. It can be also checked that:

$$\lim_{\varepsilon \to 0} \oiint_{S_\varepsilon} p^* \frac{\partial p}{\partial n} dS = 0 \qquad \text{(C.15)}$$

due to the fact that p^* is proportional to $(1/r)$ and dS to (r^2), i.e., as r tends to zero the latter term goes to zero much faster than the former. Evaluating the integration of the remaining term in equation (C.12) in spherical coordinates and taking its limit as r tends to zero one has:

$$\lim_{\varepsilon \to 0} \oiint_{S_\varepsilon} p \frac{\partial p^*}{\partial n} dS = p(P). \lim_{\varepsilon \to 0} \oiint_{S_\varepsilon} \frac{\partial p^*}{\partial n} dS = p(P) \qquad \text{(C.16)}$$

the term $p(P)$ comes out of the integral because at the limit it has the value of the pressure at point P, i.e., it is a value that does not depend on the boundary. Using results from equations (C.15) and (C.16) into equation (C.12) for P in the domain:

$$p(P) = \oiint_S \left(p^* \frac{\partial p}{\partial n} - p \frac{\partial p^*}{\partial n} \right) dS \qquad \text{(C.17)}$$

By using the fact that the normal derivative of sound pressure is related to the particle normal velocity by:

$$\frac{\partial p}{\partial n} = -i.\rho.\omega.v_n \qquad \text{(C.18)}$$

Equation (C.17) then becomes,

$$p(P) = - \oiint_S \left(i.\rho.\omega.v_n.p^* + p \frac{\partial p^*}{\partial n} \right) dS \qquad \text{(C.19)}$$

Equation (C.19) states that the sound pressure p at any point P inside the acoustic domain can be obtained by integrating the equation on the boundary. This is the main idea behind the BEM because only the boundary information is needed to obtain the solution. Since the singular point P is not on the boundary surface, equation (C.19) is nonsingular. However, it is not really ready

93

to be used because for a well-posed boundary value problem p and v_n are both not known from the boundary conditions, i.e., only half of the boundary data are prescribed as the boundary conditions.
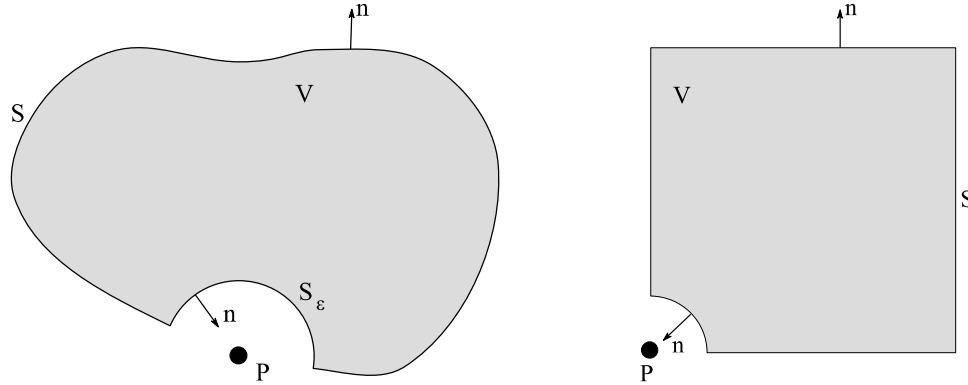
Figure C.3 - Point P excluded from the domain on a smooth boundary (left) and at a corner (right).

To find the other half of the boundary data, it is necessary to collocate P on the boundary not directly, but with a tiny volume circumscribing the point like shown in Figure C.3. This time there is not a spherical volume anymore, but instead a hemisphere in a smooth boundary or a portion of a sphere such as in a corner. In both cases, equation (C.12) is still valid and its left hand side is zero because of the exclusion of the singular point P from the domain., i.e.:

$$0 = \oiint_{S+S_\varepsilon} \left(p^* \frac{\partial p}{\partial n} - p \frac{\partial p^*}{\partial n} \right) dS \tag{C.20}$$

and

$$\lim_{\varepsilon \to 0} \oiint_{S_\varepsilon} p^* \frac{\partial p}{\partial n} dS = 0 \tag{C.21}$$

for the same reasons as those used in equation (C.15). However, equation (C.16) does not produce $p(P)$ anymore because S_ε is not the surface of a full sphere. If P is collocated on a smooth boundary, S_ε is the surface of a hemisphere and equation (C.16) becomes:

94

$$\lim_{\varepsilon \to 0} \oiint_{S_\varepsilon} p \frac{\partial p^*}{\partial n} dS = p(P). \lim_{\varepsilon \to 0} \oiint_{S_\varepsilon} \frac{\partial p^*}{\partial n} dS = \frac{1}{2}. p(P) \tag{C.22}$$

Using equations (C.21) and (C.22) in equation (C.20) yields:

$$\frac{1}{2}. p(P) = - \oiint_S \left(i.\rho.\omega.v_n.p^* + p \frac{\partial p^*}{\partial n} \right) dS \tag{C.23}$$

where the value of ½ is referred to be the solid angle of the interior volume at *P*. For a boundary that is not smooth, such as an edge or a corner, the leading coefficient is different from ½. By denoting it as $C^0(P)$, the boundary integral equation can be rewritten as:

$$C^0(P).p(P) = - \oiint_S \left(p^*.i.\rho.\omega.v_n + p \frac{\partial p^*}{\partial n} \right) dS \tag{C.24}$$

where the value of $C^0(P)$ can be determined using equation (C.23):

$$C^0(P) = \lim_{\varepsilon \to 0} \oiint_{S_\varepsilon} \frac{\partial p^*}{\partial n} dS \tag{C.25}$$

Equation (C.25) is still not useful because it is impractical to numerically evaluate an integral over an infinitesimal surface. A first step to convert it into something that can be numerically evaluated is to note that:

$$\lim_{r \to 0} p^* = \lim_{r \to 0} \frac{e^{-i.k.r}}{4.\pi.r} = \lim_{r \to 0} \frac{1}{4.\pi.r} = p_L^* \tag{C.26}$$

where p_L^* is the fundamental solution of the Laplace equation. Similarly,

$$\lim_{r \to 0} \frac{\partial p^*}{\partial n} = \lim_{r \to 0} (1 - i.k.r). \frac{e^{-i.k.r}}{4.\pi.r} = \lim_{r \to 0} \left(-\frac{1}{4.\pi.r} \right) = \lim_{r \to 0} \frac{\partial p_L^*}{\partial n} \tag{C.27}$$

Therefore, equation (C.25) becomes:

95

$$C^0(P) = \lim_{\varepsilon \to 0} \oiint_{S_\varepsilon} \frac{\partial p_L^*}{\partial n} dS \tag{C.28}$$

Still, equation (C.28) is an integral over an infinitesimal surface. By forming Green's second identity for an imaginary Laplace problem $\nabla^2 \phi = 0$ occupying the same domain V as the acoustic problem, we can derive an integral equation similar to equation (C.20):

$$0 = \oiint_{S+S_\varepsilon} \left(p_L^* \frac{\partial p}{\partial n} - p \frac{\partial p_L^*}{\partial n} \right) dS \tag{C.29}$$

By remarking that $\phi = 1$ is a particular solution to the Laplace equation and substituting into equation (C.29) gives:

$$0 = \oiint_{S+S_\varepsilon} \frac{\partial p_L^*}{\partial n} dS \to \oiint_{S_\varepsilon} \frac{\partial p_L^*}{\partial n} dS = - \oiint_{S} \frac{\partial p_L^*}{\partial n} dS \tag{C.30}$$

Using equations (C.30) and (C.28) the leading coefficient becomes:

$$C^0(P) = - \oiint_{S} \frac{\partial p_L^*}{\partial n} dS \tag{C.31}$$

where the integral can be numerically be evaluated over the boundary surface S. Summarizing all the discussion above presented, the boundary integral equation for an interior acoustic problem is given by equation (C.24), which is normally referred as Helmholtz integral equation. The leading coefficient $C^0(P)$ is equal to 1 if P is in the domain, $\frac{1}{2}$ if P is on a smooth boundary and 0 if P is outside the acoustic domain. As a final comment, it should be noted equation (C.24) becomes singular when P is collocated on the boundary.

3. Exterior problems

The objective in an exterior problem is to solve the Helmholtz equation in an unbounded fluid domain V due to the acoustic radiation from a vibrating structure without boundary surface S. The normal vector n on the structure surface S is pointing away from the acoustic domain and, as in the interior problems, the boundary conditions on the structure surface may be specified by the general expression of equation (C.11).
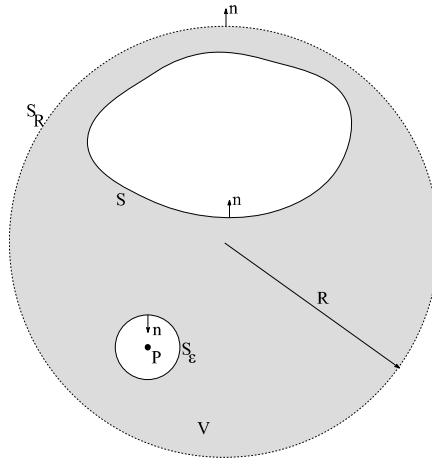
Figure C.4 - Point P excluded from an exterior domain.

Using a far-field boundary surface S_R of radius R temporarily constructed to bound the acoustic domain V and applying Green's second identity in p and p^* neglecting the internal volume enclosing the singular point P yields:

$$\iiint_{V-V_\varepsilon} \left(p^* \, \nabla^2 p - p \, \nabla^2 p^* \right) dV = \oiint_{S+S_\varepsilon+S_R} \left(p^* \frac{\partial p}{\partial n} - p \frac{\partial p^*}{\partial n} \right) dS \tag{C.32}$$

As the singular point P is already excluded from the domain, the left-hand side is zero due to cancellation of the two terms. Therefore, like in the interior formulation one has:

$$\lim_{\varepsilon \to 0} \oiint_{S_\varepsilon} p^* \frac{\partial p}{\partial n} dS = 0 \tag{C.33}$$

97

and

$$\lim_{\varepsilon \to 0} \oiint_{S_\varepsilon} p \frac{\partial p^*}{\partial n} dS = p(P). \lim_{\varepsilon \to 0} \oiint_{S_\varepsilon} \frac{\partial p^*}{\partial n} dS = p(P) \qquad \text{(C.34)}$$

Due to the Sommerfeld radiation condition[17], any physical solution p can be represented by an equivalent point source of certain strength when the solution at infinity is desired. In other words:

$$p \to \frac{e^{-i.k.r}}{r} \qquad \text{(C.35)}$$

as r goes to infinity and A is a constant. Since p has the same form as p^* at infinity, it can be shown that:

$$\lim_{R \to \infty} \oiint_{S_R} \left(p^* \frac{\partial p}{\partial n} - p \frac{\partial p^*}{\partial n} \right) dS \qquad \text{(C.36)}$$

which results in the following boundary integral equation:

$$p(P) = \oiint_{S} \left(p^* \frac{\partial p}{\partial n} - p \frac{\partial p^*}{\partial n} \right) dS \qquad \text{(C.37)}$$

with P in the domain. Equivalently:

$$p(P) = - \oiint_{S} \left(i.\rho.\omega.v_n.p^* - p \frac{\partial p^*}{\partial n} \right) dS \qquad \text{(C.38)}$$

which is identical to equation (C.19) except by the fact that the normal direction is inverted on S.

---

[17] The Sommerfeld radiation condition basically ensures that sources radiate waves instead of absorbing them.

For *P* on the boundary, *P* is excluded from the acoustic domain as shown in leading to the boundary integral equation given by:

$$C(P).p(P) = -\oiint_S \left(p^* . i.\rho.\omega.v_n + p\frac{\partial p^*}{\partial n} \right) dS \qquad \text{(C.39)}$$

where *C(P)* is defined by:

$$C(P) = \lim_{\varepsilon \to 0} \oiint_{S_\varepsilon} \frac{\partial p^*}{\partial n} dS = \lim_{\varepsilon \to 0} \oiint_{S_\varepsilon} \frac{\partial p_L^*}{\partial n} dS \qquad \text{(C.40)}$$
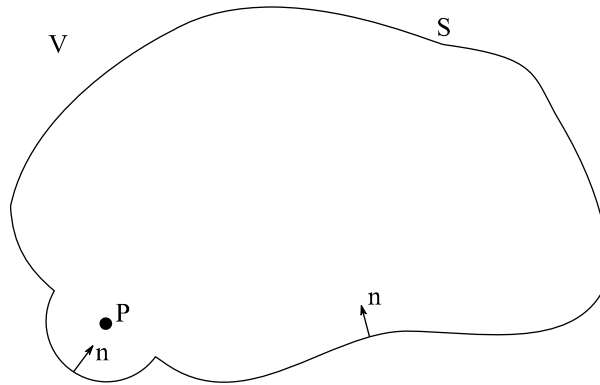
Figure C.5 - Point P excluded from an exterior domain with a smooth boundary.

Equation (C.40) is almost equal to equation (C.28) except that S_ε is now on the interior side of *S*. Defining a complementary surface S_ε' on the interior side of *S* such that S_ε and S_ε' form a full spherical surface of radius ε centered at *P* as shown in Figure C.5.The normal in this case is point toward *P*, therefore:

$$\oiint_{S_\varepsilon + S_\varepsilon'} \frac{\partial p_L^*}{\partial n} dS = 1 \qquad \text{(C.41)}$$

Noticing that the integral over the complimentary surface is $C^0(P)$ given by equation (C.28), it can be said that:

$$C(P) = 1 - \lim_{\epsilon \to 0} \oiint_{S'_\epsilon} \frac{\partial p^*_L}{\partial n} \, dS = 1 - C^0(P) \qquad \text{(C.42)}$$

Using equation (C.31) in equation (C.42) and realizing that the normal direction on *S* for an exterior problem is actually opposite to the normal for an interior problem:

$$C(P) = 1 - \oiint_S \frac{\partial p^*_L}{\partial n} \, dS \qquad \text{(C.43)}$$

C(P) is equal to 1 for *P* in the acoustic domain, ½ for *P* on a smooth boundary and 0 for *P* outside the acoustic domain (inside the solid structure). Therefore, equation (C.43) is used only *P* is on the boundary.

4. Boundary conditions

There are three types of boundary conditions which can be used in the BEM summarized in Table C.1 and further discussed in this section:

Table C.1 - Boundary conditions for the wave and Helmholtz equation after von Estorff (2000).

BC	Wave equation	Helmholtz equation
Dirichlet	$p(\vec{r}, t) = \bar{p}(\vec{r}, t)$	$p(\vec{r}, \omega) = \bar{p}(\vec{r}, \omega)$
Neumann	$\dfrac{\partial p(\vec{r}, t)}{\partial n} = -\rho \dfrac{\partial v_n(\vec{r}, t)}{\partial t}$	$\dfrac{\partial p(\vec{r}, \omega)}{\partial n} = -i \rho \omega \bar{v}_n(\vec{r}, \omega)$
Robin	$\dfrac{\partial p(\vec{r}, t)}{\partial n} = -\bar{A}(\vec{r}) \dfrac{\partial p(\vec{r}, t)}{\partial t}$	$p(\vec{r}, \omega) = -\bar{Z}(\vec{r}, \omega) \bar{v}_n(\vec{r}, \omega)$

where $\bar{A}(\vec{r})$ and $\bar{Z}(\vec{r}, \omega)$ are the surface admittance and impedance respectively, assumed to be known quantities.

4.1. Dirichlet boundary condition

The surface Helmholtz integral equation for an exterior Dirichlet problem (p prescribed on S) is:

$$\oiint_{S} i.\rho.\omega.v_n.p^*dS = -\frac{1}{2}.p(P) - \oiint_{S} p\frac{\partial p^*}{\partial n}dS \qquad \text{(C.44)}$$

where n is the unit normal vector directing away from the exterior acoustic domain or into the solid body and the unknown v_n has been moved to the left-hand side. Also, consider an auxiliary Dirichlet interior Dirichlet problem defined inside the body V'. If the same normal is kept (as used in the exterior problem), the interior Helmholtz equation for the auxiliary Dirichlet problem is:

$$\oiint_{S} i.\rho.\omega.v_n.p^*dS = \frac{1}{2}.p(P) - \oiint_{S} p\frac{\partial p^*}{\partial n}dS \qquad \text{(C.45)}$$

Comparing equation (C.44) with (C.45), it can be noticed that they have the same left-hand side. Since equation (C.45) is for an interior problem, it will have resonances defined by its eigenfrequencies. Although the exterior problem will not have any resonances, equation (C.44) has the same left-hand side of equation (C.45), which determines the coefficient matrix in the BEM. When equation (C.45) breaks down at resonance frequencies, its coefficient matrix becomes singular and so does the coefficient matrix of equation (C.44).

4.2. Neumann boundary condition

For a Neumann boundary condition (v_n prescribed on S), the unknown is p and the right-hand sides of equations (C.44) and (C.45) become the left-hand sides. Although it can be thought that the exterior and interior problems do not have the same coefficient matrix in this case, the non-uniqueness problem still exists. Hence, rewriting equation (C.44) for an exterior Neumann problem:

$$\frac{1}{2} \cdot p(P) + \iint_S p \frac{\partial p^*}{\partial n} dS = - \iint_S i.\rho.\omega.v_n.p^* dS \qquad \textbf{(C.46)}$$

In order to explain the non-uniqueness difficulty for the exterior Neumann problem, the indirect formulation shall be used. Consider an auxiliary interior Dirichlet problem defined inside the body V'. If the same normal vector (as used in the exterior problem) is kept unchanged, the indirect boundary integral equation for P in V' using the classical double-layer formulation is:

$$p(P) = \iint_S \frac{\partial p^*}{\partial n} \mu \, dS \qquad \textbf{(C.47)}$$

where μ is the unknown dipole distribution on S necessary to generate the solution p. The physical meaning of the dipole is that $\mu = p^+ - p^-$, where p^+ *and* p^- are the pressures on the interior and exterior sides of S. Equation (C.24) can actually be derived by adding the interior and exterior Helmholtz integral equations together and assuming the same normal velocity on the surface for both the interior and exterior equations. In order to solve the auxiliary interior Dirichlet problem, the collocation point P has to be taken to the boundary. There will be a jump associated with the limiting process and equal to $\mu(P)/2$, which can be explained by comparing equations (C.19) and (C.23) and construct the Jump theorem.

4.2.1. The jump theorem

For any smooth density function μ defined on a smooth boundary surface S with the normal vector pointing away from the domain, the jump of $\iint_S \frac{\partial p^*}{\partial n} \mu \, dS$ as P approaches the boundary from the domain is $-\frac{1}{2}\mu(P)$.

The meaning of the jump theorem is actually the result of integration over an infinitesimal area (such as a disk of radius ε) on the boundary surface near point P when it is pushed very close to the boundary from the domain. Although it is infinitesimal, the contribution is finite because of

the singularity involved in the kernel $\dfrac{\partial p^*}{\partial n}$.

Since the normal in equation (C.47) is pointing into instead of away from the interior domain, the jump is $\frac{1}{2}\mu(P)$ as P approaches the boundary from the interior. Taking the limit it produces:

$$p(P) = \frac{1}{2}\mu(P) + \oiint_S \frac{\partial p^*}{\partial n}\, \mu\, dS \qquad\qquad \text{(C.48)}$$

Since the unknown for the indirect formulation is μ, equation (C.48) is rewritten in such a way that the unknown stays on the left-hand side:

$$\frac{1}{2}\mu(P) + \oiint_S \frac{\partial p^*}{\partial n}\, \mu\, dS = p(P) \qquad\qquad \text{(C.49)}$$

Comparing equations (C.49) and (C.44) it can be seen that both have the same form on the left-hand side except that equation (C.44) uses p whereas equation (C.49) uses μ as the unknown variable. Since equation (C.49) is for an interior problem, its solution breaks down at certain characteristic frequencies which are the resonance ones for the interior Dirichlet problem. Although there is no resonance for the exterior Neumann problem, equation (C.44) will not yield a unique solution at these characteristic frequencies.

4.3. Robin (or general) boundary condition

A general boundary condition can be written in a general form as:

$$\alpha.p + \beta.v_n = \gamma \qquad\qquad \text{(C.50)}$$

where α, β and γ user-specified constants. It should be noted that the Dirichlet and BCs are just special cases of equation (C.50) and, in order to deal with this general BC, it is necessary first to express v_n in terms of p by isolating it in equation (C.50) (providing that $\beta \neq 0$), i.e.:

$$v_n = \frac{\gamma - \alpha.p}{\beta} \qquad\qquad (C.51)$$

Substituting the previous equation in the exterior surface Helmholtz integral equation (C.38) results in:

$$\frac{1}{2}p(P) + \oiint_S p\left(\frac{\partial p^*}{\partial n} - i.\rho.\omega.\frac{\alpha}{\beta}.p^*\right)dS = - \oiint_S i.\rho.\omega.\frac{\gamma}{\beta}.p^*dS \qquad\qquad (C.52)$$

where the unknown variable is p. It is noticed that the left-hand side coefficient matrix in equation (C.52) is a linear combination of the left-hand side coefficient matrices of equations (C.44) and (C.46). Since both equations break down at the same characteristic frequencies associated with the interior Dirichlet problem, equation (C.52) also breaks down at the same set of characteristic frequencies.

4.4. The CHIEF method

The simplest way of overcoming the non-uniqueness problem is to use the CHIEF method proposed by (Schenck, 1968). The method simply collocates the Helmholtz integral equation at a few interior points inside the body V' as constraint equations in addition to the existing surface Helmholtz integral equation (normally referred as CHIEF points). Since $C(P) = 0$ for an exterior problem when P is collocated inside the body, the CHIEF equations take the form:

$$0 = - \oiint_S \left(i.\rho.\omega.v_n.p^* + p\frac{\partial p^*}{\partial n}\right)dS \qquad\qquad (C.53)$$

The CHIEF equations together with the existing Helmholtz integral equation form an overdetermined system of equations, which may then be solved by a least-square procedure. Also, they enforce the zero pressure condition at the CHIEF points as a constraint to the surface Helmholtz integral equation. Usually this constraint is strong enough to distinguish an exterior problem from the interior Dirichlet problem. However, when a CHIEF point falls on any interior

nodal surface associated with a characteristic eigenfrequency, the CHIEF equation will not provide any constraint effect at that particular frequency because the pressure on the interior nodal surface is also zero for the interior problem. This drawback is compounded by the fact that as the frequency increases the eigenfrequencies and the nodal surfaces of the interior problem become more closely spaced. The usual practice is to use the CHIEF points for all frequencies and increase the number of points as frequencies go up. However, there is always a question about how many CHIEF points are necessary and where to place them. The method has been proved very effective for problems at low and intermediate frequencies.

4.5. Calculations

This section presents a brief discussion about the calculation procedures concerning the solution of a BEM problem inside Virtual.Lab®.

4.5.1. Direct BEM

For the direct BEM, the following system of equations must be created and solved for each selected analysis frequency:

$$[A(\omega)].\{p\} = [B(\omega)].\{v_n\} \tag{C.54}$$

where $[A(\omega)]$ and $[B(\omega)]$ are non-symmetric, full-populated and frequency dependant matrices, $\{p\}$ is a vector of nodal pressures on the BEM surface and $\{v_n\}$ is a vector of nodal normal velocities on the BEM surface. The nodal pressure and nodal normal velocity on the BEM surface are also called primary surface results or potentials. From these primary surface results, pressure, velocity and intensity values are automatically calculated if field points are defined before the analysis. The pressure at an arbitrary field point P is obtained from surface pressure and normal velocity values by field point post-processing, using the expression:

$$P_p = \{a\}^T\{p\} + \{b\}^T\{v_n\} \tag{C.55}$$

The calculation of the primary surface results are given by equation (C.54) and is the most expensive in terms of CPU (Central Processing Unit) time because it involves the inversion of a complex and fully populated matrix. Since it only involves numerical integration, field point post-processing from these primary surface results given by equation (C.55) is relatively fast unless there a very large number of field points is used.

4.5.2. Indirect BEM

Differently from the direct method, in the indirect BEM approach the system of equations that must be created and solved for each selected analysis frequency is:

$$
\begin{bmatrix} B & C^T \\ C & D \end{bmatrix} \begin{Bmatrix} \sigma \\ \mu \end{Bmatrix} = \begin{Bmatrix} f \\ g \end{Bmatrix}
\qquad \text{(C.56)}
$$

where σ is a vector of single layer potentials (jumps of velocity), μ is a vector of double layer potentials (jump of pressure) and f and g excitation vectors. It is worth to note that the first matrix is fully populated but symmetric. The single layer and double layer potentials on the BEM surface are also called primary surface results. Pressure, velocity and intensity values can be calculated from them at field points by using post-processing as seen previously in section 4.5.1.

If field points are defined on the boundary element surface, it must be specified on which side of the surface they are, i.e., either positive or negative, where positive means the sense of the local element normal axis. Their pressures and velocities can then also be evaluated, although the numerical procedure has to handle hyper-singular integrals. It is recommended to have such surface field points only at nodes of the boundary element mesh. As in the case of direct BEM , the calculation of the primary surface results is the most expensive in terms of CPU time because it involves the inversion of a complex and fully-populated matrix, and field point post-processing from the primary surface results is relatively fast, unless a very large number of them is used.

4.5.3. Structural coupling

The frequency analysis procedure computes the response of a structure and the surrounding fluid to harmonic excitations. Two techniques are available for representing the structural behavior:

- Physical coordinates (Direct Response);
- Modal coordinates (Superposition).

Excitations can be structural loads (forces) or acoustic loads (wave sources) taking into account any other boundary condition defined on the structure such as constrained displacements, admittance values and known acoustic (surface) velocities. From these input data, the procedure computes both the structural response (displacements) and the acoustic potentials (single and double layer potentials). From these primary results, it is then possible to evaluate the acoustic field (pressure, velocity and intensity) at any field point inside or outside the vibrating surface.

The calculation procedure sets up and solves a coupled system of equations involving both structural displacements and acoustic jumps of pressure as unknowns. For physical coordinates, this system of equations is of the form:

$$\begin{bmatrix} K_s - \omega^2.M_s & C^T \\ C & \dfrac{H(\omega)}{\rho.\omega^2} \end{bmatrix} \begin{Bmatrix} u \\ \mu \end{Bmatrix} = \begin{Bmatrix} F_s \\ \dfrac{F_A}{\rho.\omega^2} \end{Bmatrix} \tag{C.57}$$

Where $H(\omega)$ is the BEM indirect influence matrix, K_s and M_s the structural stiffness and mass matrices, C the geometrical coupling matrix, F_s and F_A the structural and acoustic load vectors, u the vector of nodal displacements an μ the vector of nodal jumps of pressure. In modal coordinates the system takes the form:

$$\begin{bmatrix} \widehat{K}_s - \omega^2.\widehat{M}_s & \widehat{C}^T \\ \widehat{C} & \dfrac{H(\omega)}{\rho.\omega^2} \end{bmatrix} \begin{Bmatrix} a_s \\ \mu \end{Bmatrix} = \begin{Bmatrix} \widehat{F}_s \\ \dfrac{F_A}{\rho.\omega^2} \end{Bmatrix} \tag{C.58}$$

Where the caret symbol indicates a projection in the structural modal basis and $\{a_s\}$ are the structural modal participation factors.

4.6. The Fast Multipole BEM (FMBEM)

Physically large systems result in vast structural and acoustic models in the frequency range of interest due to the small size of elements determined by (3.1. As an example given by (Hallez, 2009), an engine with approximated dimensions of 5 x 2 x 2 meters and a analysis frequency target of 3 kHz would have around 50 elements per meter or 2500 elements per square meter, therefore resulting in an overall number of 125000 elements. This discretization is extremely huge for BEM calculations since the matrices involved are normally fully populated, therefore resulting in considerable amounts of RAM usage, disk storage and processing needs. This trend is better summarized in Figure C.6 for structures with increasing sizes.
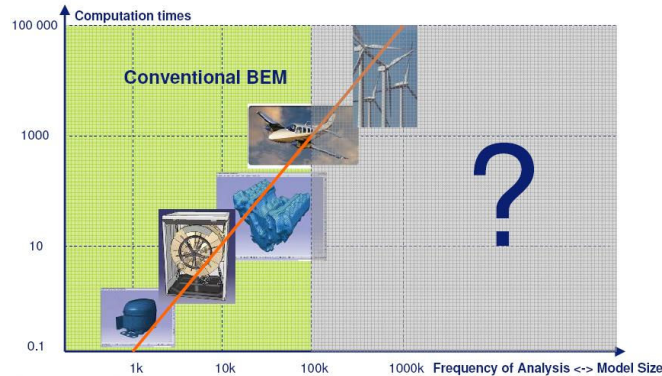

Figure C.6 - Illustration showing the computation time versus the model size for traditional BEM (Hallez, 2009).

Since in traditional BEM the computation time increases with the number of elements cubed, a new approach is necessary to solve ultra-large scale models. As demonstrated in the previous sections, in that kind of modeling each node must have its interaction calculated with all other nodes. An important observation that can be done is the fact that the intensity of the interactions decreases with the distance because of exponential behavior of the fundamental solution ((C.10), which opens a new possibility to treat nodes far apart from the source point simultaneously: this is the key feature behind the FMBEM as depicted in Figure C.7.
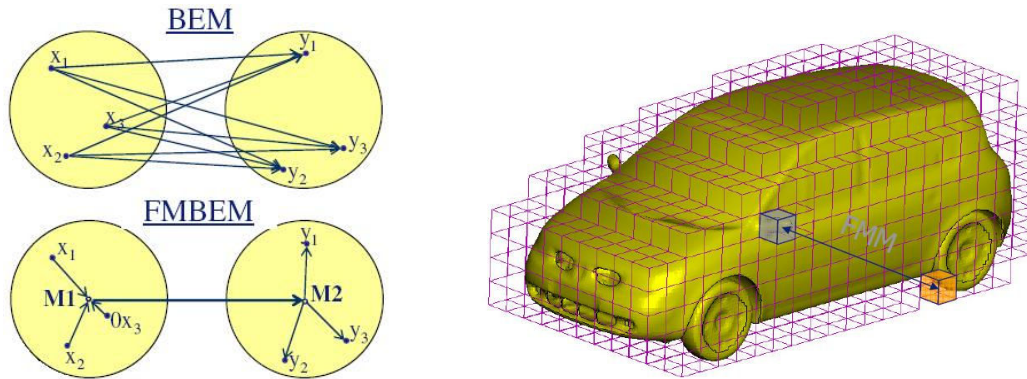
Figure C.7 - Differences between approaches taken by BEM and FMBEM (Hallez, 2009). In the first case, the interactions between all nodes must be evaluated. In the second case the structure is subdivided in small blocks where the internal interactions of the nodes with a central node are computed to be further interacted with the central nodes of other blocks.

An introductory and excellent discussion about the FMBEM is made by (Liu et al., 2006), in which the authors try to demonstrate the new concepts involved by using a potential problem. Nevertheless, as the authors mention, the method is much more complex than the traditional BEM, which is beyond the objective of this short discussion. Although complex, the technique is very promising and was considered one of the top 10 algorithms in scientific computing that were developed in the 20th century due to the huge savings in computational times as demonstrated in Figure C.8.

Method	DOFs	Time when doubling frequency
BEM	$O(n^3)$	64 times more
FMBEM	$O(n \cdot \log^2(n))$	4 to 6 more
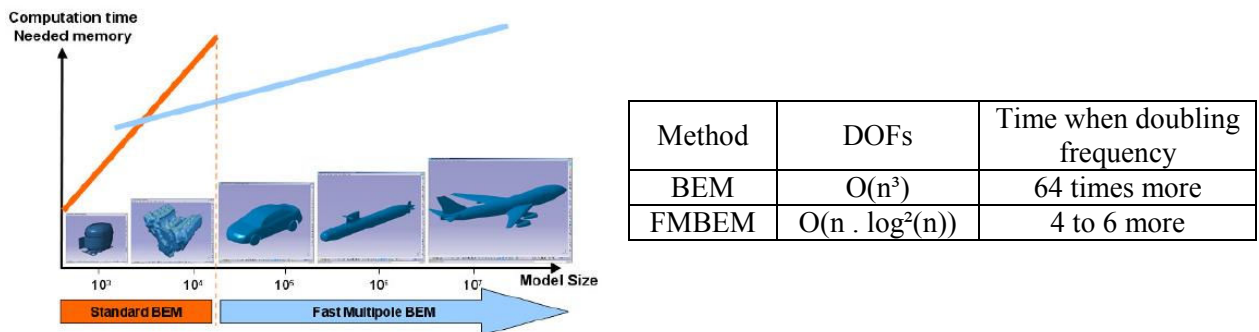
Figure C.8 - Demonstration of the most suitable method according to the model size and the number of elements (Hallez, 2009).

A final word about the FMBEM is that it is available in Virtual.Lab® as a solution possibility. However, the method works only with triangular elements and accepts only constant boundary conditions such as panel pressure, velocity or displacement. Some time has been spent in order to make the solution work in Virtual.Lab® but none of the tries has succeeded.

Appendix D - Mass normalization of modes

An undamped Multiple Degree Of Freedom (MDOF) system can be modeled by equation (D.1):

$$[M]\{\ddot{u}\} + [K]\{u\} = \{F\}$$ <div style="float:right">(D.1)</div>

where $[M]$ and $[K]$ are the system mass and stiffness matrices, $\{\ddot{u}\}$ and $\{u\}$ are the acceleration and displacement vectors at the DOFs and $\{F\}$ is the excitation force vector. Assuming a periodic excitation type $\{F\} = \{\tilde{F}\}e^{s.t}$ and a response $\{u\} = \{\tilde{u}\}e^{s.t}$, the following homogeneous eigenproblem can be established:

$$([M].s_r^2 + [K])\{\Psi\}_r = \{0\}$$ <div style="float:right">(D.2)</div>

where $\{\Psi\}_r$ and s_r are the shape (relative displacement among all DOFs) and pole for a specific mode r. Therefore, if $\{\Psi\}_r$ is an eigenvector of the MDOF system solution, the same vector scaled by a constant $\gamma_r\{\Psi\}_r$ will also be and infinite choices for shape amplitudes are possible. Although their normalization is arbitrary, the mass-normalization is the most frequent used in structural modal analysis and is based in the weighted orthogonality (He et al., 2001) of the mode shapes in relation to the mass matrix (symmetry of *M* and *K*). Therefore:

$$\{\Psi\}_r^T[M]\{\Psi\}_r = m_r$$ <div style="float:right">(D.3)</div>

where m_r is the modal mass for an individual mode *r*. Hence, if the procedure above is followed for the eigenvector $\{\Psi\}_r$, a new mass-normalized vector $\{\Phi\}_r$ can be written such as:

$$\{\Phi\}_r^T[M]\{\Phi\}_r = 1$$ <div style="float:right">(D.4)</div>

and the scaling constant becomes:

$$\gamma_r = \frac{1}{\sqrt{m_r}} \tag{D.5}$$

Applying the same principle to the stiffness matrix in equation (D.1) yields:

$$\{\Phi\}_r^T [K] \{\Phi\}_r = \omega_r^2 \tag{D.6}$$

with ω_r^2 the natural frequency of mode r. In matrix notation one would have the following results for mass and stiffness matrices respectively:

$$[\Phi]^T [M] [\Phi] = [I] \tag{D.7}$$

and

$$[\Phi]^T [K] [\Phi] = [\omega_r^2]_d \tag{D.8}$$

where the subscript d means a diagonal matrix. By applying the definition of the receptance matrix:

$$[\alpha(\omega)] = ([K] - \omega^2 [M])^{-1} \tag{D.9}$$

Equation (D.9) combined with equations (D.7) and (D.8) yields:

$$[\alpha(\omega)] = [\Phi] [\omega_r^2 - \omega^2]_d^{-1} [\Phi]^T \tag{D.10}$$

It can be shown that results from equation (D.10) are symmetric (Ewins, 1984), thus indicating the principle of reciprocity[18]. Also, operations between matrices can be rewritten and their results can be further generalized in the modal superposition theorem:

$$\alpha_{jk}(\omega) = \sum_{r=1}^{N} \frac{\phi_{ir} \phi_{jr}}{\omega_r^2 - \omega^2} \tag{D.11}$$

---

[18] The principle of reciprocity states that if a response at a node j is caused by an excitation at node i, then a response at node i caused by an excitation at node j will lead to the same results.

where N is the number of modes, ω the excitation frequency in radians per second, j and k are the indexes for response and excitation respectively and the terms ϕ_{ir} and ϕ_{jr} are those from the receptance matrix. The most important result shown by equation (D.11) is that the resulting FRF comprises the contributions of all individual modes, thus indicating their "superposition". An extension of equation (D.11) for the case where a damping symmetrical matrix exists is (He et al., 2001):

$$\alpha_{jk}(\omega) = \sum_{r=1}^{N} \frac{\phi_{ir}\phi_{jr}}{m_r.\left(\omega_r^2 - \omega^2 + i.2.\zeta_r.\omega.\omega_r\right)} \tag{D.12}$$

with ζ_r the damping ratio for mode r defined by equation (D.13) and c_r the modal damping for mode r defined by:

$$\zeta_r = \frac{c_r}{2.m_r.\omega_r} \tag{D.13}$$

For the cases where the damping matrix is not symmetrical, a state formulation is necessary and better discussed by Ewins (1984) and He et al. (2001). It is clear from the discussion above that the modal mass normalization plays an important role in structural modal analysis and is directly related with the FRF matrix determination, having an enormous influence in the simulations discussed in section 3.6.

Appendix E - Author's publications

Cóser, L. F., Pasqual, A. M., Arruda, J. R. F. "Sound field radiated by a spherical loudspeaker array using a flexible membrane model", In: Proceedings of 39th International Congress and Exposition on Noise Control Engineering - INTERNOISE, 13-16 June, Lisbon, Portugal, 2010.

Batista, F.B., Fabro, A.T., Cóser, L. F., Arruda, J.R.F., Albuquerque, E. L., "In-plane modal testing of a free isotropic plate using laser Doppler vibrometer measurements", In: Proceedings of 9th International Conference on Vibration Measurements by Laser and Noncontact Techniques – AIVELA, 22-25 June, Ancona, Italy, 2010.

Siviero, D. A., Goldstein, A. L., Souza, S., Arruda, J. R. F., Cóser, L. F., "An experimental investigation of a hybrid active/passive panel for increased transmission loss at low frequencies", In: Proceedings of International Conference on Noise and Vibration Engineering – ISMA, 20-22 September Leuven, Belgium, 2010.

Oliveira, A., Cóser, L. F., "Particle Velocity Measurements as a Breakthrough for Determining Acoustic Absorption Coefficient in Brazilian Trucks", In: Proceedings of the 2nd SAE Brazil International Noise and Vibration Congress, 17-19 October, Florianópolis, SC, Brazil, 2010.

Oliveira, A., Cóser, L. F., Porto, V., Macêdo, B., Oliveira, C., Vilaboim H., Figueiredo T., "Reducing Sound Radiation of an Automated Transmission by Means of Viscoelastic Multilayer Damping", In: Proceedings of the 2nd SAE Brazil International Noise and Vibration Congress, 17-19 October, Florianópolis, SC, Brazil, 2010.